Ontwikkeling van een geavanceerde sonde
en studie van randplasmastromingen en transport in tokamaks

Development of an Advanced Probe
and Study of Edge Plasma Flows and Transport in Tokamaks

Peter Peleman

Promotor: prof. dr. ir. G. Van Oost
Proefschrift ingediend tot het behalen van de graad van
Doctor in de Ingenieurswetenschappen: Toegepaste Natuurkunde

Vakgroep Toegepaste Fysica
Voorzitter: prof. dr. ir. C. Leys
Faculteit Ingenieurswetenschappen
Academiejaar 2006 - 2007

UNIVERSITEIT
GENT

ISBN-10 90-8578-117-5
ISBN-13 978-90-8578-117-2
NUR 926
Wettelijk depot: D/2006/10.500/75

Promotor

prof. dr. ir. G. Van Oost[1]

Examencommissie

prof. dr. ir. G. Van Oost
prof. dr. ir. C. Leys[1], secretaris
prof. dr. em. W. Wieme[1]
prof. dr. ir. J.-M. Noterdaeme[2]
dr. R. Morent[1]
dr. J. Stöckel[3]
prof. dr. C. Boucher[4]
prof. dr. ir. D. De Zutter[5], decaan, voorzitter

Leescommissie

prof. dr. ir. G. Van Oost
dr. J. Stöckel
prof. C. Boucher
prof. dr. ir. J.-M. Noterdaeme

[1] Faculteit Ingenieurswetenschappen, Vakgroep Toegepaste Fysica, Jozef Plateaustraat 22, 9000 Gent.

[2] Faculteit Ingenieurswetenschappen, Vakgroep Elektrische energie, systemen en automatisering, Technologiepark Zwijnaarde 914, 9052 Zwijnaarde.

[3] Institute of Plasma Physics, Academy of Sciences of the Czech Republic, Za Slovankou 3, 182 00 Praag 8, Tsjechië.

[4] Université du Quebec, Institut National de la recherche scientifique (INRS), boul. Lionel-Boulet 1650, J3X1S2 Varennes (Quebec), Canada.

[5] Faculteit Ingenieurswetenschappen, Vakgroep Informatie-technologie, Sint-Pietersnieuwstraat 41, 9000 Gent; Decanaat faculteit Ingenieurswetenschappen, Jozef Plateaustraat 22, 9000 Gent.

november 2006,

Peter Peleman

Enkele woorden van dank . . .

– Expression of gratitude – . . .

Een proefschrift schrijf je niet alleen. Daarom wil ik iedereen die, op welke manier dan ook, heeft bijgedragen aan het tot stand komen van dit doctoraatswerk van harte bedanken. Hier wil ik me beperken tot het noemen van enkele individuen en groepen die een bijzondere rol hebben gespeeld.

Allereerst gaat mijn dank uit naar mijn promotor Prof. Guido Van Oost voor het brede scala van raad & daad waarmee u mij hebt bijgestaan tijdens de ontwikkeling van dit proefwerk. De verkregen financiële ondersteuning uit projecten maakte het mogelijk om onderzoek te doen op twee internationale locaties en gaf me de vrijheid mijn werk voor te stellen tijdens verschillende conferenties. Guido, je leerde me om mijn, door gretigheid gevoede, impulsiviteit te beheersen.

In onze vakgroep Toegepaste Fysica wens ik vooreerst Prof. em. W. Wieme te bedanken voor de mij geboden kans als wetenschappelijk onderzoeker en voor het in mij gestelde vertrouwen bij mijn aanstelling als assistent in de vakgroep.
De wetenschappelijke gesprekken die ik met Prof. em. E. Desoppere voerde waren erg leerrijk en stimulerend, waarvoor ik mijn welgemeende appreciatie wens te uiten.
De ondersteuning van de technici van onze vakgroep heeft ongetwijfeld een meerwaarde betekend bij het tot stand komen van dit werk. Daniël, de ontwikkeling van de sonde heeft je vele slapeloze nachten bezorgd maar het eindresultaat was verbluffend. Uw vakmanschap en leiderscapaciteiten betekenen een serieuze meerwaarde voor onze technische dienst. Verder wens ik Peter Guns te bedanken voor het grondig doorlichten en het documenteren van het elektronische circuit van de sondediagnostiek. Beide bedankt voor jullie inzet en bereidwilligheid voor de verschillende verplaatsingen naar Jülich.

Van mijn meeste directe collega's in de onderzoeksgroep nucleaire fusie wens ik Geert en Thibaut te vermelden voor de vele aangename uren die we samen in de auto doorbrachten tijdens onze vele ritten naar het 'verre' Duitsland. De soms hilarische gespreksonderwerpen hebben me vaak wakker gehouden en hielden het fileleed draaglijk. Geert, onze bijna wekelijkse Duitse 'nouvelle cuisine?' ervaringen en de vele daarop voorafgaande cocktails deden de soms zware pil van het van huis weg zijn verzachten.
Op educatief vlak heb ik erg genoten van de nauwe samenwerking met de Prof. C. Leys die me ongetwijfeld een aantal waarden en normen bijbracht.
Alle andere collega's van de vakgroep wens ik te bedanken voor de vele gezellige uren die we in de laatste 5 jaar hebben mogen doorbrengen.

In Duitsland heb ik in de beginfase van mijn doctoraat nauw samengewerkt met Stefan Jachmich die lid is van de Koninklijke Militaire School (KMS). Stefan, although in the last few years we both went our one way, I would very much like to express my gratitude for the time you invested in me. I enjoyed our social gathering. I wish you the very best in your new work environment at JET. I'm sure you will make your way there. Ook wens ik Prof. M. Van Schoor (KMS) te danken voor zijn geduld die hij opbracht tijdens de verschillende inleidende gesprekken die we voerden. Je wijdde me in de theoretische wereld van de plasmafysica in en was diegene die me hielp met het schrijven van mijn allereerste internationale publicatie. Michael, de aanpassingen die u toen maakten waren, op zijn zachts gezegd, broodnodig en leerrijk. Dr. Y. Xu (KMS) verdient een expliciet woord van dank. Yuhong, it was a pleasure working together with you. Your unconditional assistance, experience and knowledge have been very helpful in order to upgrade the scientific level of my research. Thanks a lot. Ten slotte wens ik Prof. R. Weynants te danken voor de morele en financiële steun die noodzakelijk waren voor de wekelijkse verplaatsingen naar Jülich. Langs deze weg wens ik

alle andere betrokken medewerkers in Brussel en Jülich te danken voor hun bijdrage tot dit werk.

In februari 2005 besloten mijn promotor en mezelf om het onderzoek uit te breiden naar de CASTOR tokamak te Praag in Tsjechië. Ik was onmiddellijk onder de indruk van de aangename manier waarop ik hier werd ontvangen.
In particular, I would like to express my gratitude to the head of the Institute of Plasma Physics (IPP), Dr. J. Stöckel. Jan, it was a pleasure working in your department. The kind way in which you introduced me in your group has clearly accelerated my work progress. Our cooperation led to splendid scientific results which were correspondingly celebrated with some proper liquid. I would also like to thanks all the other members of the IPP in Prague.

Furthermore, I would like to thank Prof. C. Boucher. Dear Claude, I first met you in Jülich where you and your student were helping with the design of our new probe. I was impressed by your great personality and the passionate way of how you talked about probe diagnostics and plasma physics in general. Your excellent experimental knowledge has certainly led to improvements in our probe design. The big distance between Belgium and Canada has never interfered with our teamwork for which I'm very grateful. CHEERS!

De leden van de lees- en examencommissie ben ik dankbaar voor de waardevolle commentaren, correcties en suggesties die zonder twijfel de kwaliteit van het proefschrift verder hebben verbeterd.

Vervolgens is er een welgemeend woord van dank op zijn plaats voor mijn schoonnonkel Dirk Van Tieghem. Bedankt voor het kritisch overlezen van het doctoraatswerk. Al was het voor u vaak Latijn, het Engels werd er toch beter van….

Mijn ouders wil ik in het bijzonder vermelden. De vrijheid die jullie me gaven in de keuze van mijn studierichting en het vertrouwen en morele steun die daarop volgde zijn alles behalve

vanzelfsprekend. De opvoeding die ik van jullie mocht genieten vormt de basis van wat ik tot nog toe presteerde en wat ik nog bereiken zal. Het staat dan ook buiten kijf dat jullie invloed op dit doctoraatswerk groot is en laat dit werk een beloning zijn voor alles wat jullie voor me deden.

Ook mijn schoonouders verdienen een hartelijk woordje van dank. Onder andere de opvang van ons dochtertje tijdens mijn vele afwezigheden zijn we niet vergeten. Zonder jullie steun en toeverlaat zou het allemaal veel moeilijker geweest zijn.

Els, zonder twijfel ben ik jou de meeste dank verschuldigd. Op een belangrijk moment kwam je in mijn leven. We hebben samen onze studies succesvol doorlopen waarna we een mooi gezinnetje opstarten. Mijn wekelijkse 2-daagse verblijf in Duitsland en vele afwezigheden door het bijwonen van internationale conferenties en de experimentele campagnes in Praag zijn ongetwijfeld vaak moeilijke momenten geweest. Ook na de komst van ons dochtertje Lore ben jij er steeds in geslaagd om alles organisatorisch te doen kloppen. Enkel diegene die je goed kennen weten dat jij een emotionele maar ijzersterke vrouw bent die zichzelf telkens opnieuw wegcijfert in functie van anderen. Deze zeldzame eigenschap vertaalt zich in je onvoorwaardelijke steun, liefde en geduld. Keppe, jij maakt van ons huis een thuis waarnaar ik keer op keer verlang. Woorden schieten daarom ruim tekort om te beschrijven wat jij voor mij betekent. Een ding staat echter als een paal boven water; de stabiliteit in mijn privé situatie vormt de basis voor mijn prestaties op het werk. Het is daarom een grote eer om dit werk aan jou op te dragen.

Peter Peleman
Gent, november 2006

Table of Contents

2 Probe modelling

List of Tables

List of Figures

1

2

List of Acronyms and Abbreviations

1...

1D	one-dimensional
2D	two-dimensional
3D	three-dimensional

A

AC	Alternating Current
ACF	Auto-Correlation Function
ASDEX	Axially Symmetric Divertor EXperiment

C

CASTOR	Czech Academy of Science TORus

D

DC	Direct Current
DED	Dynamic Ergodic Divertor
DRAM	Dynamic Random Access Memory

E

ECHR	Electron Cyclotron Resonance Heating
ETB	Edge Transport Barrier
ELM	Edge Localized Mode

F

FWO	Fonds voor Wetenschappelijk Onderzoek – Vlaanderen. Fund for Scientific Research - Flanders

H

H-mode	High confinement tokamak regime
HFS	High Field Side

I

ICE	Improved Confinement Event
ICHR	Ion Cyclotron Resonance Heating
IGP	Ideal Gundestrup Probe
INTAS	INTernational ASsociation for the promotion of co-operation with scientists from the new independent states of the former Soviet Union
ISS	International Space Station
ISTTOK	Instituto Superior Tecnico TOKamak
ITB	Internal Transport Barrier
ITER	International Thermonuclear Experimental Reactor

J

JET	Joint European Tokamak
JT-60U	Japan Tokamak

L

LCFS	Last Closed Flux Surface
LHH	Lower Hybrid Heating
L-mode	Low confinement tokamak regime

M

MHD	Magneto-hydrodynamics
MPSE	Magnetic Presheath Entrance

N

NBI	Neutral Beam Injection

P

PIC	Particle-In-Cell
PDF	Probability Density Function

R

RI-mode	Radiative Improved mode

S

SOL	Scrape-off Layer

T

TEXTOR	Tokamak Experiment for Technology Oriented Research
TFTR	Tokamak Fusion Test Reactor
Tokamak	TOroidalnaya KAmera MAgnitnaya Katushka, Toroidal Chamber in Magnetic Coils
Tore Supra	Superconducting Torus
TdeV	Tokamak de Varennes

Nederlandstalige samenvatting
– Summary in Dutch –

De toenemende economie in ontwikkelingslanden zorgt ervoor dat de wereldwijde energieconsumptie proportioneel sneller toeneemt dan de bevolkingsgroei. Het overgrote deel (90%) van onze huidige energie wordt geproduceerd door verbranding van fossiele brandstoffen. Olie is de onbetwiste leider en wordt verwacht deze positie te behouden in de eerstvolgende decennia. De gevolgen voor het milieu zijn problematisch. De opwarming van de aarde, als gevolg van het overmatig uitstoten van broeikasgassen in onze atmosfeer, is zonder enige twijfel een groot probleem.

Voorlopig zijn hernieuwbare energie, nucleaire splijting en thermonucleaire kernfusie de enige gekende opties voor grootschalige elektriciteitsproductie op lange termijn. Hernieuwbare energievormen, waarbij gebruik gemaakt wordt van 'oneindige' voorraden uit de natuur zoals wind, zon, water en biomassa hebben echter slechts beperkte mogelijkheden qua opslag en efficiëntie. Daarom kunnen ze onmogelijk beantwoorden aan de huidige en toekomstige energievraag. Ze zullen eerder een beperkte complementaire rol spelen.

Een andere optie is nucleaire energie. Twee verschillende processen, waarbij gebruik gemaakt wordt van atoomkernen, kunnen aangewend worden voor de productie van energie: nucleaire kernsplijting en thermonucleaire kernfusie. De meest aantrekkelijke eigenschap van deze energievormen is dat ze geen rechtstreekse broeikasgassen of andere luchtvervuilende stoffen produceren. Verschillende nadelen bezorgen die nucleaire kernsplijting een onderwerp van discussie. Ze bemoeilijken zijn groei als toekomstige energievorm. Radioactief afval, misbruik voor militaire doeleinden en de veiligheid van nucleaire installaties vormen vaak onderwerp van discussie.

Thermonucleaire kernfusie is een (bijna) niet-vervuilende, veilige en zo goed als onuitputtelijke energievorm voor de toekomst. Ernstige technische en wetenschappelijke hindernissen moeten echter nog overwonnen worden alvorens kernfusie economisch kan wedijveren met de andere energievormen.
Fusie van lichte positief geladen deeltjes (kernen) kan enkel gebeuren bij extreem hoge temperaturen vanwaar de naam 'thermonucleaire' kernfusie vandaan komt. De brandstof is dan volledig geïoniseerd. We spreken dan over een plasma, ook wel de vierde aggregatietoestand genoemd. Het plasma kan worden opgesloten en gecontroleerd door middel van magnetische opsluiting. Een verscheidenheid van magnetische configuraties wordt gebruikt. De tokamak blijkt hierbij de meest veelbelovende configuratie. Zijn ontwerp vormt de basis voor de ontwikkeling van de volgende generatie fusiereactor ITER [Weyn94, ITER01]. De plasmaopsluiting is nog niet perfect. Verscheidene fysische en technische uitdagingen staan de hedendaagse praktische realisatie van een economische reactor nog in de weg.

Een belangrijk probleem is dat deeltjes- en energieverliezen ontstaan in het randplasma. De opsluitingstijd van het hete en dichte plasma in het centrum wordt hierdoor beperkt. Dit transport van energie en deeltjes in de rand van de tokamak staat haaks op het magneetveld (radiaal). De oorzaak is vooral gelegen in het turbulente karakter van het plasma. Het begrijpen en beheersen van randplasma's is daarom een belangrijke doelstelling bij de reductie van turbulent plasmagedrag.
De tokamaks CASTOR en TEXTOR zijn bijzonder geschikt voor het bestuderen van randplasma's en plasmawandinteracties gelet op hun grote variëteit aan diagnostieken. Het experimentele werk, voorgesteld in dit doctoraatswerk, is uitgevoerd op beide tokamaks en geconcentreerd op onderzoek van randplasma's met behulp van sondes. De elektrische sondemethode is één van de meest directe technieken in plasmadiagnostieken voor het bestuderen van randplasma's. Gundestrupsondes worden gebruikt bij de bepaling van

plasmastromingen. Sondes lijden helaas onder de empirische wet van diagnostieken; het 'gemak' van interpretatie is omgekeerd evenredig met het gemak van implementatie [Matt94]. De moeilijkheid bij de interpretatie van gemeten plasmastromen ligt in het beschrijven ervan. Hoe precies stoort de sonde lokaal het plasma? Hoe zijn de lokale plasmaparameters gerelateerd tot het ongestoorde plasma veraf? Toch is er de laatste drie decennia grote vooruitgang geboekt in de sondemodellering.

Het eerste theoretische gedeelte van deze thesis neemt een ééndimensionaal quasi-neutraal vloeistofmodel onder de loep. [Hut87, VG99a]. Dit model resulteert in transportvergelijkingen bestaande uit twee gekoppelde differentiaalvergelijkingen die worden benaderd door een analytische vergelijking. Hiermee kan men onmiddellijk de parallelle en loodrechte Machgetallen (de verhouding van de gemiddelde stroming van de hoofdionen (waterstof en zijn isotopen) en de ionengeluidssnelheid) bepalen uit de stromen van de (vlakke) sondecollectoren.
Een zorgvuldig uitgevoerde parameterstudie test de betrouwbaarheid van het model. Dit resulteert in een verbeterde analytische formule die nu de verschillende afhankelijkheden van parallelle en loodrechte Machgetallen en de hoekverandering tussen de sondecollectoren en de magnetische veldlijnen in rekening brengt [Pel05]. Bovendien is het kader van toepasselijkheid van het model nu duidelijk gedefinieerd. Dit is noodzakelijk in het licht van het ontwerp van een nieuwe sonde (zie verder). Dit verbeterde model is vergeleken met een tweedimensionale, quasi-neutrale deeltjes-in-cel (PIC) simulatiecode. De goede overeenkomst valideert dit verbeterde model binnen zijn goed gedefinieerde toepasselijkheid. Dit geeft het volste vertrouwen voor de verdere analyse van de sondedata [Pel06a].
Wereldwijd gebruikt men twee verschillende types Gundestrupsondes: sondes met vlakke collectoren (TEXTOR) en sondes met ronde collectoren (CASTOR). Het hierboven vermelde sondemodel is uitgebreid om ons in staat te stellen de Machgetallen te bepalen uit data van sondes met ronde collectoren. Het effect van ronde collectoren op de bepaling van

de loodrechte stroming is onder de loep genomen. Dit onderzoek leidt tot de ontdekking dat ronde collectoren geen invloed hebben op de bepaling van parallelle stromingen bij het vloeistofmodel. De nieuw opgestelde vergelijking voor de bepaling van de loodrechte Machgetallen, houdt nu rekening met het effect van verkromming bij niet-vlakke collectoren [Pel06a]. Deze uitbreiding tot het vloeistofmodel stelt ons nu in staat om op een correcte manier de meetresultaten van de CASTOR Gundestrupsonde te interpreteren.

Een compleet nieuwe en gesofisticeerde sondediagnostiek is ontworpen en geïnstalleerd op TEXTOR gedurende de termijn van dit doctoraatswerk. Een veelzijdige snelscannend en roterend sondesysteem kwam in werking op de TEXTOR tokamak in november 2005. De wederkerige lineaire beweging van het systeem stelt ons in staat de lokale randplasmaparameters te meten met een hoge tijds- en ruimtelijke resolutie.
In het tweede deel van dit werk staat een nieuwe geavanceerde Gundestrupachtige sonde centraal. Deze sonde wordt bevestigd op de snelle, heen - en weer bewegende manipulator. De unieke design van deze sonde laat het gelijktijdig meten toe van de toroïdale en poloïdale plasmastromingen, de ionensaturatiestroom, dichtheid, elektronentemperatuur, vlottende potentiaal (dus elektrisch veld). De eerste experimentele resultaten van deze verschillende plasmaparameters tonen aan dat deze diagnostiek betrouwbaar en accuraat is [Pel06b]. Het simultaan meten van al deze plasmaparameters en hun fluctuaties is een wereldwijd unicum.
Nu de robuustheid is aangetoond en rekening houdend met de gebruiksvriendelijkheid en de hoge tijds- en ruimtelijke resolutie, is de sondediagnostiek uitgegroeid tot één van de meest gebruikte diagnostieken voor het meten van randplasmaparameters op TEXTOR.

Het laatste deel van dit doctoraatswerk behandelt de presentatie en discussie van experimentele resultaten op de CASTOR tokamak gedurende randplasmapolarisatie-

experimenten. Dit onderzoek kadert in de studie naar mechanismen die verantwoordelijk zijn voor de geobserveerde toename van deeltjestransport tijdens instabiliteiten in randplasma's.

De techniek die het randplasma polariseert veroorzaakt een regime van verbeterde opsluiting van het centrale plasma. In CASTOR induceert de polariserende elektrode een radiale stroom wat een sterk gelokaliseerd radiaal elektrisch veld E_r teweegbrengt. De verbeterde opsluiting wordt toegewezen aan de stabilisatie van de turbulentie door de afschuiving in de $E_r \times B_\phi$ poloïdale stroming geïnduceerd door het elektrische veld [VOost03]. De onderdrukking van turbulentie reduceert het deeltjestransport naar buiten toe.

Tijdens deze polarisatie-experimenten observeren we een duidelijke en reproduceerbare transitie naar een verbeterde plasmaopsluiting, in combinatie met de creatie van een zogenaamde deeltjestransportbarrière. Deze barrière is gekarakteriseerd door een (i) belangrijke toename van de dichtheidsgradiënt in de rand; (ii) afname in deeltjesregeneratie in de rand; (iii) substantiële toename van de globale deeltjesopsluitingstijd; (iv) duidelijke onderdrukking van het niveau in fluctuaties van dichtheid en potentiaal (dus turbulentie).

Voor het eerst zijn snelle periodieke oscillaties (fluctuaties) waargenomen bovenop de gemiddelde verandering van E_r, plasmastromingen, deeltjesregeneratie en de deeltjestransportbarrière. Deze verschijnselen zijn waargenomen gedurende de volledige fase van de globaal verbeterde plasmaopsluitingstijd [Spo05, Pel06c]. Deze fenomenen zijn geïdentificeerd als relaxatie-evenementen (REs). Interessant is ook dat deze REs slechts weinig invloed hebben op de globale opsluiting. Ze brengen eerder een modulatie op de lokale randplasmaparameters en transportbarrière teweeg. Een belangrijke ontdekking is de dynamische relatie tussen de toroïdale stroming en de toename in deeltjestransport. Deze verhoogde radiale deeltjesflux brengt mogelijks energie over naar de toroïdale stroming via hun dynamische koppeling waardoor deze stroming substantieel toeneemt. Deze koppeling

kan ontstaan via turbulentie afkomstig uit Reynolds-spanningen. Gelijkaardige fenomenen van niet-lineaire dynamische interacties tussen turbulent transport en toroïdale stroming zijn gerapporteerd op de tokamak JET [Hid03a,b] in experimenten zonder polarisatie van het randplasma. In deze experimenten bleken vooral de hoogfrequente componenten met een frequentie van 12,5 kHz een dominant effect te hebben. In onze experimenten wordt de periodieke link tussen turbulent transport en parallelle stroming vooral waargenomen bij een frequentie van 10 kHz (vrijwel zeker veroorzaakt door E_r). Dit ligt erg dicht bij de geobserveerde dominante frequentie in JET. Dat deze gelijkaardige eigenschappen ontstaan in het randplasma van twee totaal verschillende tokamaks en onder volledige verschillende plasmacondities, suggereert dat de achterliggende fysica van universele aard is. De resultaten suggereren verder dat de parallelle turbulente kracht een belangrijk ingrediënt is voor het verklaren van stromingsimpulsredistributie in de rand van fusieplasma's. Dit impliceert bovendien dat de fysica van stromingen in het randplasma nood heeft aan een driedimensionale beschrijving. Theoretisch is aangetoond dat in zulke driedimensionale omgeving de verschillende componenten van het fenomeen moeten worden beschouwd. Het blijft een uitdaging voor experts om gelijktijdig de veranderingen van deze componenten tijdens het ontstaan van deze relaxatiefenomenen te meten.

English Summary

Due to the growing economies in the developing countries, the world energy consumption is supposed to grow more rapidly than the increase of the population. Most of our energy comes from burning fossil fuels (90%) and it will stay this way in the near future. Oil currently provides a larger share of the world energy consumption than any other energy source and is expected to keep that position throughout the next decennia. The environmental consequences of the massive use of fossil fuels due to the release of huge quantities of greenhouse gasses (like CO_2) in our atmosphere, is beyond all doubt a serious problem, as it is generally believed to be responsible for global warming.

The only long-term alternatives to burning fossil fuels are renewables, nuclear fission and fusion. The limited prospect of renewable energy, when using infinite elements of nature such as - water (hydropower), biomass, wind, heat from the earth (geothermal), and the sun (solar energy), clearly implies that they are not really 'alternative' energy sources to replace fossil fuels but will rather complement existing and future cleaner energy sources [Klee98]. Another option is given by nuclear energy. Two distinct processes involving the nuclei of atoms can be harnessed for energy production: fission – the splitting of nucleus – and fusion – the joining together of two nuclei. The most attractive feature of these energy-producing reactions is that they do not directly produce greenhouse gases or other forms of air pollution. However, several problems cloud fission's potential as an acceptable power source today and in the future: the disposal of radioactive waste; the concern about nuclear weapons proliferation; and concern about the safe operation of plants.

Nuclear fusion holds the promise of a clean, safe and almost inexhaustible energy and is candidate for the energy production

in the future. However, significant technical barriers must be overcome before fusion can economically compete with these other energy sources.

The fusion of light particles (nuclei) can only be obtained at extremely high temperatures. By far the most promising fusion reaction is that in which the nuclei of deuterium and tritium fuse to produce an alpha particle with the release of a neutron which carries most of the released energy. At such high temperatures the gas is fully ionized and a 'plasma', a fourth state of matter (along with solid, liquid and gas) is formed. Although it is the most common state of matter in the universe (99%), it is the least well known. The free electric charges make the plasma electrically conductive so that it strongly responds to electromagnetic fields. In laboratory experiments, magnetic or inertial forces must be used instead of the gravitational force (like in stars) to control the dimension of the plasma volume and to confine the particles during a sufficiently long time (at the required high densities and temperatures) in order to allow a certain number of fusion reactions to occur. This technique rests upon the property that the charged particles will travel (gyrate) along the lines of a magnetic field due to the Lorentz force. A variety of magnetic configurations can be used. So far, the tokamak has proved to be the most promising as its design was chosen to manufacture the next generation fusion reactor ITER [Weyn94, ITER01]. However, this confinement is not perfect and the practical realisation of an economic reactor still awaits the solution of a number of physical and technical challenges.

A major issue is that particle and energy losses originate in the edge plasma and consequently limit the confinement time of the hot and dense core plasma. This cross-field (radial) transport of energy and particles in the boundary of the tokamak is found to be mainly driven by turbulence. Understanding and controlling edge plasmas is therefore an important goal in order to reduce turbulent plasma behaviour.

Tokamaks like CASTOR and TEXTOR have engaged to specialize in edge studies and plasma-surface interactions by employing extensive equipment of edge diagnostics. The experimental work presented in this thesis was performed on both tokamaks and especially concentrates on edge plasma diagnosis by means of probes. The electrical probe method is one of the most straightforward techniques in plasma diagnostics to study edge plasmas. Mach probes, in particular, are used to determine edge plasma flows. Unfortunately, probes suffer from the first law of diagnostics; the ease of interpretation is inversely proportional to the ease of implementation [Matt94]. The difficulty with measurements of direct plasma particle fluxes is in establishing an understanding of just how the probe perturbs the plasma locally and how the local plasma parameters are then related to the unperturbed plasma far from the probe. Nevertheless, in the last few decades a tremendous progress in probe modelling has been accomplished.

In the first theoretical part of this thesis a one-dimensional quasi-neutral fluid probe model is reviewed in detail [Hut87, VG99a]. The resulting transport equations constitute a set of coupled differential equations which were, for convenience, approximated by an analytical expression in order to directly determine the parallel and perpendicular (with respect to the magnetic field) Mach numbers (defined as the ratio between the mean ion flow and ion sound speed) from the currents measured by the probe's (flat) collectors. A numerically-based full-parameter study has been performed to carefully examine the reliability of this analytical model resulting in the formulation of an improved approximated expression. This new analytical expression now takes into account the various dependencies of the parallel and perpendicular Mach numbers and the inclination angle of the collectors with respect to the magnetic field [Pel05]. Furthermore, its range of applicability has clearly been defined, which was necessary in the context of designing a new probe (see further). Consequently, the improved model now bears comparison with a two-dimensional quasi-neutral particle-in-cell simulation code. In this way, the improved model is

validated and it more carefully describes a Mach probe making us confident for future analysis of probe data [Pel06a].
Worldwide two different types of Gundestrup probes are employed: probes with flat collectors, for example in TEXTOR, and probes with round collectors, as in CASTOR. The aforementioned probe model has been extended to be able to correctly determine the Mach numbers from data retrieved from probes with round collectors. The effect of a round collecting surface on the perpendicular flow has been investigated and it was found that the parallel flow appeared to be insensitive to the shape of the collector. The perpendicular flow, however, clearly depends on the curvature of the collector. A new analytical expression has been proposed in which this dependency is taken into account [Pel06a]. This extended fluid probe model can now also correctly be used to interpret Mach probe data from CASTOR.

During the full time span of this doctoral work a complete new sophisticated probe diagnostic has been developed and manufactured on TEXTOR. A versatile fast scanning and rotating probe system became in operation on the TEXTOR tokamak in November 2005. The reciprocating linear movement of the system enables us to measure local plasma edge parameter profiles with high temporal and spatial resolution.
In the second part of this work a novel advanced Gundestrup-like probe head is presented. The probe is mounted on the fast reciprocating manipulator. The unique probe assembly enables us to simultaneously determine the toroidal and poloidal plasma flows, the ion saturation current, density, electron temperature, floating potential (thus electric field), as well as their fluctuating properties. The first experimental results of these measured plasma parameters are now known. The diagnostic based on them was found to be reliable and accurate [Pel06b]. Now that the robustness of the new probe diagnostic has been demonstrated and taking into account the high spatial and time resolution and user-friendliness, the fast scanning probe diagnostic has become one of the most frequently used edge diagnostics on TEXTOR.

The last part of this doctoral thesis consists of the presentation and discussion of experimental results performed on the CASTOR tokamak during edge biasing experiments. The research fits in the framework of the investigation of mechanisms which are responsible for the observed enhanced transport during plasma instabilities.

In the tokamak CASTOR a regime of enhanced particle confinement can be triggered by applying sufficient voltage to an electrode located several centimetres inside the plasma; a technique generally known as edge biasing or polarization. A biased electrode drives a radial current in the plasma edge inducing a strong and localized radial electric field E_r and thus a sheared $E_r \times B_\phi$ poloidal flow, which suppresses turbulence and related transport [VOost03].

During these edge biasing experiments, we observed a clear and reproducible transition to an improved confinement along with the creation of a so-called particle edge transport barrier (ETB). This barrier is characterized by a (i) substantial increase of the edge density gradient; (ii) reduction in recycling; (iii) substantial increase of the global particle confinement time; (iv) suppression of the density and potential fluctuation level (thus turbulence).

For the first time fast periodic oscillations (fluctuations) on E_r, plasma rotations, edge recycling and the edge transport barrier during the globally improved confinement phase on top of the biasing-imposed DC E_r, were observed [Spol05, Pel06c]. These phenomena were dubbed as relaxation events (REs). Interestingly enough, they do not much affect the global confinement properties, but modulate the local edge plasma parameters and edge transport barrier as well. An important finding is the discovery of a dynamic relation between the toroidal flow and the enhancement in transport. The enhanced radial outflux may transfer energy to the toroidal flow via dynamical coupling and thus increase the toroidal flow substantially. This coupling can occur through the turbulence-driven Reynolds stress. Similar phenomena for the non-linear dynamical interaction between the turbulent transport and the toroidal flow have been reported on JET [Hid03a,b] in non-

biasing experiments, where, in particular, the large scale components $(\sim 12.5\ \text{kHz})$ show dominant effects. In our case, the periodic link between the turbulent transport and the parallel flow takes place at an almost fixed frequency of $f \approx 10\ \text{kHz}$, which is probably triggered by E_r and interestingly close to the dominant frequencies in JET.
The fact that these features occur in the plasma boundary of two complete different tokamaks under entirely different plasma conditions might suggest that the physics are of universal nature. The results suggest that parallel turbulent force is an important ingredient to explain flow momentum redistribution in the boundary of fusion plasmas (i.e. flow physics requires a three-dimensional (3D) description). Because of the 3D nature of the shear flow physics in fusion plasmas and the experimental evidences shown, several components of the production term, including radial-parallel $\left(\left\langle \tilde{v}_{//}\tilde{v}_r \right\rangle\right)$ and radial-perpendicular $\left(\left\langle \tilde{v}_{\perp}\tilde{v}_r \right\rangle\right)$ components of Reynolds stress, should be considered [Verg05]. It remains a challenge for experimentalists to simultaneously measure the evolution of the whole production term during the development of the observed relaxations.

1 Introduction

Energy, 'the ability to do work', is essential for meeting basic human needs, extending life expectancy and providing a rising living standard.[1]

1.1 The world energy problem

Together with the increasing energy consumption, it has been possible for the world to sustain an ever increasing population. At present, however, three quarters of the world energy production is consumed by one quarter of the world's population living in the industrialised countries. It is interesting to note that the largest energy consumers are to be found among those countries which are also large energy producers and exporters (Qatar, United Arab Emirates, Kuwait, Norway, etc.) or dispose of cheap and abundant energy (Iceland, Canada, etc.) [Ong06]. Lowest energy consumption is found in developing countries. Power consumption in Japan and the European Union is about half of that in the USA. With 6.5 billion people and a world average power consumption of about 2.23 kW, the total amount of energy that is currently consumed amounts to about 14 TWyr. An estimate of the total energy that might be needed in the future can be found when assuming the following two assumptions:

[1] Uranium Information Centre (UIC), http://www.uic.com.au/

(1) the average power consumption per capita (this is the average annual total primary power consumption per country divided by the number of its inhabitants) will rise from 2.23 kW to 3 kW (i.e. about half of what is already used in Europe and about one third of what is used in the USA[2]), and
(2) the world's population will rise from the present 6.5 billion to 9.1 billion by 2050, and perhaps 10 billion later in the century, as predicted by the United Nations (press release on the World Population Prospect, revision 2005). Most of the population growth will be in the developing countries, which is where already more than three quarters of the world's people live.

For 10 billion people we thus find an estimated future energy need of 30 TWyr or about two times more than is consumed now. Thus, worldwide energy use has been increasing and is projected to keep on increasing as shown in figure 1.1, especially the demand of oil. Oil currently provides a larger share of the world energy consumption than any other energy source and is expected to remain in that position throughout the mentioned period. Natural gas is projected to be the fastest-growing component of primary world energy consumption, more than doubling between 1997 and 2020. Therefore, most of our energy is currently (and in the near future) produced by burning fossil fuels (90%). The environmental consequences of the massive use of fossil fuels due to the release of huge quantities of CO_2 in our atmosphere, is beyond all doubt a serious problem. Carbon dioxide is neither the only greenhouse gas (GHG) responsible for the enhanced greenhouse effect (global warming), nor is it the most potent, but is by far the most common, and this is why it is being focussed on more than other greenhouse gases. There is a general agreement among specialists that the enhanced greenhouse effect causes the

[2] Energy Information Administration (EIA), International Energy Annual 2004, http://www.eia.doe.gov/iea/

average temperature on earth to increase. The side effects of changing a large and global component (the atmosphere) of our climate system on such a very short geological time scale is therefore frightening and might even be irreversible. Although the present energy resources and supplies (Table 1.1) seem to be sufficient to go on as we are doing now for at least a few decades, the further depletion of the world energy reserves will inevitably lead to political and environmental instabilities. Fossil fuels have served us well, it is time for alternatives!

Fuel	Proved recoverable reserves (2003)	Years of use at current rate of consumption
Coal	0.9 10^{12} tons	210
Crude Oil	1.2 10^{12} barrels	30-40
Natural Gas	170 10^{12} m^3	60-70
Uranium	2.0 10^6 tons	40-50 (2400-3000)*

* if breeder technology is employed.

Table 1.1: Years of use of different fuels at current rate of consumption. Source: [Ong06].

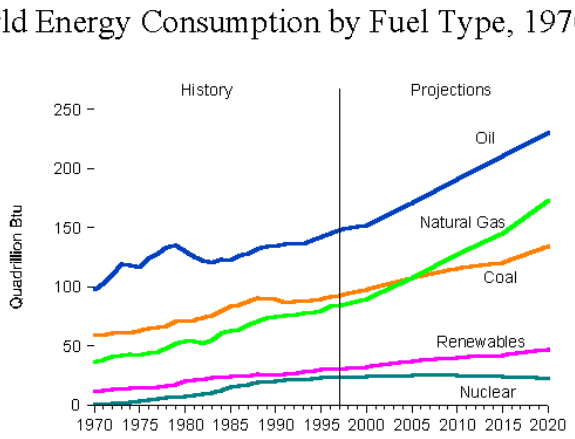

Figure 1.1: World Energy Consumption by Fuel Type, 1970-2020.[3]

[3] Energy Information Administration (EIA), official energy statistics from the US government.

1.2 Long-term energy sources

The only long-term alternatives to burning fossil fuels are renewables, fission and fusion. Whereas, fossil fuels are exhaustible renewable energy sources nearly infinite elements of nature such as - water (hydropower), biomass, wind, heat from the earth (geothermal), and the sun (solar energy) - regenerate and can be sustained indefinitely. "Green" renewables contribute much less to global warming and climate change by offsetting fossil fuels used to generate electricity. Although renewable resources in the world are large and inexhaustible, they have, unfortunately, only a limited potential. Natural obstacles met by renewables are low energy density and/or fluctuations in time, implying the need for storage which reduces again the efficiency and leads to extra costs and environmental constraints [Ong06]. The limited prospect for this kind of energy clearly implies that they are not really 'alternative' energy sources to replace fossil fuels but renewables will rather complement existing and future cleaner energy sources. Modest growth in renewable energy is projected to continue, maintaining an 8% share of the total energy consumption over the forecast horizon [Klee98].
Another option is given by nuclear energy. Two distinct processes involving the nuclei of atoms can be harnessed for energy production: fission – the splitting of nucleus – and fusion – the joining together of two nuclei. The most attractive feature of these energy-producing reactions is that they do not directly produce greenhouse gases or other forms of air pollution. On 2 July 2006 442 nuclear power plant units with an installed electric net capacity of about 370 GW were in operation in 33 countries world-wide. Another 33 nuclear power plants are presently under construction which will provide an extra 28 GW.[4] Fission power currently provides about 6% of the world's electric power [Ong06]. If fossil plants were used to produce the amount of electricity generated by these nuclear plants, more

[4] The European Nuclear Society (ENS), http://www.euronuclear.org

than an additional 300 million tons of carbon would be emitted each year.[5] Worldwide, 15 countries obtain at least 30% of their electricity from nuclear fission power (e.g. 77% in France). However, several problems cloud fission's potential as an acceptable power source today and into the future: disposal of radioactive waste; concern about nuclear weapons proliferation; and concern about safe operation of plants. Nuclear waste remains radioactive and hazardous for many centuries, and no nation has developed a satisfactory long-term solution for disposal. Accidents at nuclear plants have the potential to unleash vast amounts of radiation, such as occurred at Chernobyl in 1986. After this accident some political parties became solidly opposed to nuclear energy. Recently, Germany and Belgium have passed laws to abandon nuclear energy but without any definite plan for replacing it. Very likely, after some time, the countries whose policies turn out badly will copy the countries whose policies turn out well.

Given the projected growth in global energy demand as developing nations industrialize, and the need to stabilize and then reduce GHG emissions, it is important to establish fission energy as an acceptable and viable option, if at all possible, and to develop the capability to harness fusion.

Fusion's promise as an energy source comes from its inexhaustible fuel supply, and from its potential for almost negligible environmental impact compared to the environmental costs of competing energy sources: the air pollution and carbon dioxide emission from fossil fuel combustion; high-level radioactive waste generated by nuclear fission; and the emissions from the production of the larger quantities of concrete, steel, glass and other materials required to collect energy from renewable energy sources [Toki02]. However, significant technical barriers must be overcome before fusion could economically compete with these other energy sources.

[5] U.S. Department of Energy, Nuclear Energy Research Initiative (NERI), http://nuclear.energy.gov/neri/neNERIresearch.html

1.3 Controlled thermonuclear fusion

The Future of Energy on Earth is the Energy of Stars

The fusion process has been studied as part of nuclear physics for much of the 20th century. In the late 1930s the German-born physicist Hans A. Bethe first recognized that the fusion of hydrogen nuclei (protons) to form deuterium is exoergic (i.e. there is a net release of energy), and together with subsequent reactions, accounts for the fundamental energy source of stars. In a typical fusion reaction the reacting nuclei both have a positive electric charge, and their natural electrostatic repulsion, called Coulomb repulsion, must be overcome before they can join. For fusion reactions to occur at sufficiently high rates to produce useful energy, light elements (the Coulomb barrier is smallest for isotopes of hydrogen) must be confined at sufficiently high density and temperature for a sufficiently long time to overcome this energy barrier. In the sun and other stars energy is produced by fusion reactions of hydrogen nuclei (protons). The energy released in these nuclear reactions is much larger than that for chemical reactions, because the binding energy that holds a nucleus together is far greater than the energy that holds electrons to a nucleus. An overview of the binding energy per nucleon as a function of the atomic mass number A is shown in figure 1.2. The release of nuclear energy can occur at the low end of the binding energy curve (low Z, number of protons) through the fusion of two light nuclei into a heavier nucleus. It appears that the mass of the fusion product is less than the total mass of the two separate nuclei. This mass difference Δm , called the mass defect or mass deficiency, is converted into a net release of energy, thus the binding energy, according to Einstein's law $E = \Delta mc^2$ where c is the speed of light in vacuum. In the sun protons have one chance in a million to fuse to helium during a period of ten thousand years, which is calculated to be effective in stars because of the high densities and huge volumes but has not been observed in laboratory plasmas.

Therefore, in laboratory experiments, magnetic or inertial forces must be used instead of gravitational force to control the dimension of the plasma volume and to confine the particles during a sufficiently long time (at the required high densities and temperatures) in order to allow a certain number of fusion reactions to occur. So far, the most promising way towards a fusion reactor based on magnetic confinement is the tokamak (section 1.5). For two reasons man-made fusion energy generation requires one of the following reactions with the hydrogen isotopes deuterium (D or ${}_1^2H$) and tritium (T or ${}_1^3H$):

$$\begin{cases} D+T \rightarrow {}_2^4He + n + 17.59 \text{ MeV} \\ D+D \rightarrow T + {}_1^1H + 4.0 \text{ MeV} \\ D+D \rightarrow {}_2^3He + n + 3.3 \text{ MeV} \\ D+{}_2^3He \rightarrow {}_2^4He + {}_1^1H + 18.3 \text{ MeV} \end{cases} \quad (1.1)$$

(n is neutron and He - isotope ${}_2^4He$ being an α - particle)

First, their rate of reactions is much faster than that between protons and, second, the net energy release from these reactions is up to 40 times greater than that from a proton-proton reaction. The energies given are the total energies released, for D - T being the kinetic energy of the neutron (80%, 14.03 MeV) and the α -particle (20%, 3.56 MeV). This total liberated energy is many times more than what is needed to overcome the energy barrier, i.e. 0.1 MeV. The measure of the probability of a fusion reaction to occur as a function of the relative velocity of the two reactant nuclei is defined as the reaction cross-section, σ. Figure 1.3 represents σ as a function of energy E for $D-D$, $D-{}^3He$ and $D-T$ reactions. For practical energies that are currently achievable in laboratory plasma (order of 10 keV, i.e. 6 times hotter than the centre of the sun), the $D-T$ reaction has a 100 to 1000 times higher probability to occur compared to the two other reactions shown in figure 1.3. Along with the fact that during a $D-T$ reaction a high amount of energy is released explains why deuterium-tritium will most likely be the type of fuel used in first generation fusion reactors [Glass60]. At such high temperatures the gas is fully ionized and a 'plasma', a fourth state of matter (along with solid, liquid and

gas) is formed. Although it is the most common state of matter in the universe (99%), it is the least well known. The free electric charges make the plasma electrically conductive so that it strongly responds to electromagnetic fields and can therefore be controlled by magnetic fields.

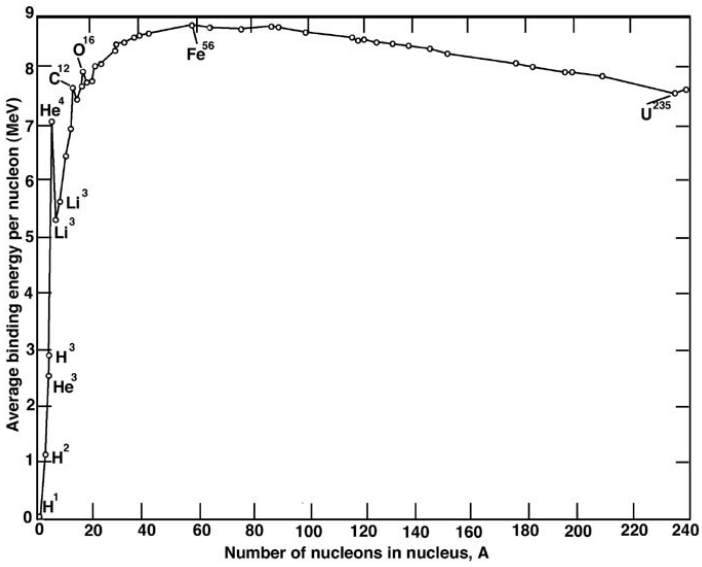

Figure 1.2: Average binding energy per nucleon as a function of mass.[6]

[6] NASA's imagine the universe! http://imagine.gsfc.nasa.gov/

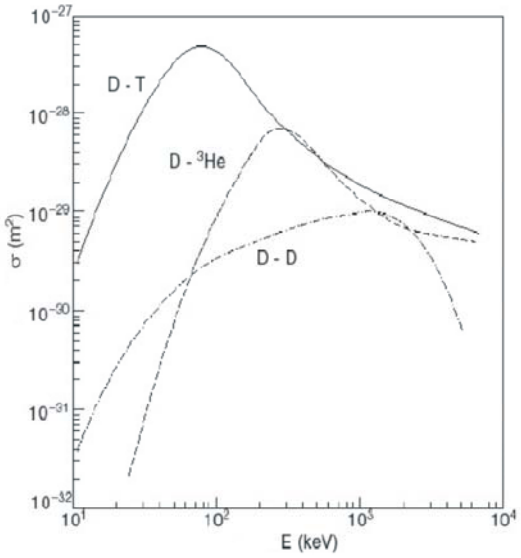

Figure 1.3: Comparison of the cross-sections of *D-T*, *D-D* and *D-*$^{3}_{2}He$ reactions as function of energy *E*. [7]

1.4 Lawson criterion

The fusion energy gain factor Q is the ratio of fusion power to the input power required to maintain the plasma in steady state:

$$Q = \frac{P_{fusion}}{P_{input}} \tag{1.2}$$

The condition $Q = 1$ is referred to as breakeven. It is the goal of a future fusion reactor to reach ignition $(Q = \infty)$, in which a self-sustained plasma heats itself by fusion energy without any external input. However, the condition for a fusion reactor to

[7] Duplicate lecture notes, 'Plasmafysica 1' (2005-2006), Prof. dr. ir. G. Van Oost, Department of Applied Physics, Ghent University

sell power ($Q = 20$) requires quality of confinement almost as good as that required to achieve ignition.
A practical general measure of a system that defines the conditions needed for a fusion reactor to reach ignition was originally formulated by Lawson [Law57] in a criterion which gives a minimum required value for the product of the plasma electron density n_e and the energy confinement time τ_E. Later this condition was improved to an even more useful figure of merit based on the (fusion) triple product of n_e, τ_E and the plasma temperature T. The energy confinement time indicates the quality of the magnetic confinement as defined by the energy content of the plasma W divided by the plasma's power loss to its environment P_{loss}:

$$\tau_E = \frac{W}{P_{loss}} \tag{1.3}$$

For the D-T reaction, the physical value is about $n_e T \tau_E \geq 10^{21}$ keV.s.m^{-3}. The apparent saturation of the 'fusion triple product' in figure 1.4 reflects the fact that the present large experiments (JET, TFTR, JT-60U) are basically at the limit of their capability and that a new larger device such as ITER, the next generation nuclear fusion machine (see paragraph 1.5), is required to reach and go beyond the ignition point [Wolf96]. Comparing the speed of progress of fusion research and development with that of DRAM (Dynamic Random Access Memory, indicated in figure 1.4) as a typical high technology in the last century is a popular way of promoting the progression of nuclear fusion.
Since plasmas act like fluids, they have no permanent shape and will quickly disperse if not confined. Fortunately, the free electric charges (ionized gas) make the plasma electrically conductive so that it responds strongly to electromagnetic fields. Magnetic confinement rests upon the property that the charged particles will travel (gyrate) along the lines of a magnetic field due to the Lorentz force. The other approach to contain hot plasmas is the so-called inertial confinement which is beyond the scope of this thesis. A variety of magnetic configurations can be used of which 'tokamaks' and 'stellerators' (not discussed

here) are so far proved to be the most promising and advanced concepts [Weyn94]. Although both concepts have their advantages and disadvantages, the tokamak nowadays seems to have the upper hand as its design was chosen to manufacture ITER [ITER01].

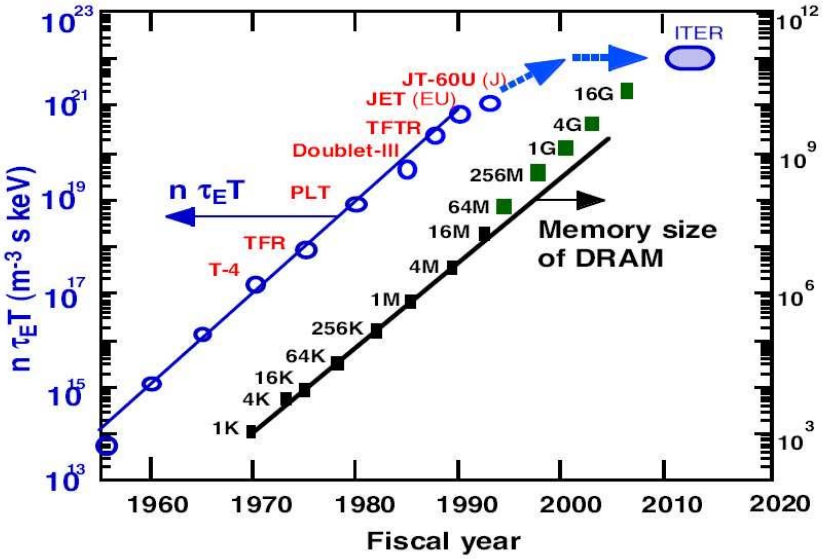

Figure 1.4: Comparison of fusion research and development with that of DRAM technology showing that they have a comparable progress speed of 10 times increase in 5 years.[8]

[8] Internal report of K. Mitsuru, member of the Japan Atomic Energy Research Institute, Japan; http://fire.pppl.gov/energy˙ja˙wec01.pdf

1.5 The tokamak

In magnetically confined fusion plasmas it is necessary to contain and isolate from material surfaces ionized gases whose temperatures and densities exceed 10 keV (10^8 K) and 10^{13} particles/cm^3. Moreover, confinement must be of sufficient duration for fusion interactions to replenish the heat lost from neutral fluxes, radiation, and transport. In most devices, the plasma is toroidal. The word 'tokamak' is an acronym derived from the Russian words "TOroidalnaya KAmera ee MAgnitnaya Katushka," meaning "Toroidal Chamber in Magnetic Coils".

1.5.1 Geometry of a tokamak

The vacuum chamber of the tokamak is toroidal, or doughnut-shaped, thus having no open ends and therefore no end-losses as shown in figure 1.5. The torus has a major radius R_0, from its centre to the axis of the vacuum chamber, which has a minor radius a (figure 1.5). This device is axisymmetric and is characterized by a large magnetic field B_ϕ in the toroidal direction and a smaller poloidal magnetic field B_θ [Tayl97]. The magnitude of B_ϕ is typically a few Tesla, an order of magnitude bigger than $|B_\theta|$. In addition, extra coils are suitably placed to create a vertical magnetic field B_z used for control of position and shape of the plasma. B_ϕ is produced by large external field coils which are wrapped around the reactor. B_θ is generated by a toroidal current (plasma current I_p) induced in the plasma that acts as the secondary circuit of a transformer (figure 1.5). This current is pulsed implementing a non-continuous regime which might be one of the major drawbacks of the tokamak design. However, in view of a continuous reactor operation, methods are being studied to sustain plasma current via other means.

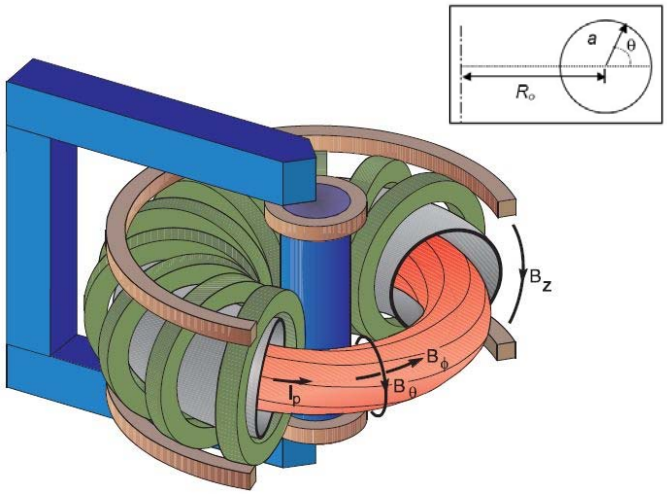

Figure 1.5: Schematic drawing of a tokamak device.

1.5.2 Systems of reference

Two systems of reference can be used to describe the motion of particles as shown in figure 1.6(b). One is linked to the local magnetic field line $(r, \perp, //)$; the other to the toroidal axis of the machine (r, θ, ϕ). The radial direction is identical for both systems, i.e. perpendicular to the magnetic surface pointing outwards. The angle between the parallel and toroidal direction is defined as the pitch angle α. The toroidal system is axi-symmetric, i.e. all quantities are independent of the toroidal coordinate. In the (r, θ, ϕ) reference system a radius R is defined as

$$R = R_0 + r\cos(\theta) \tag{1.4}$$

where r is the distance to the plasma centre and R the distance to the vertical torus axis. The displacement of the magnetic

surfaces, generally known as the Shafranov shift, is rather unimportant in the edge region and is therefore neglected. The edge plasma parameters, for example the ion velocity v, can then be transformed from one system to the other via the projection relations:

$$\begin{cases} v_{\perp} = \cos(\alpha) v_{\theta} - \sin(\alpha) v_{\phi} \\ v_{//} = \sin(\alpha) v_{\theta} + \cos(\alpha) v_{\phi} \end{cases} \tag{1.5}$$

or via the inverse transformation

$$\begin{cases} v_{\theta} = \cos(\alpha) v_{\perp} + \sin(\alpha) v_{//} \\ v_{\phi} = -\sin(\alpha) v_{\perp} + \cos(\alpha) v_{//} \end{cases} \tag{1.6}$$

Some useful expressions for the toroidal and poloidal magnetic field can be obtained:

$$\begin{aligned} B_{\phi} &= \frac{B_0 R_0}{R} = B\cos(\alpha) \\ B_{\theta} &= B\sin(\alpha) = B_{\phi}\tan(\alpha) = B_{\phi}\Theta \end{aligned} \tag{1.7}$$

with $\Theta = B_{\theta}/B_{\phi}$ defined as the pitch of the magnetic field. On each flux surface the magnetic field has a different winding number $q = m/n$ defined as the ratio of the number of toroidal m and poloidal n rotations needed before the field line joins up on itself (or closes). It can also be written as

$$q = \frac{rB_{\phi}}{R_0 B_{\theta}} \tag{1.8}$$

This number is also called 'the safety factor' because of the role it plays in determining stability. In general, higher values of q lead to greater stability. It also appears as an important factor in transport theory.

1.5.3 Confinement of turbulent plasmas

The Lorentz force makes charged particles to gyrate around the magnetic field lines. The toroidal field line configuration in a tokamak seems, at first site, an ideal situation since the particles are forced to follow the lines of force and run around ad infinitum. However, since this field is stronger towards the centre of the machine it is easy to show, using Ampère's law for a toroidal geometry, that a gradient in the magnetic fields exists which is directed towards the centre of the configuration leading to a drift velocity [Chen74, VS98a]:

$$\bar{v}_{D,\bar{\nabla}B} = -\mu \frac{\bar{\nabla}B \times \bar{B}}{qB^2}, \tag{1.9}$$

with μ the magnetic moment of the gyrating particle. Due to the curvature of the field additional centrifugal forces exist, creating drifts which add to this ∇B drift. These drift velocities are opposite for electrons and ions so that the two species are separated and an electric field is created, resulting in an additional drift

$$\bar{v}_{D,\bar{E}} = \frac{\bar{E} \times \bar{B}}{B^2} \tag{1.10}$$

which is directed outwards, away from the centre and is the same for the two species. The result is that the plasma drifts out of the confining field and that a more complex magnetic field configuration is necessary to eliminate these drifts. Therefore, onto the major toroidal filed, a field in poloidal direction, perpendicular to the first one, is added so that the total field line twists around the torus, thus mixing positive and negative charges again, thus eliminating the drift caused by the electric field.
So, by design, the combination of B_ϕ and B_θ creates helical magnetic field lines that spiral around the torus and maps out toroidal ion shell like magnetic (or flux) surfaces in which the current lines lie and where the plasma pressure $(p = nkT)$

remains constant. Together, the current and magnetic field exert a bulk force on the plasma given by their vector cross product. This force is normal to the flux surfaces and can therefore contain the pressure of the plasma, as indicated in figure 1.6(a). For simplicity of presentation only flux surfaces with circular cross section and which are concentric are considered in figure 1.6. In this case, the normal direction is radially outward. The balance of magnetic force and pressure specifies a steady state of the mean ideal magneto-hydrodynamics (MHD) equations. Experience has established that ideal MHD adequately reflects the force balance as measured in plasmas, with the magnetic field determined from the current density through Ampère's law. The mean states of ideal MHD are referred to as equilibriums. However, different processes, such as collisions and resistive instabilities, cause the plasma to evolve from one ideal equilibrium to another and radial variations (fluctuations) of the pressure (∇p) and the plasma current (∇B) are set. Together with collisions, these fluctuations produce a flux of heat and particles moving radially outwards of the plasma. In particular, the fluctuations characterized by spatial scales that are small compared to the dimensions of the plasma generally dominate the losses of heat and particles [Liew85, Woot90]. Although it has not been possible to attribute the dominant measured losses to fluctuations associated with a specific collective plasma mode, measurements have confirmed that the losses are due to fluctuations and not collisions (for example, see [Ritz89]). In some cases the fluctuation-driven loss rates exceed those due to collisions by orders of magnitude. These fluctuations in the plasma are generally known as turbulence. Reducing this turbulent plasma behaviour has therefore been one of the most challenging tasks for fusion scientists in the last few decades.

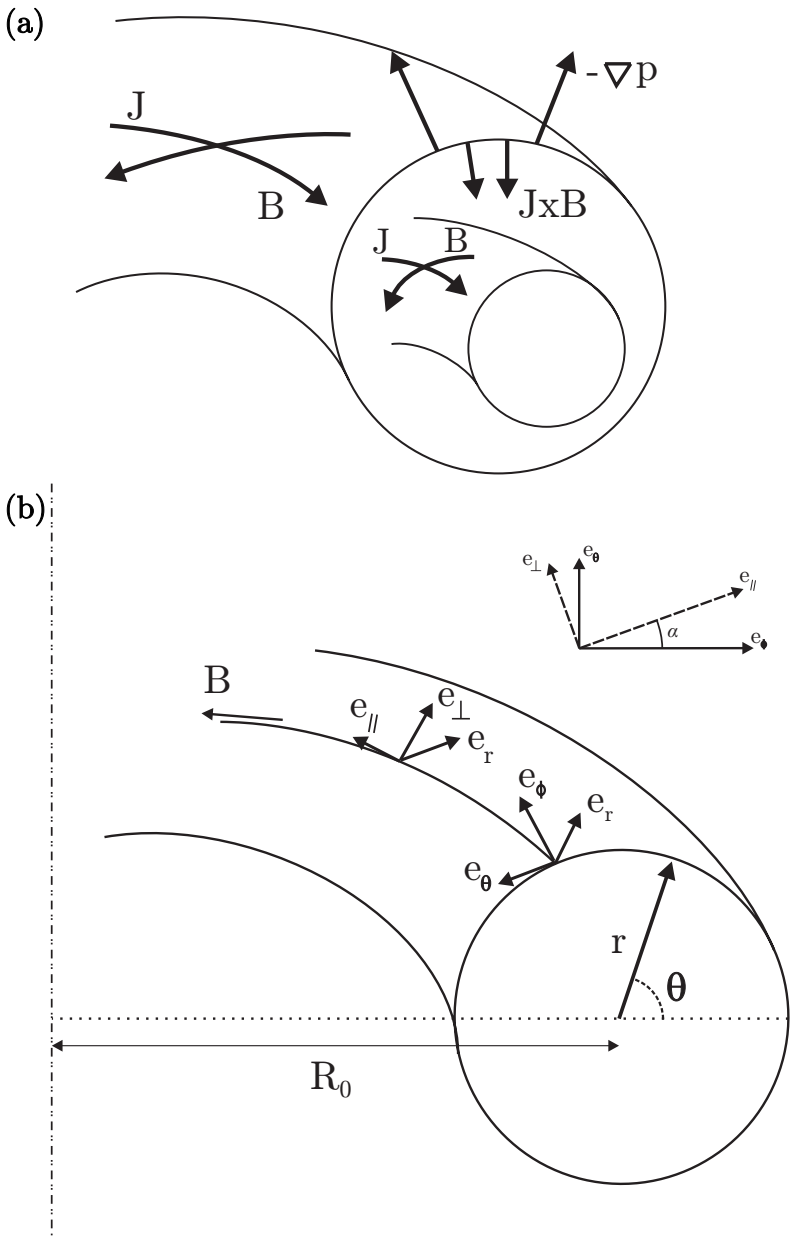

Figure 1.6: Flux surfaces with circular cross section of a magnetically confined toroidal plasma. In (a), the currents and magnetic-field lines lie on nested tori. The $J \times B$ force balances the plasma pressure. In (b), the toroidal and parallel system of reference.

1.5.4 Plasma heating systems

The plasma current ohmically heats (by dissipation) tokamak plasmas. However, because the resistivity of the plasma decreases with increasing temperature, ohmic heating is limited to a few keV. The required temperatures of more than 10 keV (needed for *D-T* fusion) are achieved by applying additional auxiliary heating sources. One method is to launch electromagnetic waves into the plasma, where they are absorbed by the gyrating particles which are in resonance with this wave and are accelerated (thus heated). These techniques are called Electron/Ion Cyclotron Resonance Heating (ECRH/ICRH) and Lower Hybrid Heating (LHH) [Koch06a, Wes06]. Another possibility is to use very fast neutral particles which are injected into the plasma. These high energy neutrals become ionized as they enter and circulate several hundred times around the torus while slowing down due to collisions with the plasma particles. The energy transferred due to these collisions heats up the plasma. This technique is called NBI (Neutral Beam Injection) [Koch06b]. The plasma can also be heated through rapid compression by moving the plasma to an area of a higher magnetic field, generally known as the High Field Side (HFS) of the tokamak.
The plasma density n_e is typically in the range 10^{19}-10^{20} m^{-3}. The duration of a pulse (or discharge) t_p can go from milliseconds to tens of seconds. Conventional tokamaks to date generally demonstrate a stability limit to β defined as the ratio of the kinetic or plasma pressure (p) and the magnetic pressure $\left(B^2/2\mu_0\right)$:

$$\beta = \frac{p}{B^2/2\mu_0} = \frac{n_e kT_e + \sum n_i kT_i}{B^2/2\mu_0} \tag{1.11}$$

with μ_0 being the permeability of vacuum. Since the total fusion power scales with the square of the density and thus with $\beta^2 B^4$, high values of β and B are desired but restricted by operational limits [Waid96].

1.5.5 Limiters and divertors

In the simplest way one can divide tokamak plasmas in two distinct regions. In the core region the magnetic flux surfaces never intersect any material structure keeping the field lines closed. The edge or boundary region is separated from the confined plasma by the separatrix or the Last Closed Flux Surface (LCFS) where the closed magnetic surfaces are interrupted by a material object, namely either by a limiter or by divertor plates, forming a scrape-off layer (SOL) region with open field lines where plasma particles are 'scraped' from the core plasma and directed towards the targets.
The properties of the SOL determine both the particle removal as well as the power exhaust. The particle flows in the SOL and their radial decay give constraints for the construction of the main plasma facing components and for systems which are capable of adequate particle and power removal.
It is clear that the core of a burning fusion reactor must provide a very good isolation against heat losses; therefore the magnetic field forms onion shell like magnetic surfaces. However, also the plasma edge on fusion reactors has to fulfil specific tasks. The power and the particles – in particular the helium ash and other impurities – coming from the core of the reactor have to be removed at an adequate rate. We know already [Reit06] that helium particles, newly born in the fusion process, have to be pumped in a time corresponding to 5 - 10 times the energy confinement time τ_E. This high removal rate can only be obtained if the particle flux is highly compressed when it enters a pumping channel. Two separate systems capable of sufficient particle removal have been invented: the pumped limiter and the divertor (figure 1.7).
A limiter (figure 1.7a) is a material structure providing the first contact with the plasma. It is designed in such a way that the field lines graze the plasma facing surface to distribute the energy fluxes and particles and therefore limit the local power load. We can distinguish three types of limiter configurations. First, the poloidal limiter is a ring going around in the poloidal direction forming a bottle neck which limits the plasma. As the

power input and pulse duration increased, toroidal limiters became in use forming a belt going around the machine in the toroidal direction as schematically shown figure 1.7a. Some machines also have local limiters which have no toroidal or poloidal symmetry helping to optimize the power handling capability. A limiter is generally coated with carbon tiles to withstand high particle and power fluxes which heat it up and unfortunately erode its surface and so risks to contaminate the plasma.

The more complex system of a magnetic divertor (figure 1.7b) requires special magnetic fields which modify the outer magnetic field of the reactor and allow for a particle flow into a separate chamber, the divertor chamber. Here the separatrix forms one singular point, the X-point, where two magnetic field lines intersect as shown in figure 1.7b. The particles are directed towards the divertor plates during which the plasma radiates part of its energy away (cools down) and becomes denser. As a result, the erosion and power load on the targets can be minimized and is situated away from the main plasma. After neutralization of the plasma at the target plates the neutral gas, some of the created impurities and the helium ash is more effectively pumped away compared to the pump limiter concept and therefore many modern tokamaks are equipped with divertors.

However, the desired high particle flux density into a divertor chamber or towards a pumped limiter is accompanied by an undesired strong power flux. This power flux density is at upper tolerance limit of even the best suited materials. In our present understanding, the simultaneous requirement of particle exhaust and power handling in the SOL remains a critical issue for future thermonuclear burning plasma in a tokamak.

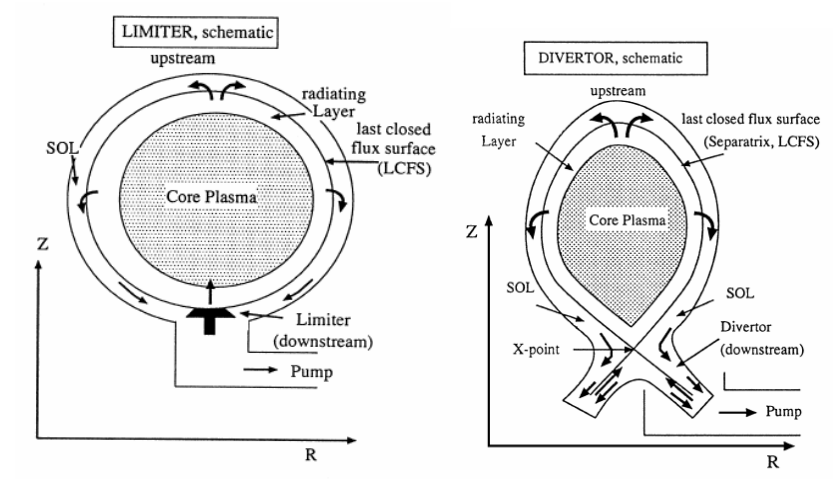

(a) (b)

Figure 1.7: Axi-symmetric toroidal pump limiter (a) and poloidal divertor (b) configuration. The typical plasma flow patterns are also sketched.[9]

1.5.6 CASTOR, TEXTOR and ITER

The experimental work within the framework of this thesis is performed on CASTOR and TEXTOR, a small- respectively medium-sized tokamak of which the main parameters are summarized in table 1.2 and compared to the huge next-generation tokamak ITER.

Parameter	CASTOR	TEXTOR	ITER
R_0 [m]	0.4	1.75	6.2
A [m]	0.085	0.47	2
Plasma cross-section	Circular	Circular	D-shape
$B_{\phi,\max}$ [T]	1.5	3	5.3
$I_{p,max}$ [MA]	0.025	0.8	15
$t_{p,max}$ [s]	0.050	10	400
$n_{e,max}$ [m^{-3}]	$3*10^{19}$	10^{20}	10^{23}
Input Power P [MW]	0.035	9	73+

Table 1.2: Typical tokamak parameters of CASTOR, TEXTOR and ITER.

[9] Internal report , *'Edge Physics, divertors, pump limiters'*, K. H. Finken, Institut für Plasmaphysik (IPP), Forschungzentrum Jülich

CASTOR is an abbreviation for Czech Academy of Sciences TORus, a small-sized tokamak with a circular cross section. This tokamak is operational since 1977 in the Institute of Plasma Physics (IPP) of the Academic of Science in Prague, Czech Republic (figure 1.8). The LCFS is defined by a poloidal limiter and the working gas is hydrogen. It is probably the world-leading machine for probe research, a plenitude of electric and magnetic probes are available to study the edge plasma.

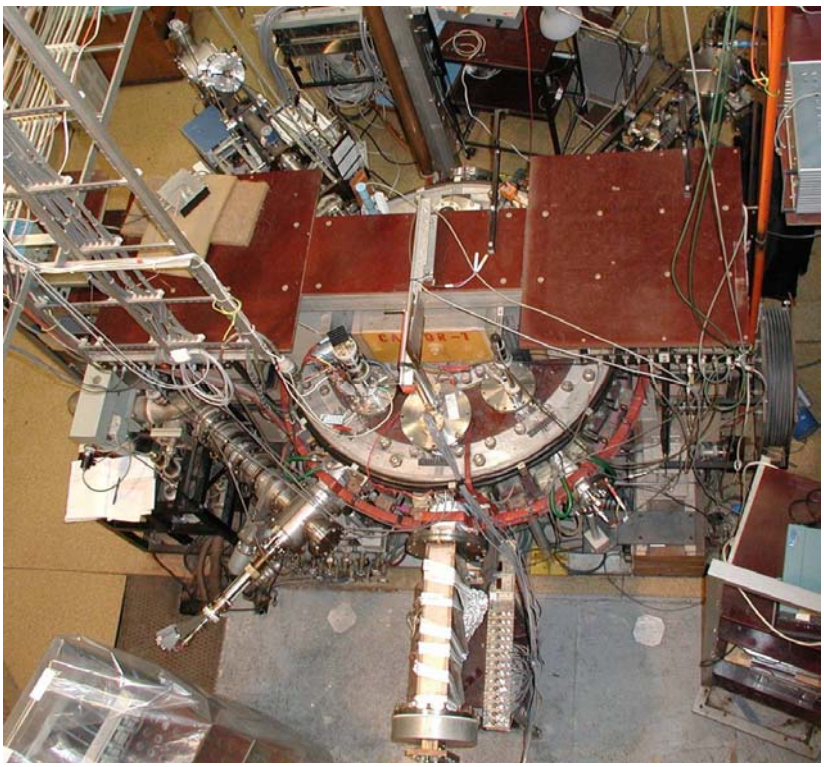

Figure 1.8: Top view of CASTOR.

The Tokamak Experiment for Technology Oriented Research, TEXTOR, is aimed at the field of plasma wall interaction. It is a medium-sized device with a circular cross-section. The inner wall consists of a removable liner (covers the full toroidal circumference), a toroidal pump limiter (ALT-II), three poloidal limiters and an inner bump limiter which is mounted on top of the liner as shown in figure 1.9. TEXTOR is located at the Forschüngszentrum in Jülich, Germany, where in collaboration with the EURATOM associations ERM/KMS (Belgium) and FOM (The Netherlands) under the framework of the "Trilateral Euregio Cluster" (TEC), mainly detailed studies of particle and energy exchange between the plasma and the surrounding chamber (plasma surface interaction) are performed. Recently the Dynamic Ergodic Divertor (DED) has been installed in order to influence transport parameters at the plasma edge and to study the resulting effects on heat exhaust, edge cooling, impurity screening, plasma confinement and stability. The number of special features and the flexibility of TEXTOR provide excellent opportunities for important contributions to fusion research.

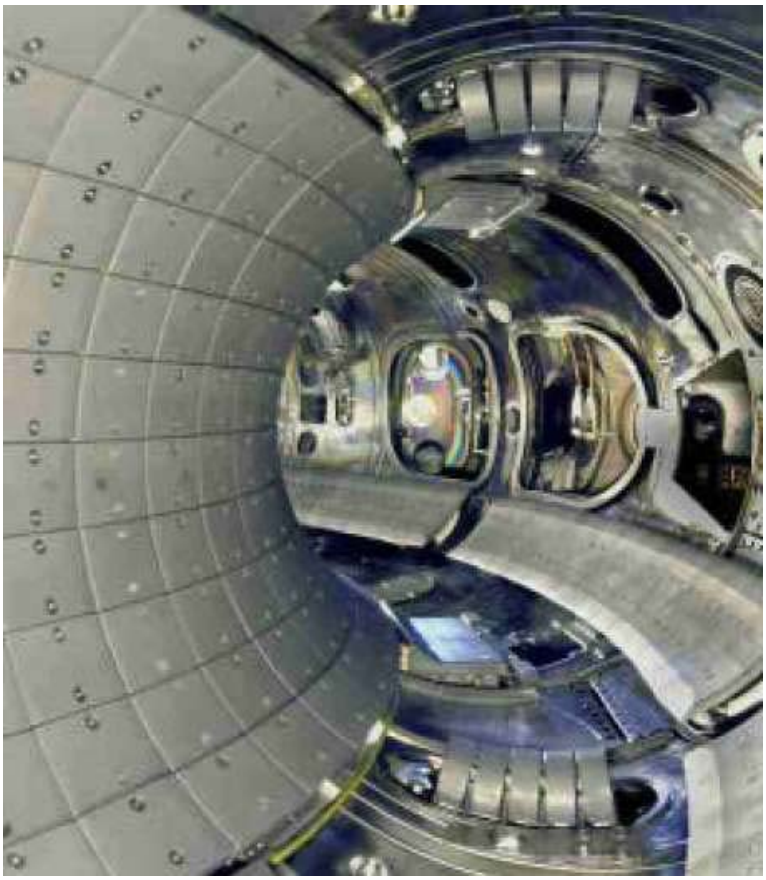

Figure 1.9: Photograph of the TEXTOR limiters protecting the liner from the plasma energy, shaping the plasma, and partly being designed for material testing. Shown are the bumper limiter (left), the main limiters (top and bottom), and the ALT-II limiter (right).

ITER is a joint international research and development project that aims to demonstrate the scientific and technical feasibility of a full-scale fusion power reactor [ITER01]. ITER is an acronym standing for International Thermonuclear Experimental Reactor but it also means 'the way' in Latin, and this double meaning reflects its role in harnessing nuclear fusion as a peaceful power source. The partners in the project are the European Union (represented by EURATOM), Japan, the Peoples Republic of China, India, the Republic of Korea, the Russian Federation and the USA. ITER will be constructed in Europe, at Cadarache in the South of France and the first plasma operation is expected in 2016. The program is anticipated to last for 30 years (10 years for construction, and 20 years of operation) and costs approximately €10 billion making it the second most expensive scientific project after the International Space Station (ISS). This machine will have about double the size of today's biggest tokamak JET (Joint European Tokamak). ITER is designed to produce approximately 500 MW of fusion power sustained for up to 500 seconds. It is a significant amount of power for a fusion research project; a future fusion power plant would generate about 3000-4000 MW of thermal power. Although ITER will produce net power in the form of heat, the generated heat will not be used to generate any electricity.

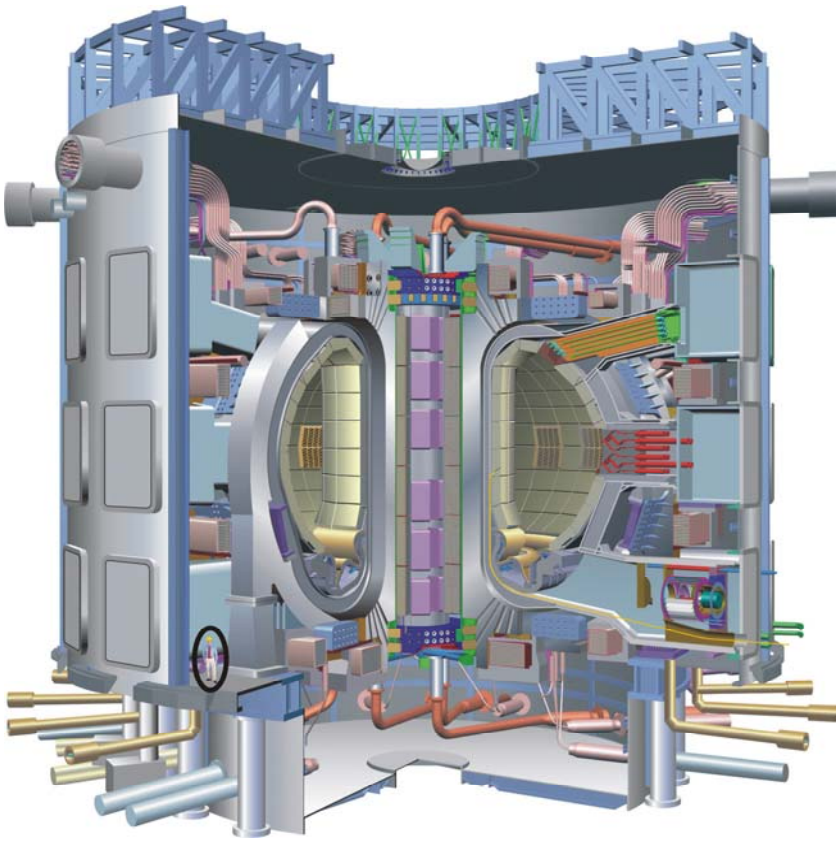

Figure 1.10: Technical cutaway of the ITER tokamak. The person in the bottom indicates the scale.[10]

[10] http://www.iter.org/

1.6 Context of this thesis and outline

1.6.1 Importance of edge plasmas and plasma flow

As in most systems in physics the condition of the boundary strongly influences the process. For more than a decade it has become increasingly clear that edge or boundary plasmas play an important role in magnetic fusion experiments. The strong relation between the edge and central (core) plasma has clearly been recognized worldwide in particular its role in particle and energy exhaust. First, the level of impurity concentration (helium, neutrals,...) in the fusion volume must be kept sufficiently low by means of effective heat removal and particle exhaust. Second, the cross-field transport of energy and particles originating in the edge plasma due to different mechanisms limits the confinement time of the hot and dense core plasma. Therefore, fusion research dedicated to a better understanding of edge plasmas and controlling it is of essential importance. Tokamaks like CASTOR and TEXTOR have engaged to specialize in edge studies and plasma-surface interactions by employing extensive equipment of edge diagnostics.
One of the main progresses in tokamak research is the discovery of a so-called high confinement plasma regime, generally abbreviated as H-mode (in contrast to L-mode, a regime of low confinement). Such an improved confinement regime was first observed on the large tokamak ASDEX [Wag82]. The H-mode can occur spontaneously in large divertor tokamaks when the neutral beam power exceeds a certain threshold [Ten97]. However, it was later found that the onset of an L-H transition can also be induced in ohmically heated plasmas by applying sufficient voltage to an electrode several centimetres inside the plasma [Weyn93]. This active method of forcing a current through the plasma to control the plasma edge is called edge biasing or polarization. In both cases a strong, localized radial electric field is observed. The shear in the radial electric field is supposed to be important for the suppression of turbulence in the edge, thus improving the confinement of energy and

particles. This is usually referred to as the creation of a transport barrier. The underlying idea is that the shear (thus difference in velocity) in the plasma flow, in particular the shear in the $E_r \times B_\phi$ poloidal flow v_θ, destroys the turbulent eddies and thus reduces cross-field transport. Thus the main effect of the induced radial current is to create a torque in the poloidal direction, enabling the plasma to rotate. Although many models were able to reproduce the shape and magnitudes of the measured electric fields and plasma flows, the measured transport coefficients still remain much larger than what the neoclassical theory predicts. It is believed that the enhanced cross-field transport (anomalous transport) originates from high frequent electrostatic turbulent mechanisms which are not included in the neoclassical transport theory. Although these mechanisms are not yet well understood, transport experiments can now probe the substructure of tokamak turbulence.
Recently, experimental evidence of a dynamical coupling between turbulent transport and toroidal flows v_ϕ has been reported on JET [Hid03a]. This empirical link could provide new insights in the physics of edge plasmas in order to explain the discrepancy between the measured and theoretical radial transport. In this thesis we report a similar observation on CASTOR. Although we did not measure turbulence directly, a clear and reproducible relationship between the turbulent transport and toroidal flows was found [Pel06c]. This important finding does not only concur with the results on a much bigger tokamak such as JET, but the completely different plasma conditions in which these experiments took place could indicate that the mechanism to couple transport and toroidal flows might be a universal feature of tokamak edge plasmas.

1.6.2 Plasma edge diagnosis by probes

The electrical probe method is one of the most straightforward techniques in plasma diagnostics to study the plasma boundary. Inserting some kind of probe that directly senses the local particle flux is probably the most natural approach to measure

the particle distribution functions. In fusion plasmas only the plasma edge is accessible due to the heat load on the probe. Electric probes are usually referred to as Langmuir probes, associated to the Nobel Prize for Chemistry (1932) winning physicist Irving Langmuir [Lang23, Lang29] who did pioneering work on probes using an electrical measurement technique. Shielding effects at the plasma-probe interface causes a non-ohmic current-voltage (*I-V*) characteristic used to determine the electron temperature, density and plasma potential. To measure the plasma flow a so called Mach probe has to be employed [Oth78]. A Mach probe consists typically of two oppositely facing collectors (Langmuir probes) insulated from each other and aligned with the magnetic field. In order to determine also the perpendicular Mach number, additional collectors inclined with respect to the magnetic field, are necessary. Such an array of collectors, poloidally distributed over the probe's circumference, is generally known as a 'Gundestrup' probe [Mac92].

1.6.3 Probe modelling

The difficulty with direct plasma particle flux measurements lies mainly in the understanding of the local perturbation of the plasma by the probe and of the relation of the local plasma parameters to the unperturbed plasma far from the probe. In this context probe modelling is important in correctly interpreting the observed particle energies and currents. Hutchinson developed an analytical one dimensional (1D) fluid model in which the ratio of the measured upstream and downstream ion saturation current yields the Mach number (defined as the ratio of the plasma flow velocity to the ion acoustic velocity) parallel to the magnetic field [Hut87; 88a,b]. Van Goubergen extended this model which allows us to determine not only the parallel but also the perpendicular flow [VG99a]. We have investigated the reliability within the range of applicability of this model for Mach probe measurements based on a numerical study. This investigation resulted in an

improvement of the model by formulating a new analytical expression which now takes into account the various dependencies of the parallel and perpendicular Mach numbers and the inclination angle of the collectors with respect to the magnetic field [Pel02]. In addition, this refined 1D fluid model has been validated by comparing it to a two-dimensional (2D) quasi-neutral Particle-In-Cell (PIC) simulation code [Pel05].
On CASTOR and TEXTOR two different types of Gundestrup-like probe designs are employed: one with round and one with flat collectors. We have studied the effect of the collector shape on the accuracy of the measurement of the flows [Pel05]. Here we have formulated a new analytical expression which takes into account the curvature of non-flat collectors and show that this extension in the model significantly reduces the error on the determination of the perpendicular flow when it reaches a certain threshold. However, this threshold was found to be out of range of our experimental results making us confident in choosing flat collectors for our design of a new probe.
Reviews of other techniques used for edge plasma diagnosis can for example be found in [Hut00, Sta90].

1.6.4 New probe diagnostic at TEXTOR

Very recently (Nov. 2005) a versatile fast scanning and rotating probe system became in operation on the TEXTOR tokamak. The reciprocating linear movement of the system enables us to measure local plasma edge parameter profiles with high temporal and spatial resolution. We have designed and manufactured a novel advanced Gundestrup-like probe head. The unique design of this probe makes it possible to simultaneously obtain a large variety of edge plasma parameters with a high spatial and temporal resolution which has never been reported on other tokamaks. From the moment this probe assembly came in operation and its reliability was demonstrated [Pel06a], it has been one the most favourable edge diagnostics on TEXTOR.

1.7 Outline of this work

The present work is described in three chapters. First theoretical probe modelling is presented. The two subsequent chapters are dedicated to experimental (probe) work performed on two different tokamaks, TEXTOR and CASTOR respectively. Each chapter includes one or two relevant publication(s) published (or accepted for publication) in international journals with refereeing system. The thesis is organised as follows.

Chapter 2 begins with a review of a 1D fluid probe model followed by an investigation of the reliability of this analytical model. Subsequently, an improvement is proposed showing that under certain circumstances an ameliorated analytical approach is recommended. This improved model is then validated using a 2D Particle-In-Cell simulation code. Finally, we have investigated the effect of implementing round collectors on probes when using this validated 1D fluid model for the interpretation of the raw probe data which consequently resulted in an extension of the model.

In Chapter 3 the design of a new advanced Gundestrup-like probe head is introduced. The main features of the fast reciprocating probe system, on which the probe head is mounted, are described. This chapter closes with the first results of probe measurements in the plasma edge of the tokamak TEXTOR discussing the reliability and accuracy of the probe assembly.

Chapter 4 presents and discusses the experimental results performed on the CASTOR tokamak during biasing experiments. The work is mainly focussed on the interrelationship between radial electric fields, plasma flows and enhancement of radial transport in particular during plasma edge instabilities. Overall conclusions are given in Chapter 5.

1.8 Publications

This work resulted in the following publications.

1.8.1 Publications in international journals

1. 'Investigation of the reliability of a 1-D fluid probe model for Mach probe measurements'; P. Peleman, S. Jachmich, M. Van Schoor, and G. Van Oost; Czechoslovak Journal of Physics, 55(3):381, 2005.

2. 'Relaxation phenomena induced by edge biasing experiments in the CASTOR tokamak'; M. Spolaore, P. Peleman, J. Brotankova, P. Devynck, H. Figueiredo, G. Kirnev, E. Martines, J. Stöckel, G. Van Oost, J. Adamek, E. Dufkova, I. Duran, M. Hron, and V. Weinzettl; Czechoslovak Journal of Physics, 55(12):1597, 2005.

3. 'Comparative Study of Flat and Round Collectors Using a Validated 1D Fluid Probe Model'; P. Peleman, S. Jachmich, M. Van Schoor, G. Van Oost, W. Knaepen, C. Boucher; Contributions to Plasma Physics, 46(5-6):432, 2006.

4. 'Highly resolved measurements of periodic radial relaxation in edge biasing experiments'; P. Peleman, C. Boucher, J. Brotankova, P. Devynck, J. Stöckel, M. Spolaore, and G. Van Oost; to be published in Journal of Nuclear Materials (accepted), 2006.

5. 'Novel advanced Gundestrup-like probe for the measurements of flows and edge plasma parameters in TEXTOR'; P. Peleman, S. Jachmich, Y. Xu, C. Boucher, G. Van Oost, B. Schweer, and M. Mitri; to be published in Review of Scientific Instruments (accepted), 2006.

1.8.2 Publications in international conferences

6. 'Study of the accuracy of Mach probes to measure the parallel and perpendicular flow in the plasma edge'; P. Peleman, S. Jachmich, M. Van Schoor, C. Boucher, F. Michon, and G. Van Oost; 29th European Physical Society (EPS) conference on Plasma Physics and Controlled Fusion, Montreux, Switzerland, ECA 26B, 2.126, 2002.

7. 'Turbulent transport reduction by ExB velocity shear during edge plasma biasing in tokamaks'; G. Van Oost, J. Adámek, V. Antoni, P. Balan, J. A. Boedo, P. Devynck, I. Ďuran, L. Eliseev, J.P. Gunn, M. Hron, C. Ionita, S. Jachmich, G.S. Kirnev, E. Martines, A. Melnikov, P. Peleman, R. Schrittwieser, C. Silva, J. Stöckel, M. Tendler, C. Varandas, M. Van Schoor, V. Vershkov, and R. R. Weynants; First Cairo Conference on Plasma Physics & Applications, Cairo, Egypt, International Cooperation, Bilateral Seminaries Vol. 34, 2003.

8. P. Peleman, G. Van Oost, S. Jachmich, and M. Van Schoor, 'Measurements of the parallel and perpendicular flow in the electrode biased plasma edge of Textor-94 using an improved theoretical model'; 4th Deutsche Physikalische Gesellschaft (DPG) Spring Conference, Aachen, Germany, P 10.30, 2003.

9. 'Improvement of a 1D fluid probe model for Mach probe measurements'; P. Peleman, S. Jachmich, M. Van Schoor, and G. Van Oost; 12th International Congress on Plasma Physics (ICPP), Nice, France, e-proceeding, 2004

10. 'Relaxation phenomena during edge biasing in the CASTOR tokamak'; M. Spolaore, J. Brotankova, P. Peleman, P. Devynck, H. Figueiredo, G. Kirnev, E. Martines, J. Stöckel, G. Van Oost, J. Adamek, E. Dufkova, I. Duran, M. Hron, and V. Weinzettl; 32th European Physical Society (EPS) conference on Plasma Physics and Controlled Fusion, Tarragona, Spain, P4.031, 2005.

11. 'Relaxation phenomena induced by edge biasing experiments in the CASTOR tokamak'; M. Spolaore, J. Brotankova, P. Peleman, P. Devynck, H. Figueiredo, G. Kirnev, E. Martines, J. Stöckel, G. Van Oost, J. Adamek, E. Dufkova, I. Duran, M. Hron, and V. Weinzettl; 8th Workshop on Electric Fields, Turbulent Structures and Relaxation in Edge Plasmas (EFSREP), Tarragona, Spain, 2005.

12. P. Peleman and G. Van Oost, 'Enhanced Mach probe data analysis for the determination of flows in the tokamak TEXTOR with an innovative electrostatic probe', 8th International Workshop on the Interrelationship between Plasma Experiments in Laboratory and Space (IPELS), Trömso, Norway, p.81, 2005.

13. 'A novel advanced Gundestrup-like probe for the measurements of flows and edge plasma parameters in TEXTOR'; P. Peleman, S. Jachmich, Y. Xu, C. Boucher, G. Van Oost, B. Schweer, and M. Mitri; 16th Annual Conference on High-Temperature Plasma Diagnostics (HTPD), Williamsburg Virginia, USA ,TP-29, 2006.

14. 'Highly resolved measurements of periodic radial relaxation in edge biasing experiments'; P. Peleman, C. Boucher, J. Brotankova, P. Devynck, J. Stöckel, M. Spolaore and G. Van Oost; International Conference on Plasma Surface Interactions (PSI), Hefei (Anhui), China, P3-23, 2006.

15. 'Experimental and theoretical investigations of the role of microturbulence and electric fields in the establishment of improved confinement in tokamak plasmas through inter-machine comparisons'; G. Van Oost, P. Peleman, *et al.*; 13th International Congress on Plasma Physics (ICPP), Kiev, Ukraine, IP003, 2006.

16. 'Detailed measurements of momentum balance during the periodic collapse of a transport barrier'; M. Hron, P. Peleman, M. Spolaore, R. Dejarnac, O. Bilykova, J. Brotankova, J. Sentkerestiova, I. Duran, L. van de Peppel, J. Gunn, J. Stöckel, G. Van Oost, J. Horacek, J. Adamek, and M. Stepan; 33rd European Physical Society (EPS) conference on Plasma Physics and Controlled Fusion, Rome, Italy, 2006.

17. 'First Mach probe measurements of rotation, electric field and particle transport in the DED-ergodized edge plasma of TEXTOR'; S. Jachmich, P. Peleman, M. Van Schoor, Y. Xu, M. Jakubowsky, M. Lehnen, B. Schweer, and R. Weynants; 33rd European Physical Society (EPS) conference on Plasma Physics and Controlled Fusion, Rome, Italy, 2006.

18. 'Periodic collapse of a transport barrier induced by biasing experiments in the CASTOR tokamak'; M. Spolaore, J. Brotankova, J. Stöckel, I. Duran, M. Hron, P. Peleman, R. Dejarnac, O. Bilykova, J. Sentkerestiova, L. van de Peppel, J. Gunn, G. Van Oost, J. Adamek, M. Stepan, and E. Martines; 9th Workshop on Electric Fields, Structures, and Relaxation in Edge Plasmas (EFSREP), Rome, Italy, 2006.

1.8.3 Oral Presentations in international workshops

19. 'Investigation of the reliability of a 1-D fluid probe model for Mach probe measurements'; P. Peleman, S. Jachmich, M. Van Schoor, and G. Van Oost; 7th Workshop on Electric Fields, Turbulent Structures and Relaxation in Edge Plasmas (EFSREP), Nice, France, 2004.

20. 'Comparative study of flat and round collectors using a 1D validated fluid probe model'; P. Peleman, S. Jachmich, M. Van Schoor, G. Van Oost, W. Knaepen, and C. Boucher; 6th International Workshop on Electrical Probes in Magnetized Plasmas (IWEP), Seoul, South-Korea, No.11, p.32, 2005.

1.8.4 Publications in national conferences

21. 'Measuring the flow in the plasma edge of TEXTOR-94 using Mach probes'; P. Peleman, S. Jachmich, M. Van Schoor, and G. Van Oost; 2nd FTW PhD Symposium, Universiteit Gent, p. 24, 2001.

22. 'Study of the accuracy of Mach probes to measure the parallel and perpendicular flow in the plasma'; P. Peleman, S. Jachmich, M. Van Schoor, C. Boucher, F. Michon, and G. Van Oost; 3rd FTW PhD Symposium, Universiteit Gent, p. 49, 2002.

23. 'Refinement and Extension of a 1D Fluid Probe Model for Mach Probe Measurements'; P. Peleman and G. Van Oost; 5th FTW PhD Symposium, Universiteit Gent, p.42, 2004.

In the context of my PhD. work, I completed the postgraduate diploma: 'Doctoral Training in Engineering' which was issued by the Faculty of Engineering in October 2005.

2

Probe modelling

Probes suffer from the first law of diagnostics;
The ease of interpretation is inversely
proportional to the ease of implementation [Matt94]

The electrostatic probe is one of the fundamental techniques for measuring the properties of edge plasmas. Since it has been realized that edge conditions are of great importance for magnetically confined plasmas, probe diagnostics have found increasing use in fusion research. In particular, one of the most important current applications is the diagnosis of flowing edge plasma by means of Mach probes. Such plasma drifts may play a significant role in confinement-related phenomena such as enhanced cross-field transport, edge plasma instabilities, relaxations, etc. However, the theory of probe operation in strong magnetic fields is one of notorious difficulty. The difficulty with measurements of direct plasma particle fluxes is in establishing an understanding of just how the probe perturbs the plasma locally and how the local plasma parameters are then related to the unperturbed plasma far from the probe. The nature of this perturbation depends on the potential of the probe and the electric current drawn from it.

The goal of this chapter is not to consider all existing probes and probe models but rather to provide sufficient physical background on basic probe theory to allow us to concentrate on one particular probe model. Therefore, basic principles of a long and comprehensive history in probe modelling are summarized

in section 2.1. Section 2.2 is devoted to the review of the historical development and to describe a one-dimensional fluid probe model followed by the study of the reliability of this analytical model. Subsequently, in section 2.3 the model is validated using a kinetic simulation code and an extension in the model is proposed to allow to study probes with round collectors since such probes are employed in the CASTOR tokamak (chapter 4).

2.1 Basic principles of probe theory

2.1.1 Characterisation of a probe in unperturbed plasma

Let us first consider the presence of an object, a probe, which is not perturbing the plasma. The plasma is assumed to be homogeneous, infinite and quasi-neutral. Thus the ion density n_i equals the electron density n_e. Furthermore, the electrons and ions are assumed to be in thermal equilibrium with temperature T having an isotropic Maxwellian velocity distribution $f(\bar{v})$. In unperturbed plasmas, the number of particles (ions and electrons) with mass m crossing unit area per unit time, thus the 'particle flux density Γ', is

$$\Gamma = \frac{1}{4} n \bar{v} \tag{2.1}$$

with

$$\bar{v} = \sqrt{\frac{8kT}{\pi m}} \tag{2.2}$$

the mean particle speed and k is Boltzmann's constant. Since the ions are much heavier than the electrons and the object is present in a plasma in thermal equilibrium $(T_i = T_e)$, the mean ion speed will be much smaller than the mean electron speed so

that the total electric current from a probe of area A, if the plasma were unperturbed, would be dominated by the electrons:

$$I = -eA\left(\frac{1}{4}n_i\bar{v}_i - \frac{1}{4}n_e\bar{v}_e\right) \approx \frac{1}{4}eAn_e\bar{v}_e \quad > 0 \qquad (2.3)$$

The probe would thus emit a net positive current. If, for example, a probe were electrically insulated from other parts of the plasma device, then it would rapidly charge up negatively until the electrons were repelled and the net electrical current brought to zero. The potential adopted by such a 'floating' probe is called the floating potential V_{fl}. This potential is different (more negative) from the electric potential in the plasma in the absence of any probe. This latter potential is called the plasma (or space) potential V_p. Since a plasma is generally highly conducting it is considered to be an equipotential volume at the plasma potential V_p.

2.1.2 Effect of a potential-disturbing charge in the plasma

2.1.2.1 Debye shielding

In most cases the probe potential V is negatively charged with respect to the surrounding plasma ($V < V_p$). Then an increasing fraction of the electrons are reflected from the negative potential. The effects of a potential-perturbing charge in a plasma are generally much shorter-range than in a vacuum because the charges in the plasma tend to redistribute themselves so as to shield the plasma from the electric field the perturbing charge generates. The Poisson equation can be used to determine the length of this short-range effect. We assume that the ions do not move but that the electrons adopt a thermal equilibrium distribution in which the electron density is determined by the Boltzmann factor

$$n_e = n_\infty \exp\left(eV/T_e\right). \qquad (2.4)$$

T_e here is the electron temperature in energy units (eV) and n_∞ is the density far from the perturbing charge where the potential V is taken as zero. Poisson's equation is then

$$\nabla^2 V = \frac{-\rho}{\varepsilon_0} = \frac{-e}{\varepsilon_0}\left(n_i - n_e\right) = \frac{-e}{\varepsilon_0} n_\infty \left[1 - \exp\left(\frac{eV}{T_e}\right)\right]. \quad (2.5)$$

If we now suppose that $eV << T_e$, the following equation can be obtained:

$$\nabla^2 V - \frac{1}{\lambda_D^2} V = 0 \quad (2.6)$$

where

$$\lambda_D = \sqrt{\frac{\varepsilon_0 T_e}{e^2 n_\infty}} \quad (2.7)$$

is called the Debye length. Equation 2.7 was first derived by Debye and hence the characteristic length carries his name. In one dimension the solutions of equation 2.6 are $V \propto \exp\left(\pm x/\lambda_D\right)$. The perturbing effects of a charge will thus penetrate only of the order of λ_D. For laboratory plasmas, λ_D is of the order of micrometers. For example, a 1 eV temperature plasma with a density of 10^{17} m^{-3} has $\lambda_D = 20\mu m$, so the Debye length is much smaller than typical probe dimensions a which is of the order of millimetres. The supposition of $\lambda_D \ll a$, which will be used in the next paragraph, is therefore strongly satisfied.

2.1.2.2 Sheath formation

From the discussion above it is concluded that when a solid probe is in contact with a plasma the potential drop between the plasma and probe is mostly confined to a very narrow region. This region is called the sheath. In the sheath, charge neutrality is violated and the electric field is strong. The densities of electrons and ions must be determined by self-

consistently solving Poission's equation for the potential together with the equations of motion of the charged particles and hence their densities. The case of greatest interest is considering probes which are negatively charged with respect to the plasma potential so that the probe attracts ions and repels electrons. A simplified planar approximation of the sheath analysis is then adequate. Assuming that almost all electrons are reflected before they reach the probe the electrons adopt a thermal equilibrium distribution and the electron density can be approximated by the Boltzmann factor,

$$n_e \approx n_\infty \exp\left(eV/T_e\right) \tag{2.8}$$

The ion density must be calculated from the equation of motion. When assuming that the ion temperature is considerable less than the electron temperature one can suppose that the ions have zero energy at infinity. The ion velocity can then immediately be written as

$$\left|v_i\right| = \left(\frac{-2eV}{m_i}\right)^{1/2} \tag{2.9}$$

The total ion current crossing a surface A around the probe is constant. This current J_i is then:

$$J_i = An_i v_i = \text{constant} \tag{2.10}$$

Using the Poisson equation 2.5 becomes

$$\nabla^2 V = \frac{-e}{\varepsilon_0}\left[\frac{J_i}{A}\left(\frac{m_i}{-2eV}\right)^{1/2} - n_\infty \exp\left(\frac{eV}{T_e}\right)\right]. \tag{2.11}$$

This equation splits up into two distinct regions.

First, at large distances from the probe there is a plasma region in which quasi-neutrality $\left(n_i = n_e\right)$ is satisfied and the $\nabla^2 V$ can be neglected:

$$\frac{J_i}{A}\left(\frac{m_i}{-2eV}\right)^{1/2} = n_\infty \exp\left(\frac{eV}{T_e}\right) \tag{2.12}$$

The solutions of this equation is not $V =$ constant. There is a nonzero electric field in the plasma region. However, this field is very small compared to the field in the second region (see further). This second region includes a transition and a 'sheath' region that is presently treated together and called the sheath.
Differentiating the quasi-neutrality equation 2.12 to x results in a term in dV/dx. The coefficient of this term is

$$n\left(\frac{e}{T_e}+\frac{1}{2V}\right) \tag{2.13}$$

which is zero when $V = -T_e/2e$ showing that the plasma solution has infinite derivative at this potential. Therefore, the quasi-neutral approximation must break down, and a sheath form, at or before this potential:

$$V_s \geq -T_e/2e\,. \tag{2.14}$$

For the sheath region $\nabla^2 V$ cannot be ignored. Suppose that at the plasma-sheath boundary (x_s) the potential V_s is different from V_∞ $(= 0)$ because of the fields in the plasma region. At this boundary the solutions in the two regions much match, and that $\lambda_D \ll a$ and hence that x_s (generally several times λ_D) is also much less than a, the approximation of a planar geometry is justified, that is, taking A constant.
In the vicinity of the sheath the ion fluxes at the sheath entrance and in the plasma should be equal, i.e.

$$n_i = n_{is}\left(\frac{V_s}{V}\right)^{1/2}, \tag{2.15}$$

where subscript 's' denotes the values at the plasma-sheath interface. Now considering the plasma solution,

$$n_{is} = n_{es} \quad \left[= n_\infty \exp\left(eV_s/T_e\right)\right] \tag{2.16}$$

and combining this equation and equation 2.15 the Poisson's equation becomes:

$$\nabla^2 V = \frac{-e}{\varepsilon_0} n_s \left[\left(\frac{V_s}{V} \right)^{1/2} - \exp\left\{ \frac{e(V - V_s}{T_e} \right\} \right] \tag{2.17}$$

Solving this equation in the region close to x_s gives

$$\nabla^2 V = \frac{-e}{\varepsilon_0} n_s \left[-\frac{1}{2V_s} - \frac{e}{T_e} \right] (V - V_s). \tag{2.18}$$

There is only a proper sheath solution when the square bracketed term is negative. The maximum sheath edge voltage for proper sheath formation is thus:

$$V_s \leq -T_e/2e \tag{2.19}$$

This condition can be understood in the following way. In the sheath region the ion density n_i must exceed the electron density since the sheath has positive charge. The ion velocity v_i is given by the energy conservation. The particle flux $\Gamma_i = n_i v_i$ must therefore exceed some minimum value in the sheath. Having equation 2.19 provides this minimum velocity. Qualitatively, this condition was first explicitly derived by Bohm [Bohm49a,b]. He reported that proper sheath formation, i.e. a monotonic potential change at the Debye length scale, requires a condition for the flow velocity of the instreaming ions at the sheath edge. Assuming the plasma flow through the sheath one-dimensional and therefore directed along the surface-normal, the ions must reach a minimum velocity defined as the ion sound speed c_s,

$$v_{sh} \geq c_s = \sqrt{\frac{T_e}{m_i}} \tag{2.20}$$

This inequality is known as the Bohm criterion. It demands that the ions must have a sufficiently high velocity so that the decrease of the ion density towards the surface (caused by the acceleration of the electric field) is smaller than the decrease of the electron density governed by the Boltzmann factor. Only under this condition can the ion density in the entire sheath indeed remain higher than the electron density and therefore

keep the entire sheath positively charged as discussed above. However, equation 2.20 is only valid when $T_i = 0$; for a finite ion temperature the criterion is generalized [Riem91] to:

$$v_{sh} \geq c_s = \sqrt{\frac{T_e + \gamma T_i}{m_i}} \tag{2.21}$$

with γ the specific heat ratio of the ions.

The only way to satisfy both the plasma (equation 2.14) and the sheath region (equation 2.19) requirements is if

$$V_s = -T_e/2e \tag{2.22}$$

In conclusion, this potential is where the sheath edge always forms if the probe is sufficiently negative. This is always the case in the probe experiments presented in this thesis.

The region where the plasma flow becomes accelerated along the magnetic field line to reach sonic (or supersonic) velocities at the sheath edge is called the 'presheath' region which is located upstream to the sheath. Plasma and energy are fed into this region by diffusion and heat conduction from the main plasma and by ionization due to collisions within the layer itself. Therefore, collisional transport and relaxation within the flow has to be taken into account. The electric field in the presheath is much smaller (but at a larger scale length) than in the sheath, where the ions are further accelerated to supersonic speeds. The reason for the space-charge potential is the different acceleration of electrons and ions at the plasma edge by their respective thermal pressures. Electrons, in general, are slowed down by the electric field while ions are accelerated, so that the electric field effects equal fluxes of negative and positive charges to the sheath edge. It is therefore justified to assume that the presheath is quasi-neutral.

2.1.3 Probe theory in the zero magnetic field case

For simplicity first consider a probe inserted into the plasma in absence of a magnetic field. In this way the particle transport is determined only by the electric field.

2.1.3.1 Single unmagnetized probes

Of course, one can always bias the object with respect to V_p at any desired potential using an external circuit. Such a situation is only possible when using small objects, like probes, where a much bigger reference electrode is used. In tokamaks this reference electrode is generally the grounded conducting vacuum vessel or the limiter. In any case, the dimension of the probe is so small compared to the reference electrode that the current density, due to the probe's presence, has a negligible influence on the local plasma quantities. Under these conditions the probe is referred to as a 'single' probe.
Langmuir and collaborators [Lang24, Mott26] invented this diagnostic method for measuring both temperature and density with an electrostatic single probe, now called a Langmuir probe. The operating principle is very simple and a typical probe circuit is presented in figure 2.1.

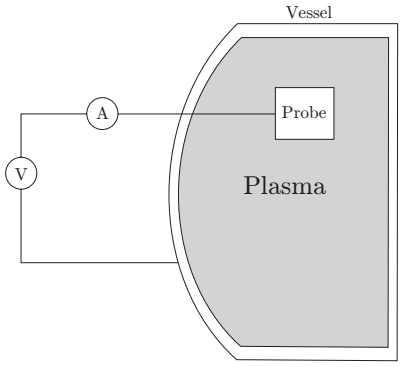

Figure 2.1: Basic operating principle of a single probe circuit.

The current I of a biased probe tip is measured as a function of bias voltage V with respect to a reference electrode resulting in a so-called I-V characteristic. Figure 2.2 shows a typical Langmuir probe I-V characteristic which can be divided into three distinct parts. To quantify the current collected by the probe as a function of the voltage it is again assumed that in the presheath the electrons adopt a thermal equilibrium distribution in the electron density (equation 2.8).

In the case when a sufficient negative probe voltage with respect to V_p is applied (part I), an increasing fraction of electrons in the sheath is repelled from the potential. Finally, the probe collects only positive ions, and the corresponding total negative current is called the ion saturation current $I_{i,sat}$ given by:

$$I_{i,sat} = -Aen_{i,sh}c_s \tag{2.23}$$

where subscript '*sh*' denotes the value at the sheath. In a quasi-neutral $\left(n_{i,sh} = n_{e,sh}\right)$ presheath the gradient in density between the unperturbed plasma and the presheath is expressed by $n_{e,sh} = \zeta n_\infty$ with ζ a value depending on the flow of the plasma ($\zeta = 0.5$ for non-streaming plasmas). Equation 2.23 can therefore be rewritten to an expression which relates the electron density at the sheath edge to the density of the unperturbed plasma:

$$I_{i,sat} \approx -Aen_{e,sh}c_s = -\zeta Aen_\infty c_s \tag{2.24}$$

In the transition part of the characteristic (part II) the potential on the surface approaches the plasma potential and the probes starts to collect both ions and electrons. The potential barrier for the electrons is lowered (becoming zero when $V = V_p$) and consequently the current increases exponentially:

$$I = I_{i,sat}\left(1 - \exp\frac{\left(V - V_p\right)}{T_e}\right) \quad \text{for } V < V_p \tag{2.25}$$

This current can also be rewritten as the product of the surface A and the current density J:

$$I = AJ_{i,sat} + AJ_{e,sat} \exp \frac{\left(V - V_p\right)}{T_e} \tag{2.26}$$

with $$J_{e,sat} = \frac{1}{4} en_{sh} \bar{v} = \frac{1}{4} en_{sh} \sqrt{\frac{8kT_e}{m_e}} \tag{2.27}$$

and $$J_{i,sat} = -en_{sh} c_s \tag{2.28}$$

When further increasing the probe voltage ($V > V_p$), all ions are repelled and the electron current is maximized since all arriving electrons are collected. In this region (part III) a current equal to the electron saturation current $I_{e,sat}$ will flow quantified by equation 2.27.
Implying the condition that $V = V_{fl}$ when $I = 0$ into equation 2.25 a total potential drop of

$$V_p - V_{fl} = \frac{T}{2} \ln \left(2\pi \frac{m_e}{m_i} \left(\gamma \frac{T_i}{T_e} + 1 \right) \right) \tag{2.29}$$

is found which results in the case of cold ions ($T_i << T_e$) to the well-known drop of approximately $3kT_e/e$ for a floating probe system. A floating probe system is thus a probe which is electrically insulated from the plasma in which the potential adjusts itself so as to reduce the electron flux to the surface until it is equal to the ion flux.

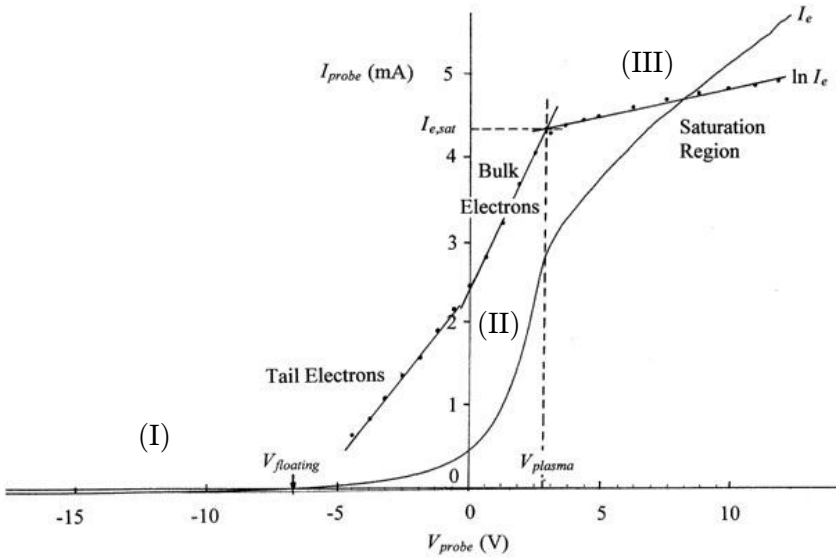

Figure 2.2: Typical Langmuir probe I-V characteristic.

2.1.3.2 Double unmagnetized probes

There are times when a single probe may be difficult to use. For example, there may be no well-defined counter-electrode to be used as a reference. There could also be large fluctuations in the plasma potential induced by waves or turbulence in the plasma which lead to noise in the measured current. Johnson and Malter [John50] developed a double probe system which floats at the plasma potential and therefore deals with these problems. In chapter 3 and 4 results of flow measurements are presented using an array of Mach probes or a so-called Gundestrup probe [Mac92]. A Mach probe consists of two collectors isolated from each other so it can be considered as a double probe system (figure 2.7). A schematic drawing of a double probe is shown in figure 2.3.

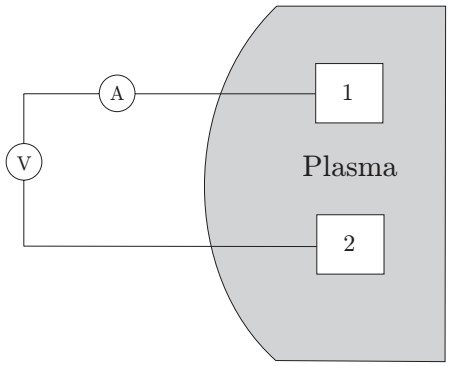

Figure 2.3: The double probe. The entire electrical circuit can be isolated from the vacuum vessel or wall.

If a potential V_{pr} is introduced between the two probes of comparable dimension, a current I_{pr} flows in the circuit. This applied voltage is independent of the plasma potential, i.e. the system is floating. The current-voltage characteristic equation can be developed by treating each probe (denoted as 1 and 2 in subscript) as a single Langmuir probe, adding the constraint that the system floats, i.e. the net current drawn from the plasma is zero thus a current I_{pr} flows in probe 1 and - I_{pr} in probe 2.

$$\begin{cases} I_1 = A_1 J_{i1,sat} + A_1 J_{e1,sat} \exp \dfrac{e\left(V_1 - V_{p1}\right)}{kT_e} \\ I_2 = A_2 J_{i2,sat} + A_2 J_{e2,sat} \exp \dfrac{e\left(V_2 - V_{p2}\right)}{kT_e} \end{cases}, \tag{2.30}$$

$$V_{pr} = V_1 - V_2, \tag{2.31}$$

and

$$I_1 = -I_2 = I_{pr}. \tag{2.32}$$

A representative double probe characteristic is shown in figure 2.4 and can be described by an analytical expression derived by combining equations 2.30-2.32.:

$$I_{pr} = -I_{i1,sat}\frac{1-\exp\left(-\dfrac{V_{pr}-\left(V_{p1}-V_{p2}\right)}{T_e}\right)}{\alpha+\exp\left(-\dfrac{V_{pr}-\left(V_{p1}-V_{p2}\right)}{T_e}\right)} \tag{2.33}$$

with $$\alpha = \frac{I_{i1,sat}}{I_{i2,sat}} \tag{2.34}$$

Here only the difference in plasma potential in front of the two probes is considered. In the practical case of a Mach probe with equal collectors $\left(A_1 = A_2 = A\right)$ the assumption $J_{e1,sat} = J_{e2,sat}$ is justified since it is anyhow much larger than $J_{i,sat}$. Furthermore, the density and temperature at both probes can be assumed equal. Note that the current in such a closed circuit can never exceed the ion saturation current of the single probe for both positive and negative voltages:

$$\begin{cases} \lim\limits_{V_{pr}\to+\infty}\left(I_{pr}\right) = -I_{i2,sat} \\ \lim\limits_{V_{pr}\to-\infty}\left(I_{pr}\right) = I_{i1,sat} \end{cases} \tag{2.35}$$

For example, if probe 1 is positive with respect to V_{p1}, the electron current is limited by ion saturation current which is drawn by probe 2 on the negative side. Consequently the electron saturation part of the characteristic is avoided which is advantageous in avoiding possible damage to the probe coming from heat fluxes mainly driven by electron saturation currents. Moreover, the electron saturation part of the characteristic provides little extra information beyond what can be deduced from the characteristic in the ion saturation and floating potential region. In a non-streaming plasma (and equal collecting area) the ion saturation currents of both probes should be equal based on equation 2.23. However, this is only the case for non-streaming plasmas. When a flow exists the ion saturation currents differ and the *I-V* characteristic becomes an asymmetric hyperbolic tangent as shown in figure 2.4. The

electron temperature can be deduced from the slope of the characteristic at $V\left(I=0\right)$ by differentiating equation 2.33:

$$T_e = \frac{I_{i1,sat} + I_{i2,sat}}{4\left(\frac{dI_{pr}}{dV_{pr}}\right)_{V(I=0)}} \tag{2.36}$$

The density can then by determined using equation 2.24 again being only valid for non-streaming plasmas.

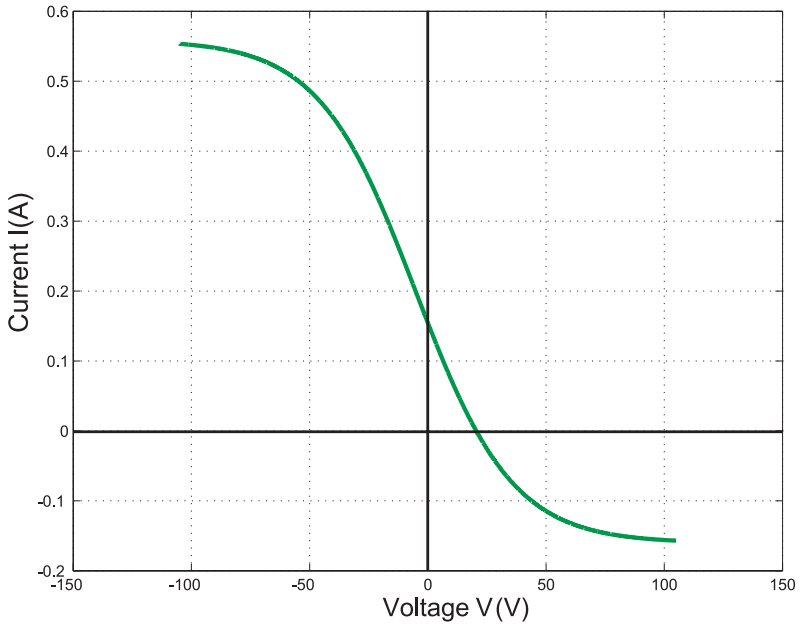

Figure 2.4: Typical Langmuir probe *I-V* characteristic of a double probe.

2.1.4 The importance of the magnetic field

All the analysis thus far has tacitly assumed that no magnetic field B is present, so the particle dynamics are determined only by the electric field. The boundary layer problem in magnetized plasmas is of particular importance for the theoretical understanding of controlled fusion experiments. In the case where probes are to be used in magnetized tokamak plasmas, the probe theory becomes much more complex and the effects of the magnetic field need to be investigated.

2.1.4.1 General remarks

A magnetic field forces charged particles to gyrate along the magnetic field lines in circular orbits of radius $\rho = mv/eB$, called the Larmor or gyro radius. In collisionless plasma the ions and electrons are no longer allowed to travel perpendicular to the magnetic field lines. The importance of the field is obviously determined by the ratio of ρ to the typical dimension a of the probe. The electrons are more strongly affected since the electron Larmor radius is clearly much smaller than the ion radius (for comparable T_i and T_e). However, in our case of interest of a strong magnetic field ($\rho_i < a$) also the ions are considerably modified. In the following it is discussed that in the condition of a strong magnetic field it might no longer be possible to formulate a completely collisionless probe theory when assuming that quasi-neutrality outside the sheath holds.

As before, the electrons are taken to be governed by the Boltzmann factor (equation 2.4). The ion density is calculated from the equation of motion assuming that the ion temperature is considerably less than the electron temperature so that the ions have zero energy at ∞. The ion velocity can then be written as:

$$v_i = \sqrt{\frac{-2eV}{m_i}} \tag{2.37}$$

Combining this equation with equations 2.8 and 2.23 the quasi-neutral equation reads:

$$\frac{I_i}{A}\sqrt{\frac{m_i}{-2eV}} = n_\infty \exp\left(\frac{eV}{T_e}\right) \tag{2.38}$$

It was found [Hut00] that in the case of a plane collector area A (one-dimensional flow) a constant potential (independent of distance) solves equation 2.38. Thus the conditions of zero potential at infinity (unperturbed plasma) and a potential drop of $V = T_e/2e$ (equation 2.22) at the sheath edge are not retrieved. The condition of a quasi-neutral presheath might only be obtained when allowing it to expand until plasma-sources or collisional terms become important. Therefore, the presheath stretches along the direction of B forming a long 'flux tube' in which the ions are collected. Consequently, in the case of a strong magnetic field the development of a 'collisional' theory may be inevitable. However, Hutchinson has shown that a reasonable (within the accuracy of measurement) estimation of the ion density can still be obtained when using a slightly adapted version of the Bohm formula for the zero field case. Based on the fact that in a strong magnetic field ions are forced to flow along the field (not across it) he concluded that equation 2.23 is still valid except that the total probe collecting area A must be replaced by the area projected onto the magnetic field direction, i.e. A'. However, this conclusion has grown from the assumption that the ion collection in a strong magnetic field is quasi-collisionless. In the following a review on the discussion of Hutchinson whether this quasi-collisionless treatment is appropriate, is given. In the same context, Chodura [Chod82] has shown that an additional region arises in the presheath imposing an extra criterion for the velocity of the ions at the entrance of that region.

2.1.4.2 Collisions in a magnetic field

The presheath can be assumed collisionless when the magnitude of the ion mean free path along the field lines l is greater than the length of the collection region L_f i.e. the presheath. If $l < L_f$, collisions must be taken into account. In this discussion only ion-electron collisions are considered since ion-ion collisions do not change the total ion momentum. The length of the collection region is assumed big enough to allow sufficient net ion flow across the magnetic field into the flux tube sources (I_1) balancing the loss of parallel collection flow when they enter the sheath region (I_2). Let us consider the 2D probe-like case of a limiter shown in figure 2.5.

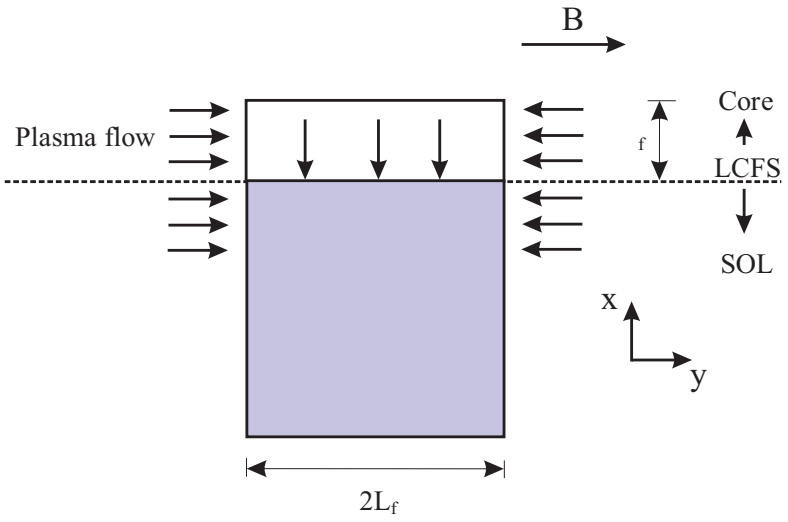

Figure 2.5: Schematic of a limiter or probe with the front face, of length $2L_f$, parallel to $\vec{B}$.

The cross-field (perpendicular) particle flux $D_\perp \nabla_\perp n$ is driven by perpendicular diffusion of ions governed by a diffusion coefficient $D_\perp$. Furthermore, the perpendicular scale length (width of the flux tube) is assumed equal to the thickness of the object extending inward over some radial distance λ_f. The decay of density towards the surface is expressed by

$n(x) = n_\infty \exp(-x/\lambda_f)$ with n_∞ the density of the unperturbed plasma. Then the ion current due to the cross-field flux along the whole tube length for a circular tube is:

$$I_1 \approx SnV_\perp = S\Gamma_\perp = SD_\perp \nabla_\perp n = -2L_f D_\perp \frac{n}{\lambda_f} \tag{2.39}$$

where $2L_f$ is the length of the front face and n the unperturbed density. This current is then balanced by the current collected at the sheath (local sink) which is described by equation 2.24:

$$I_2 = -\frac{1}{2}(2\lambda_f)\, nc_s \tag{2.40}$$

where the factor 2 on the right hand side is due to the collection from both sides, while the factor 1/2 is due to the density drop at sonic conditions. After equalization we find:

$$L_f \approx \frac{\lambda_f^2 c_s}{2D_\perp} \tag{2.41}$$

If the ions with mean ion thermal velocity v_{ti} also have a parallel diffusion coefficient $D_{//}$ the mean free path along the field lines is

$$l \approx \frac{D_{//}}{v_{ti}} \tag{2.42}$$

The ratio of l to L_f is then:

$$\frac{l}{L_f} \approx \frac{2D_\perp D_{//}}{\lambda_f^2 c_s v_{ti}} \tag{2.43}$$

Classical collisional diffusion gives

$$D_\perp = \rho_i^2 \nu_c \quad \text{and} \quad D_{//} = v_{ti}^2/\nu_c \tag{2.44}$$

with ν_c the collisional frequency and ρ_i the ion Larmor radius. Finally the ratio becomes,

$$\frac{l}{L_f} \approx 2\left(\frac{\rho_i}{\lambda_f}\right)^2 \frac{v_{ti}}{c_s} \tag{2.45}$$

Since the ion thermal speed is always less than the sound speed and $\rho_i < \lambda_f$ for a strong field, it is concluded that $l < L_f$ and collision are important. Therefore, it seems that a quasi-collisionless treatment to model the presheath when using classical collisional diffusion is not appropriate.
However in many plasmas, e.g. in tokamaks, the cross-field particle diffusion is more substantially enhanced with respect to what the classical transport theory (equations 2.44) predicts. This generally observed phenomenon in the present fusion experiments is called 'anomalous transport'. The anomaly in the transport is represented by a strong increase of $D_{\perp,//}$ which is in the present fusion experiments sufficient to make $l > L_f$ thus making the quasi-collisionless approach possibly applicable. So, even in the case when a strong magnetic field exists, the ion current might still be retrieved using equation 2.23 in which A is replaced by the projected area A' as discussed above.

2.1.4.3 The Bohm-Chodura criterion

In contrast to the so far considered case of a magnetic field perpendicular to the collectors, Chodura [Chod82] investigated the case where the magnetic field lines intersect at an angle between normal and nearly grazing. He showed that when the magnetic field is at some oblique angle to the surface, an additional presheath, the 'magnetic presheath' develops upstream of the Debye sheath. The size of the region $(\sim \rho_i)$ depends on the ion gyro radius and the angle of B to the normal of the surface. He found that in this region, in contrast to the Debye sheath, quasi-neutrality is fulfilled and that a significant electric field exists. This electric field is directed parallel to the normal of the sheath and is strong enough to deflect the ions from their motion along the magnetic field. The total potential drop in the magnetic presheath and the sheath is again $3kT_e/e$ similar to the drop which solely occurs in the Debye sheath when the magnetic field is perpendicularly directed to the surface. Beyond the Bohm criterion at the sheath edge (equations 2.20, 2.21), Chodura postulated a second condition of

supersonic flow parallel to B at the magnetic presheath entrance (MPSE), i.e. the Bohm-Chodura criterion [Chod95]:

$$v_{//,MPSE} \geq c_s \tag{2.46}$$

Thus the electric field in the presheath accelerates the ions to at least sonic speed at the MPSE and the function of the electric field in the magnetic presheath is then to turn the plasma flow from being (at least) sonic along B in the presheath to being (at least) sonic perpendicular to the solid surface and thus the particles are assumed to be collected once they have reached the MPSE. Since only $n_e = n_i$ is permitted in the quasi-neutral presheath and magnetic presheath and $n_e > n_i$ is the condition in the sheath, one might think that supersonic plasma flow into the magnetic presheath is prohibited. However, Chodura [Chod82], Riemann [Riem94] and Stangeby [Sta95a,b] showed that supersonic flow parallel to the magnetic field at the MPSE is allowed. There are thus, in general, three spatial regions schematically shown figure 2.6: (a) the electrostatic Debye sheath; (b) upstream of it, the magnetic presheath; and (c) upstream of that, the presheath.

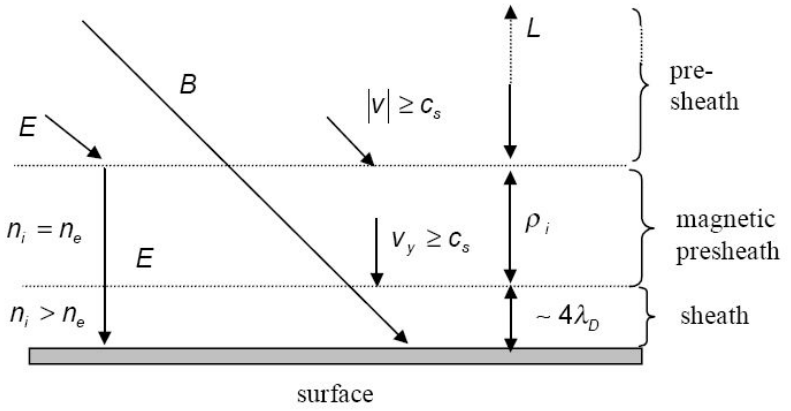

Figure 2.6: Schematic picture of the electrostatic Debye sheath, the magnetic presheath, and the presheath. v_y is the velocity component perpendicular to the surface.

2.2 Investigation of the reliability of a 1D fluid model for Mach probe measurements

In this paragraph the results of an *Investigation of the reliability of a 1D fluid model for Mach probe measurement* by P. Peleman, S. Jachmich, M. Van Schoor, and G. Van Oost published in Czechoslovak Journal of Physics, 55(12):1597, 2005 are presented. The introduction part of this publication is substantially extended in order to improve the readability of the subsequent paragraphs. In particular, the historical development and demystifying description of a 1D fluid model is presented in more detail.

2.2.1 Abstract

In this paper we show how a one-dimensional fluid model can be used to interpret data obtained from an inclined Mach probe or a Gundestrup probe. We use an analytical approximation of the solution of the differential equations describing the relation between the plasma flow and the measured ion saturation currents at the probe's surface. The parameters of the approximate analytical solution are determined by comparison with the exact numerical solution of the equations. In this way we are able to measure the parallel as well as the perpendicular Mach numbers over the whole parameter range with a minimum accuracy of 90%.

2.2.2 Introduction

Mach probes [Oth78] are common diagnostic to measure the flows and electric field profiles in the edge of fusion machines. Figure 2.7 shows a typical Mach probe geometry indicating the

parallel $(//)$, perpendicular $(\perp)$ and radial (r) directions. The probe is inclined over an angle θ with respect to the magnetic field line. The (x-y) reference indicates the parallel and perpendicular directions to the probe surface. We define the upstream collector as the one which faces the flow vector in the direction of the magnetic field. The opposite collector is then the corresponding downstream collector.

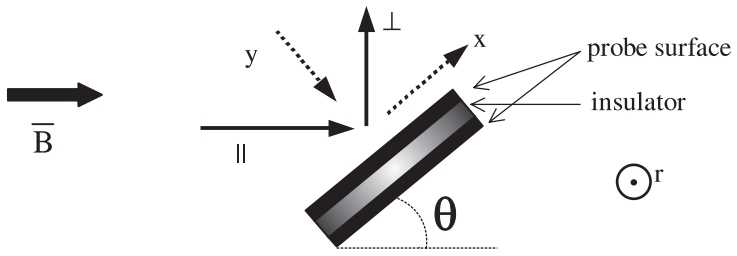

Figure 2.7: A typical Mach probe geometry.

The Mach numbers $M_{//,\perp}$ of the parallel and perpendicular (in the magnetic surface, but perpendicular to the magnetic field) flow of the unperturbed plasma are defined by the ratio of the ion plasma flow velocity $v_{//,\perp}$ to the ion acoustic velocity or sound speed c_s:

$$M_{//,\perp} = \frac{v_{//,\perp}}{c_s} \tag{2.47}$$

They can be derived from the ratio R of the up- and downstream ion saturation currents $I_{sat,\substack{up\\down}}$:

$$R = \frac{I_{sat,up}}{I_{sat,down}} \tag{2.48}$$

To derive $M_{//}$, Hutchinson [Hut87] has developed a fluid theory to describe Mach probe operation in a strong magnetic field which models a quasi-neutral presheath as a one-dimensional (1D), two-fluid plasma. One might argue that treating a two- (2D) or even three-dimensional (3D) situation might limit the accuracy of a 1D approach. Therefore, Hutchinson constructed a 2D code [Hut88a] of which the calculations have shown quite remarkable quantitative agreement with the corresponding results obtained from the 1D code. The agreement between the 1D and 2D approach is based on the fact that the nature of cross-field transport, whether it is cross-field current or coherent (perpendicular) flow, is not affecting the total collected current. The presheath can therefore be described solely in the parallel direction by treating the perpendicular diffusion equation as a source term in the parallel equations. These sources determine the parallel extend of the presheath so that the fast parallel-field flow collection is balanced by sufficient (slow) cross-field diffusion into the presheath. In absence of this source term, a quasi-neutral presheath would be forced to elongate to infinity along the $B-$ field (see discussion, section 2.1.4.1).

Van Goubergen [VG99a] extended this model to determine not only $M_{//}$ but also $M_{\perp}$. He showed that in order to study the influence of $M_{\perp}$ on R the probe must be inclined $(\theta \neq 90°)$ with respect to the magnetic field (figure 2.7).

These models essentially relate the ion saturation currents measured at the probe's surfaces to the Mach numbers of the flow of the plasma not perturbed by the probe via a set of coupled differential equations. The numerical solutions of these equations can be approximated by an analytical function $\ln(R) = c\left[M_{//} + M_{\perp}\cot(\theta)\right]$, were c is a constant equal to 2.21 [Pel02]. However, a comparison with the numerical solution of the differential equation shows that c depends on $M_{//}, M_{\perp}$ and θ, resulting in an underestimation of the Mach numbers when the analytical model with constant c is used. For values up to $M_{//,\perp} = 0.6$ the error made is rather small but increases to 25% for larger values as for example encountered in biasing experiments [Jac98, VS03, Weyn93]. Based on the numerical

(exact) solution of the differential equations we developed an expression for c in which the dependency on $M_{//}, M_{\perp}$ and θ has been taken into account. This technique allows us to drastically reduce the errors. In the following section we describe the fluid model and we show the consequences of the use of a constant c. We then introduce the proposed function for c and quantify the improvement.

2.2.3 Description of a Mach probe by a 1D fluid model

Hutchinson's model starts from the full 3D ion continuity equation 2.49 and the parallel ion momentum equation 2.50 for a steady state plasma $(\partial/\partial t = 0)$:

$$\frac{\partial}{\partial //}\left(n_i v_{//}\right) + \frac{\partial}{\partial \perp}\left(n_i v_{\perp}\right) + \frac{\partial}{\partial r}\left(n_i v_r\right) = 0 \tag{2.49}$$

$$\begin{aligned} &\frac{\partial}{\partial //}\left(m_i n_i v_{//}^2\right) + \frac{\partial}{\partial \perp}\left(m_i n_i v_{//} v_r\right) + \frac{\partial}{\partial r}\left(m_i n_i v_{//} v_r\right) \\ &\qquad - \eta \frac{\partial^2 v_{//}}{\partial r^2} = -\nabla_{//} p_i + e n_i E_{//} \end{aligned} \tag{2.50}$$

where m_i, n_i, p and v are the ion mass, ion density, the total pressure, and fluid velocity. Anomalous shear viscosity η is considered, but no volume source (e.g. ionization) or collisional friction. Combination of these equations results in a 1D model that relates the density in the presheath and the parallel Mach number at infinity $(n, M_{//,\infty})$ to the density at the probe surface (n_s) which can be measured via the ion saturation current given by $\left|I_{i,sat}\right| = e n_s c_s A$, where A is the surface of the collector and c_s the sound speed of the ions. To measure the perpendicular flow one has to incline the surface of the collectors with respect to the flow and extend the model as has

been done by Van Goubergen. The following assumptions were made:

- A quasi-neutral presheath; the Poisson's equation is therefore replaced by the quasi-neutrality equation,

$$n_i = n_e \tag{2.51}$$

- In the consideration of ion collection, the probe is sufficiently negative to repel the majority of electrons and the electron density is governed by the Boltzmann factor, i.e. equation 2.8. The electron temperature is expressed in units of energy, i.e. in eV, and assumed to be constant. Combining equation 2.8 and 2.51 the parallel electric field $E_{//}\left(=-\nabla_{//}V\right)$ can be expressed as:

$$E_{//} = -\frac{T_e}{en_i}\nabla n_i \tag{2.52}$$

Using the ion energy equation [Brag65], $p_i = c^{st} n_i^{\gamma}$, with γ the specific heat ratio of the ions and $p_i = n_i T_i = c^{st} n_i^{\gamma-1}$ gives

$$\nabla_{//} p_i = \gamma T_i \nabla_{//} n_i = -m_i c_s \nabla_{//} n_i \tag{2.53}$$

- Since the probe causes a local perturbation of the plasma and acts as a sink for particles, the radial diffusive influx can be given by

$$n_i v_r = -D\frac{\partial n_i}{\partial r} \tag{2.54}$$

with D the anomalous diffusion coefficient assumed to be constant.

- The anomalous shear viscosity η is assumed to be related to D by

$$\eta = \alpha m_i n_i D \tag{2.55}$$

with α an arbitrary constant. Introducing non-dimensional variables: $n = n_i / n_{i,\infty}$, with $n_{i,\infty}$ the unperturbed ion density; $M_{//,\perp} = v_{//,\perp} / c_s$; and non-dimensionalizing coordinate transformation: $//' = \left(D / c_s a^2\right) //$, $\perp' = \left(D / c_s a^2\right) \perp$, $r' = r/a$ and considering all the above assumptions, equations 2.49, 2.50 are transformed to:

$$\frac{\partial}{\partial //}\left(nM_{//}\right) + \frac{\partial}{\partial \perp}\left(nM_{\perp}\right) - \frac{\partial^2 n}{\partial^2 r} = 0 \tag{2.56}$$

$$\begin{gathered}\frac{\partial}{\partial //}\left(nM_{//}^2\right) + \frac{\partial}{\partial \perp}\left(nM_{\perp}M_{//}\right) - \frac{\partial}{\partial r}\left(M_{//}\frac{\partial n}{\partial r}\right) \\ - \alpha n \frac{\partial^2 M_{//}}{\partial r^2} = -\frac{\partial n}{\partial //}\end{gathered} \tag{2.57}$$

where the primes on the new co-ordinates are dropped after transformation. The assumption of a constant D is therefore justified since it only changes the length of the presheath.
Next, equations 2.56 and 2.57 can be transformed into a 1D model in the following way. The cross-field gradients over the radial dimension of the probe are linearized by replacing $\nabla_r \psi \to \left(\psi_\infty - \psi\right)$ and $\nabla_r^2 \psi \to \left(\psi_\infty - \psi\right)$, where ψ is a general variable for density and flow velocity and ψ_∞ is the unperturbed quantity. The equations are then transformed to the (x, y) coordinate system parallel and perpendicular to the probe surface (figure 2.7):

$$\begin{cases}\dfrac{\partial}{\partial //} = \dfrac{\partial y}{\partial //}\dfrac{\partial}{\partial y} = \sin(\theta)\dfrac{\partial}{\partial y} \\ \dfrac{\partial}{\partial \perp} = \dfrac{\partial y}{\partial \perp}\dfrac{\partial}{\partial y} = -\cos(\theta)\dfrac{\partial}{\partial y}\end{cases} \tag{2.58}$$

Here, it is assumed that the quantities do not vary along the probe surface $(\partial/\partial x = 0)$ which is an assumption identical to the condition of axi-symmetry in a tokamak when treating the flow towards the limiter and divertor surface [Bael91, Chod88, VS98b]. The resulting transport equations in the y - direction are then retransformed back to the $(//, \perp)$ coordinate system. The main assumption here is that $v_\perp$ remains constant in the presheath, i.e. $\partial M_\perp / \partial \perp = 0$ therefore assuming that the probe does not have a drag on the perpendicular flow [VG99b]. Finally, the resulting transport equations are:

$$\frac{\partial n}{\partial //} = \frac{\left(M_{//} - \frac{M_\perp}{\tan(\theta)}\right)(1-n) - \left(M_{//,\infty} - M_{//}\right)}{\left(M_{//} - \frac{M_\perp}{\tan(\theta)}\right)^2 - 1} \tag{2.59}$$

$$\frac{\partial M_{//}}{\partial //} = \frac{-(1-n) + \left(M_{//} - \frac{M_\perp}{\tan(\theta)}\right)\left(M_{//,\infty} - M_{//}\right)}{n\left[\left(M_{//} - \frac{M_\perp}{\tan(\theta)}\right)^2 - 1\right]} \tag{2.60}$$

with $\alpha = 1$ justified from the argumentation in [Hut88a,b]. The unperturbed plasma, i.e. the plasma at infinite distance from the probe, is thus described by the parallel Mach number $M_{//,\infty}$ and a normalized density $n = 1$. With these starting values we solve this set of coupled differential equations 2.59 and 2.60 numerically and obtain the spatial variation of the density and parallel Mach number in the presheath as shown in figure 2.8 and 2.9. The non-dimensional parallel distance is chosen such that $// = -\infty$ defines the unperturbed plasma and $// = 0$ the Magnetic Presheath Entrance (MPSE), defined by the Bohm-Chodura boundary condition (equation 2.46):

$$M_{//,MPSE} = \frac{M_\perp}{\tan(\theta)} \pm 1 \tag{2.61}$$

This condition is a result from the singularity of the denominators of equations 2.59 and 2.60 and limits the velocity at the MPSE to sonic speed. Furthermore, the treatment of values for $M_{//,\infty}, M_{\perp}$ and θ is limited by equation 2.61 so not all combinations are permitted. Figures 2.8 and 2.9 show three cases $(\theta = 50°,\ 90°$ and $130°)$ for given values of $M_{//,\infty}$ and $M_{\perp}$. We plotted the evolution of the density (figure 2.8) and of the parallel Mach number (figure 2.9), both for the up- and downstream collectors. When $\theta = 90°$, the system is insensitive to perpendicular flow and the ions reach the sound speed at the MPSE. When the probe is inclined, perpendicular flow is measured, and the parallel Mach number at the MPSE has to adapt itself to a value imposed by equation 2.61. Figure 2.8 shows that, due to the conservation of particles, the ion density in the presheath must decrease when the ions accelerate towards the MPSE.

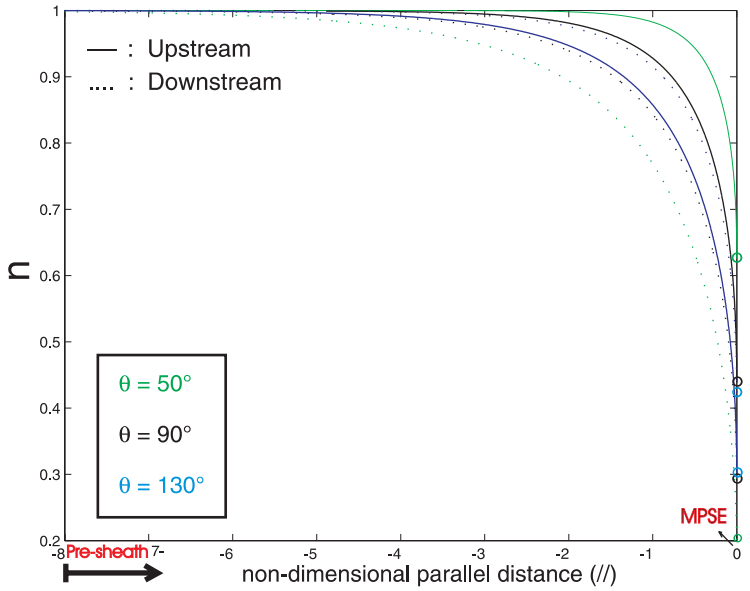

Figure 2.8: The spatial variation of the density in the presheath for $\left|M_{//,\infty}\right| = 0.2$ and $\left|M_{\perp}\right| = 0.4$.

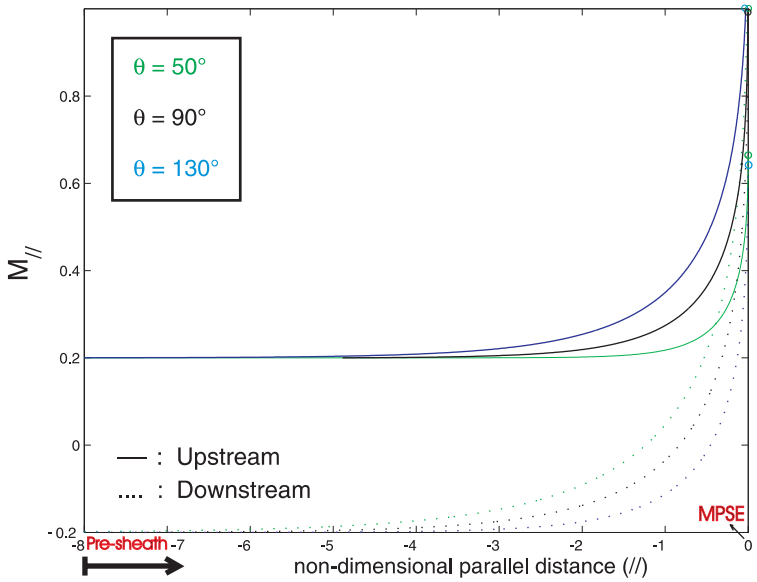

Figure 2.9: The spatial variation of the density in the parallel Mach number in the presheath for $\left|M_{//,\infty}\right| = 0.2$ and $\left|M_{\perp}\right| = 0.4$.

Dividing equation 2.59 by 2.60 immediately gives the evolution of the density as a function of the parallel Mach number:

$$\frac{\partial n}{\partial M_{//}} = n\frac{\left(M_{//} - \dfrac{M_{\perp}}{\tan(\theta)}\right)(1-n) - \left(M_{//,\infty} - M_{//}\right)}{-(1-n) + \left[\left(M_{//} - \dfrac{M_{\perp}}{\tan(\theta)}\right)\left(M_{//,\infty} - M_{//}\right)\right]} \tag{2.62}$$

A solution for a given $\left|M_{//,\infty}\right| = 0.2$ and $\left|M_{\perp}\right| = 0.4$ is shown in figure 2.10. The value at density $n = 1$ defines the parallel Mach number of the unperturbed plasma. The curves end at the MPSE, hereby defining the values of $M_{//,MPSE}$ and n_{sh}. If we apply this procedure in the range $-1 \le M_{//,\infty} \le 1$ for a given $M_{\perp}$ and θ and retain the associated sheath density at the MPSE, a relation between $M_{//,\infty}$ and n_{sh} is obtained. An

example is shown in figure 2.11 for $|M_{\perp}| = 0.4$ and four different values of θ. The curves end at a value imposed by the boundary condition (equation 2.61), e.g. for $\theta = 150°$ and $M_{\perp} = 0.4$ the maximum parallel Mach number is $\pm\ 0.3$.

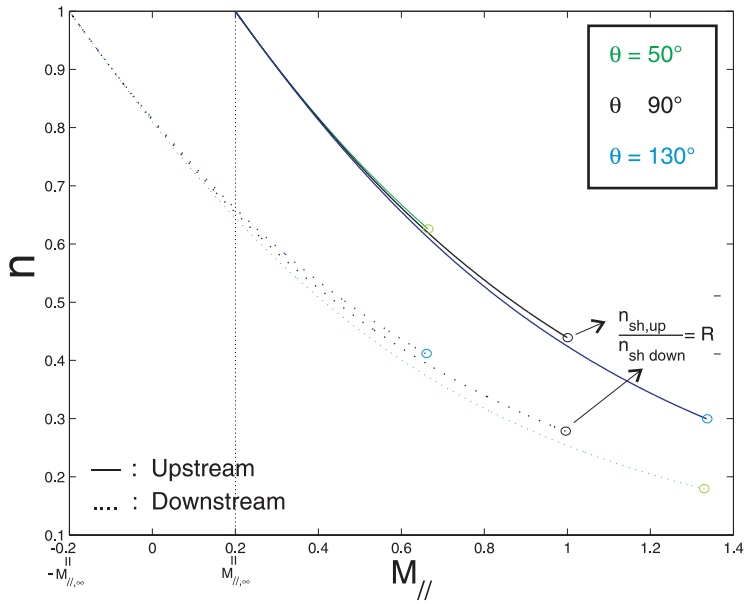

Figure 2.10: The normalized density as a function of $M_{//}$ for $|M_{//,\infty}| = 0.2$ and $|M_{\perp}| = 0.4$.

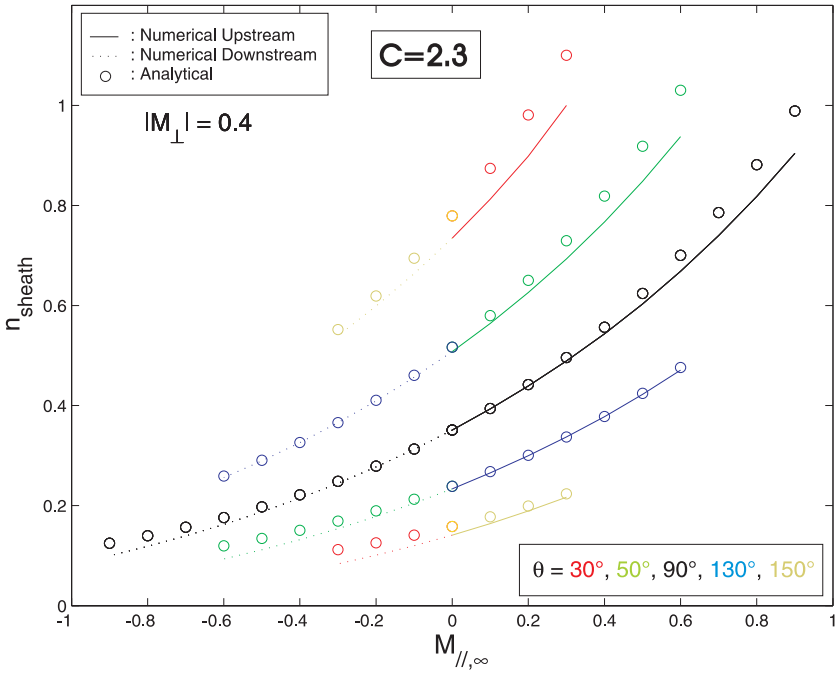

Figure 2.11: The normalized density as a function of $M_{//}$ for $|M_{//,\infty}| = 0.2$ and $|M_{\perp}| = 0.4$.

For the experiment, the ratio $R = I_{sat,up}/I_{sat,down}$ is important. With the numerical results we can determine this ratio via $R = n_{sh,up}/n_{sh,down}$. An approximate analytical solution of equation 2.62 for the density at the presheath entrance, was proposed by Hutchinson and extended by Van Goubergen:

$$n_{sh}^{up}_{down} = \exp\left[c_{\substack{up\\down}} \left(\pm|M_{//,\infty}| \pm \frac{|M_{\perp}|}{\tan(\theta)} \right) - c_0 \right] \qquad (2.63)$$

The values of $c_{\substack{up\\down}}$ and c_0 can be determined by taking values of n_{sh} produced by the numerical solution of equation 2.62. Setting $M_{//,\infty} = 0$ and $\theta = 90°$ in equation 2.63, one finds $c_0 = -\ln(n_{sh}) \approx 1.05$, while $c_{\substack{up\\down}} = \ln\left(n_{sh}^{up}_{down}\right) + c_0 \Big/ \pm|M_{//,\infty}|$

depends on $M_{//,\infty}$. This choice makes the fit between the approximate analytical solution and the exact numerical solution rather good for small values of $M_{//,\infty}$ and values of θ close to 90°. The solution however diverges for higher values of $M_{//}$ (as shown in figure 2.11) and the error can no longer be neglected. For the ratio R we get

$$\ln(R) = c\left[\left|M_{//,\infty}\right| + \left|M_{\perp}\right|\cot(\theta)\right] \tag{2.64}$$

with

$$c = c_{up} + c_{down}. \tag{2.65}$$

The dependence of c on $M_{//,\infty}$, $M_{\perp}$ and θ was found to be weak. In the past a constant value of $c = 2.3$ was used [Pel02] and the disagreement with the numerical exact solutions, when not taking into account any dependency, was ignored. However in figures 2.11 and 2.12 one can see that, under certain conditions, the error can no longer be neglected. For example, for a given $M_{\perp} = 0.5$ and $M_{//,\infty} = 0.4$ (figure 2.12, vertical dashed line) the results diverge from the numerical ones for bigger inclination angles of the probe. Figure 2.11 shows also that the approximated analytical solution for the sheath density reaches values higher than one which indicates an overestimation. The value for c is too big for those cases. On the other hand, when θ is kept constant the error builds up with growing parallel flow. The latter effect is also shown in figure 2.13 where we plot the perpendicular Mach number of the approximated versus numerical solution for a constant $\theta = 100°$. We conclude that the error increases with growing parallel Mach number. Furthermore, for these settings, the weak dependency on $M_{\perp}$ is demonstrated by a nearly constant slope of the curves.

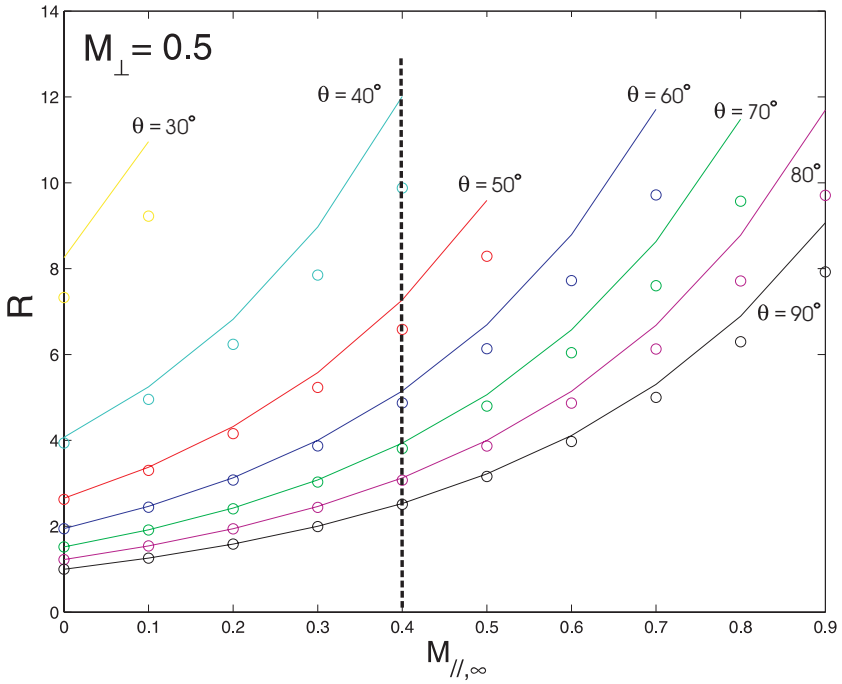

Figure 2.12: The ratio R as a function of $M_{//,\infty}$ for different inclination angles of the probe at a fixed $M_{\perp} = 0.5$.

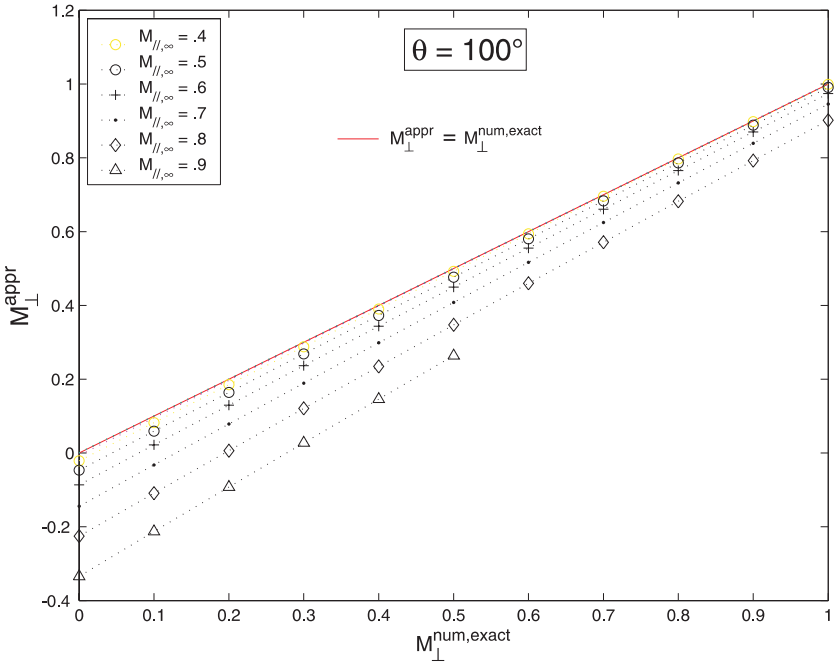

Figure 2.13: The approximated $M_{\perp}^{appr.}$ versus the numerical $M_{\perp}^{num.}$. The red solid line represents the case for which $M_{\perp}^{appr.}$ is equal to $M_{\perp}^{num.}$.

Therefore, in the following we present a better definition for c, which minimizes the error between the approximated analytical solutions and the exact numerical solution and so the underestimation of the flows.

2.2.4 Improvement of the approximated expression

Basically we will investigate the possibility to derive an analytical expression for $c\left(M_{//,\infty}, M_{\perp}, \theta\right)$ over the complete parameter range, $0 \le \left|M_{//,\perp}\right| \le 1$ and $0 \le \theta \le 180$. Instead of using a constant value for c, we assume the following expression $c\left(M_{//,\infty}, M_{\perp}, \theta\right) = c_1\left(M_{//,\infty}\right) c_2\left(M_{\perp}, \theta\right)$ which simplifies the parameter study. Based on the following results this assumption

is justified. The logarithm of R is calculated from the numerical solutions of the differential equation for a set of data of $M_{//,\infty}$, $M_{\perp}$ and $\tan(\theta)$ over the maximum defined range. We then determine

$$c = c_1\left(M_{//,\infty}\right) c_2\left(M_{\perp},\theta\right) = \frac{\ln(R)}{\left|M_{//,\infty}\right| + \left|M_{\perp}\right| \cot(\theta)} \qquad (2.66)$$

For $\theta = 90°$, c is independent of $M_{\perp}$ and θ and we can plot (figure 2.14) the numerical solutions for c_1 as a function of $M_{//,\infty}$ assuming $c_2 = 1$. An expression $c_1\left(M_{//,\infty}\right) = a + b \cdot {M_{//,\infty}}^2$ fits these points.

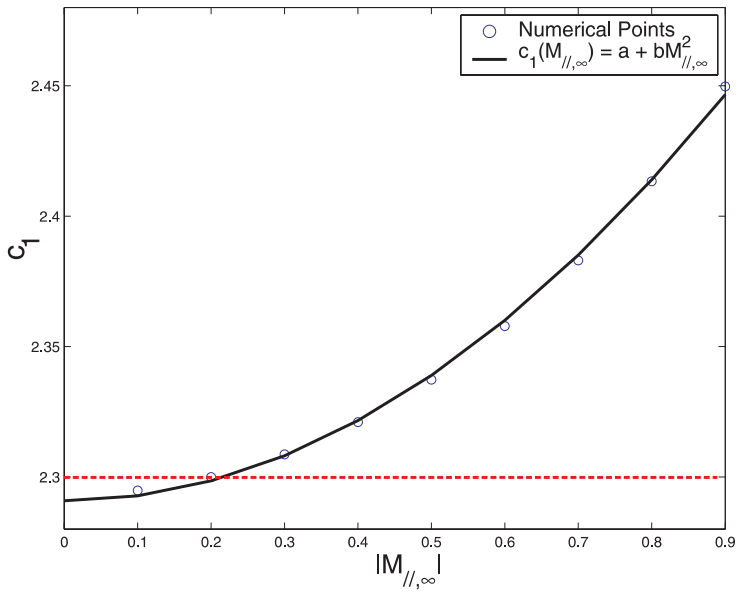

Figure 2.14: c_1 versus the parallel Mach number at the unperturbed plasma.

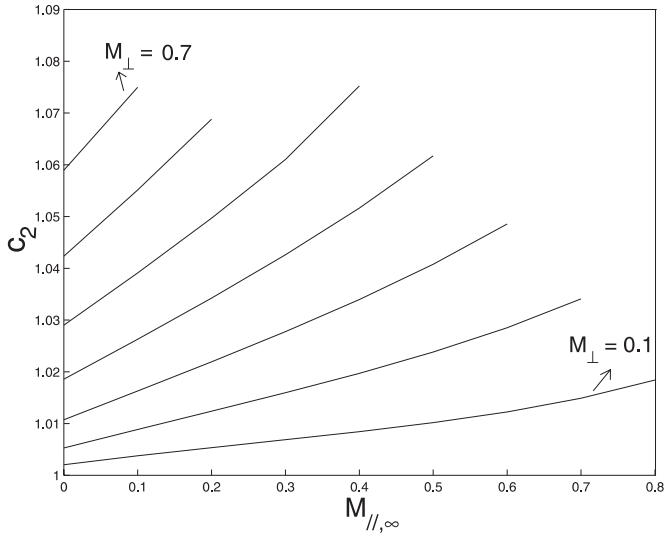

Figure 2.15: c_2 versus $M_{//,\infty}$ for $\theta = 40°$ and $M_\perp = 0.1 \rightarrow 0.7$.

To derive

$$c_2\left(M_\perp,\theta\right) = 1\Big/\left(a + b\cdot M_{//,\infty}^2\right)\ln(R)\Big/\left[\left|M_{//,\infty}\right| + \left|M_\perp\right|\cot\left(\theta\right)\right]$$

the following procedure is applied. We first keep the angle constant, for example $\theta_1 = 40°$, and vary both Mach numbers. We see that if we plot $c_2\left(M_\perp,\theta_1\right)$ as a function of $M_{//,\infty}$ (figure 2.15) the numerical solutions for all $\left|M_\perp\right| \le 1$ can be fitted by the expression:

$$c_2\left(M_\perp,\theta_1\right) = e\left(M_\perp,\theta_1\right) + f\left(M_\perp,\theta_1\right).e^{M_\perp} \qquad (2.67)$$

with

$$\begin{cases} e\left(M_\perp,\theta_1\right) = e_1\left(\theta_1\right) + e_2\left(\theta_1\right).e^{M_\perp} \\ f\left(M_\perp,\theta_1\right) = f_1\left(\theta_1\right) + f_2\left(\theta_1\right).e^{M_\perp} \end{cases}$$

We will now vary $0° \le \theta \le 180°$ to include its dependency. We found that the parameters e_1, e_2 and f_1, f_2 can be described by a common function $y(\theta) = p + q\theta^{-1}$ and write:

$$\begin{cases} e_i = e_{i,1} + e_{i,2}.\theta^{-1} \\ f_i = f_{i,1} + f_{i,2}.\theta^{-1} \end{cases} \quad (i = 1,2) \qquad (2.68)$$

Combining equations 2.66, 2.67 and 2.68 we obtain a non-linear expression of the form:

$$c\left(M_{//,\infty}, M_{\perp}, \theta\right) = a_1\left(M_{//,\infty}\right)\left[a_2\left(M_{\perp}\right).\theta^{-1} + a_3\left(M_{\perp}\right)\right] \qquad (2.69)$$

with $a_i = a_{i1}.Z^2 + a_{i2}.Z + a_{i3} \quad (i = 1,2,3)$

$$\text{for} \begin{cases} i = 1 \Rightarrow Z = M_{//,\infty} \\ i \neq 1 \Rightarrow Z = e^{M_{\perp}} \end{cases}$$

Table 2.1 gives an overview of the values of the parameters that give the best fit.

$a_{i,j}$	1	2	3
1	2.291	0	0.192
2	11.450	-18.929	7.043
3	-0.136	0.224	0.918

Table 2.1: Exact values of the parameters $a_{i,j}$ for $i, j = 1,2,3$.

In this way a much better agreement with the exact numerical solutions over the complete parameter range, $0 \le M_{//,\perp} \le 1$; $0° \le \theta \le 180°$ (those combinations limited by equation 2.61), is achieved (figure 2.16).

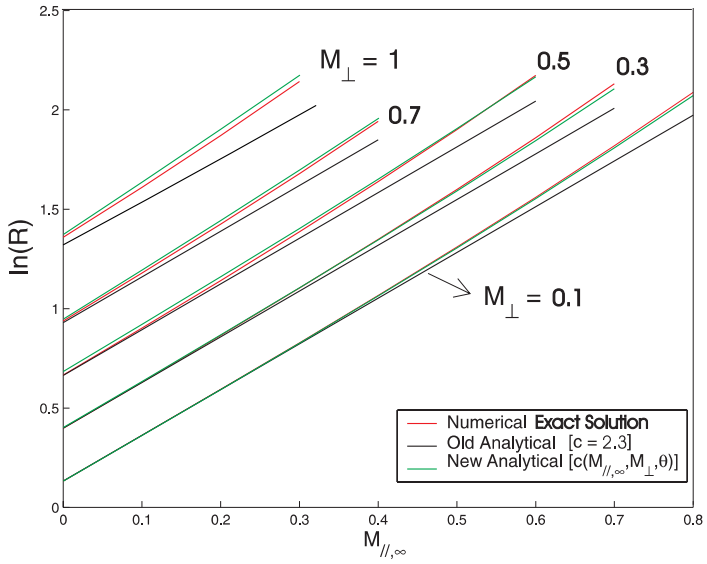

Figure 2.16: $\ln(R)$ versus $M_{//,\infty}$ for $\theta = 60°$ and $M_{\perp} = 0.1 \rightarrow 1$.

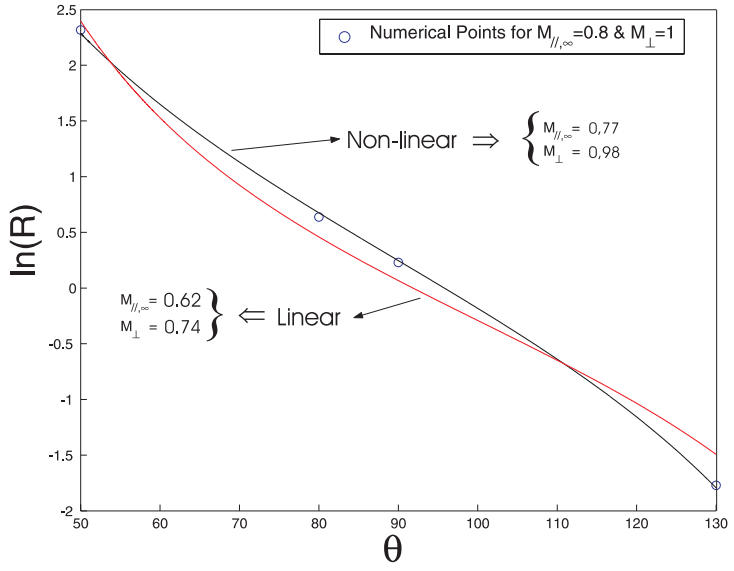

Figure 2.17: The results of the 'old' linear and 'new' non-linear fit on the Mach numbers.

Figure 2.16 shows that the improvement (for example when $\theta = 60°$) becomes important when higher flows exist. To quantify the effect, figure 2.17 shows an example of the values for the flows derived by fitting the old 'linear' and the new 'non-linear' function to four arbitrary data points (as in our experiments, four angles were available). The four input data for the least square fit are the numerical exact solutions for $M_{//} = 0.8$ and $M_{\perp} = 1$. The comparison of the two results from the linear and non-linear approach shows that, in the present case, the underestimation of the flows has been minimized. The underestimation of the perpendicular flow is reduced from 26% to 2%. The more precise value of the parallel Mach number becomes 0.77 instead the previous estimation of 0.62.

2.2.5 Conclusion

In this paper we formulated a new analytical expression for the factor $c\left(M_{//,\infty}, M_{\perp}, \theta\right)$ which takes into account the various dependencies of the parallel and perpendicular Mach numbers and the inclination angle of the collectors with respect to the magnetic field. This expression has been derived over the full parameter range $\left(-1 \le M_{//,\perp} \le 1 \text{ and } 0° \le \theta \le 180°\right)$ of which only those combinations fulfilling the limitation of the model (equation 2.61) are allowed. We showed that when a constant value for c is chosen, an error builds up when the flows grow and when the inclination angle deviates from 90°. During biasing experiments [Jac98, VS03, Weyn93] higher flows are induced in the edge plasma and the use of the improved analytical approach is recommended.

2.3 Comparative study of flat and round collectors using a validated 1D fluid probe model

We now present the results of a *Comparative study of flat and round collectors using a validated 1D fluid probe model*, by P. Peleman, S. Jachmich, M. Van Schoor, G. Van Oost, W. Knaepen, and C. Boucher, published in Contributions to Plasma Physics, 46(5-6):432, 2006.
Some parts in the abstract and the introduction are slightly repetitive with respect to sections 2.2.2 and 2.2.3 but are necessary to preserve the integrity of the paper. Furthermore, section 2.3.3 is a bit extended compared to the original version of the publication in order to further ameliorate the clarity of this section. The final part treats the design of a new Gundestrup-like probe head which is actually presented in much more detail in chapter 3. Nevertheless, this part is not left out here because the collector choice of the probe is based on motivations described in this section.

2.3.1 Abstract

In the literature two different types of Gundestrup-like probe designs are proposed: design with flat and with round collectors. In this paper we study the influence of different collector shapes of Gundestrup-like probes on the accuracy of the measurement of the parallel and perpendicular flows. A one-dimensional fluid probe model is used for deducing both Mach numbers of the unperturbed flow from the probe data. An analytical expression relates the plasma flow to the measured ion saturation currents collected at the upstream and downstream collecting surfaces of the probe. For flat collectors, the analytical model is validated by comparing it to a kinetic, two-dimensional and quasi-neutral Particle-In-Cell (PIC) simulation code. An extension of the theoretical model then allows us to study round collectors. We

performed an accuracy study which showed that systematic errors are introduced when round collectors are employed for the determination of the perpendicular flow which is systematically overestimated. The error can reach more than 70% when the perpendicular flow increases and when the angle of the collecting surface with respect to the magnetic field $(\theta \to 0)$ is small. The correct analytical expression is applied to experimental data from Gundestrup probe measurements with round collectors on the CASTOR tokamak. The analysis shows that for these measurements the error introduced by using the expression for flat collectors remains negligible, supporting our former use of the model for flat collectors. A new advanced Gundestrup-like probe design and the motivation for the choice of flat collectors are presented.

2.3.2 Introduction

Mach probes are common diagnostic to measure flow and electric field profiles in the edge of fusion machines. The probe diagnostic is based on the fact that, when a probe is inserted in a plasma with pre-existing flow, the collected current at the upstream side will be larger than that on the downstream side. The ratio (R) of the upstream to the downstream ion saturation currents, collected by the probe, proves to be a function of the ratio of the flow velocity in the parallel and perpendicular direction to the ion sound speed c_s, defined as the Mach numbers $M_{//,\perp}$. The perpendicular direction is defined to be in the magnetic surface but perpendicular to the magnetic field.
For the determination of $M_{//}$, Hutchinson [Hut87] adopted a fluid treatment which describes a probe with flat collectors perpendicular to the magnetic field $(\theta = 90°)$. Starting from the continuity and momentum equations a set of two coupled differential equations is obtained of which an approximate analytical solution gives a direct relationship between the

logarithm of R and $M_{//}$. Van Goubergen [VG99a] extended this 1D fluid model to cases where the collectors are inclined with respect to the magnetic field and showed that R becomes a function of $M_{\perp}$, which allows us to determine not only $M_{//}$ but also $M_{\perp}$. The numerical solutions of this extended model were approximated with an analytical function as expressed by equation 2.64. The parameter c was taken constant and equal to 2,21. By comparing the numerical solution of the differential equation with this analytical approximated expression, Peleman [Pel02] recently showed that c is not a constant but depends on $M_{//}$, $M_{\perp}$ and θ. By using a constant c the Mach numbers are systematically underestimated (section 2.2.3). A new analytical expression for the factor $c\left(M_{//}, M_{\perp}, \theta\right)$ now takes into account the various dependences of the parallel and perpendicular Mach numbers and the inclination angle θ of the collectors with respect to the magnetic field. This improvement makes the 1D fluid probe model for Mach probe measurements reliable over the full parameter range $\left(0° \le \theta \le 180° \text{ and } -1 \le M_{//,\perp} \le 1\right)$ within the limitation of the Bohm-Chodura boundary condition (equation 2.61).

In this paper we first compare the analytical model to a kinetic two-dimensional quasi-neutral Particle-In-Cell (PIC) simulation code [Gunn98]. It is shown that, within the applicability of the fluid model, the currents predicted by the kinetic code are comparable to those derived from the fluid model. In this way, the fluid model is validated for flat collectors. In the past several probe geometries like an Ideal Gundestrup Probe (IGP) [Gunn98], which has round collectors, and a Mach probe with flat collectors have been used to determine plasma flows. A probe with round collectors is easier to manufacture than one with flat collectors. In the second part the accuracy of the analytical function, when using a probe with round collectors, is investigated. We study the effect of a round collecting surface on the perpendicular flow. The parallel flow appears to be insensitive to the shape of the collector. It is demonstrated that the contribution of the perpendicular flow changes over the

curved collecting area. This results in a systematic overestimation of the perpendicular flow. For round collectors, a correct expression relating the ratio R to the flows is then proposed. We then apply both expressions to experimental data from the CASTOR tokamak where a Gundestrup probe with round collectors was used and we discuss the results. Finally, we present a new Gundestrup-like probe and motivate our choice of flat collectors.

2.3.3 Validation of a 1D fluid probe model for flat collectors

A PIC open[10] source simulation code was developed by J.P. Gunn [Gunn98] to simulate the ion current collected by a circular probe located at the centre of a 2D plane containing the magnetic field lines as shown in figure 2.18.

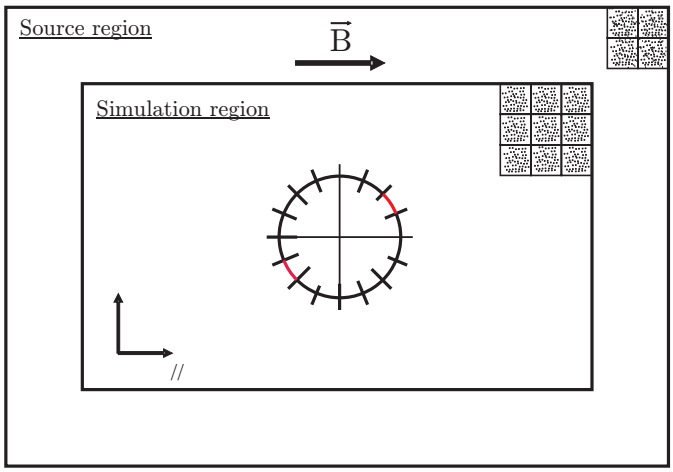

Figure 2.18: PIC code grid populated with ions (dots). The circular geometry of the probe with radius a consists of a variable array of collecting surfaces.

[10] http://claude.emt.inrs.ca/Gundestrup/CDROM/PICsimulator/index.html

The two dimensions represent the parallel and perpendicular directions on a magnetic flux surface in the tokamak edge. The condition of a strong magnetic field, i.e. $\rho_i << a$, imposes that only the guiding centres of the ions are needed to solve their parallel motion. The circular probe has a variable multi-faceted geometry of round collectors and is positioned at the centre of the simulation region. Particles whose trajectories intercept the probe surface are assumed to be absorbed (thus contribute to the collected current) and are therefore removed from the particle inventory of the simulation region. This funnel effect at the probe's surface is similar to the creation of a magnetic presheath in the fluid model and forms a gradient in density and a parallel electric field. The function of the source region is then to keep the total amount of particles in the simulation region constant. A quasi-neutral plasma $\left(n_e = n_i\right)$ is modelled and the electron temperature is assumed constant; thus electrons are not at all included in the simulations. The ions are randomly spaced in cells covering the whole simulation area. The initial parallel velocity of the ions is governed by a Maxwellian velocity distribution, shifted by a constant parallel drift. The time evolution of the velocity is obtained by solving Newton's laws in which the electric field is self-consistently calculated from the electron momentum equation as shown in [Gunn98, Joy97], i.e.

$$-eE_{//} = \frac{1}{n_e}\nabla_{//} n_e kT_e \approx \frac{kT_e}{n_i}\nabla_{//} n_i \qquad (2.70)$$

In absence of a constant perpendicular drift $\left(M_\perp = 0\right)$, the cross-field (perpendicular, vertical) motion is governed by perpendicular diffusion which is modelled by a random walk process where each ion is moved a small random perpendicular step at every time step Δt. The maximum length $\partial_\perp$ that the ions can move during one time step is proportional to the $D_\perp$:

$$\left\langle \partial_\perp^2 \right\rangle = 2D_\perp \Delta t \qquad (2.71)$$

and is assumed independent of the ion's parallel speed and oppositely the parallel speed is unmodified by the hop. However, when implementing a constant $\left(\partial M_{\perp}/\partial \perp = 0\right)$ non zero perpendicular drift $M_{\perp}$; the diffusive transport was found to be totally dominated by $M_{\perp}$ and it can therefore by turned off to save computing time. The boundary conditions at the ends of the simulation region are chosen in this way that no matter the type of cross-field transport, it is anyhow responsible for particle and momentum transport into the flux tube and is therefore balancing the parallel flow. This condition clearly influences the amount of particles present at the probe's surface whereas in the 1D fluid model this condition follows from the boundary condition expressed by equation 2.61. Finally, the perpendicular component of the electric field is ignored since it only causes a $\left(\vec{E} \times \vec{B}\right)$ - drift in the radial direction which is not incorporated in the 2D code. In order to compare the results of the 1D fluid model for flat collectors, a probe with 360 facets is simulated in the PIC code.

In figure 2.19, five values for $M_{//}$, for a given value of $M_{\perp} = 0.3$, are plotted. In figure 2.20 the parallel Mach number is kept constant (0.7), while different cases for $M_{\perp}$ were considered. A good agreement is found in the region (marked by the two vertical lines) where the fluid model is applicable as defined by equation 2.61. For small angles of theta the PIC code also gives a singularity. Indeed, the ratio R diverts to infinity since the probability of ions to be collected at the downstream side remains small relative to the upstream side (independent of the length of the simulation).

The remarkable agreement between the PIC results and the fluid model, within its range of applicability, supports the use of the (analytical) fluid model for deriving Mach numbers from experimental probe data. We will now further extend this validated model to investigate the influence of round collectors on the accuracy of the measurement of the parallel and perpendicular flows.

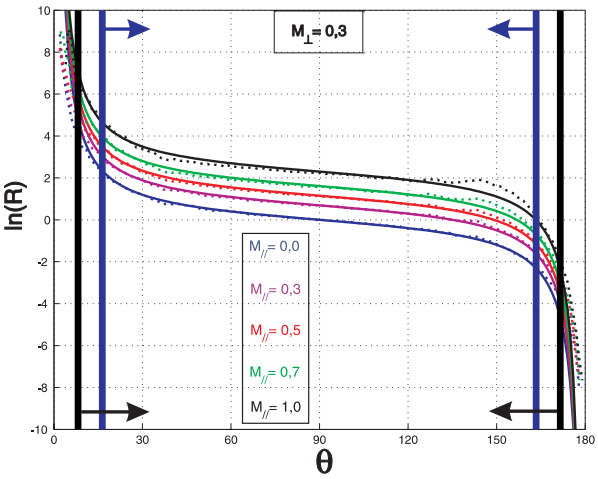

Figure 2.19: $\ln(R)$ as a function of the inclination angle of the probe for different parallel Mach numbers at a fixed $M_{\perp} = 0.3$. The solid lines represent the fluid model; the dotted lines are PIC results. The vertical lines mark two windows in which the model is applicable following the colour scheme of the figure.

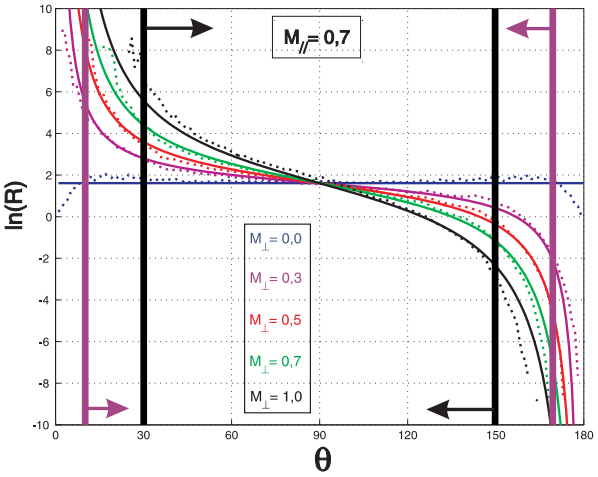

Figure 2.20: $\ln(R)$ as a function of the inclination angle of the probe for different perpendicular Mach numbers at a fixed $M_{//} = 0.7$. The solid lines represent the fluid model; the dotted lines are PIC results. The vertical lines mark two windows in which the model is applicable following the colour scheme of the figure.

2.3.4 Extension of the analytical model to round collectors

When considering round collectors the width of the flux tubes and the relative contribution of the perpendicular flow and the parallel flow changes along the collecting area (figure 2.21).

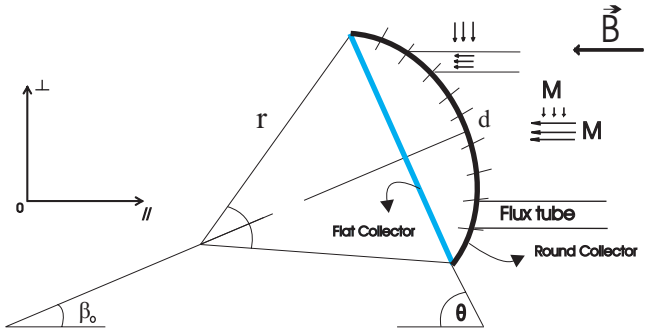

Figure 2.21: Geometry of a flat and round collector.

This means that, in the case of a round collector, the current to each collector is proportional to the integral of the sheath density over the angle α. For a flat collector, the angle (θ) between the collector surface and the magnetic field is constant. The contribution of $M_{\perp}$ to the total current is then constant and, when taking into account the projected collecting area, the current is directly related to $M_{\perp}$ as described in equation 2.64. The 1D fluid probe model relates the ion saturation currents measured at the probe surfaces to the Mach numbers of the flow of the plasma not perturbed by the probe via a set of coupled differential equations. The model starts from the continuity equation and the parallel projection of the ion momentum equation and results in two coupled differential equations (2.59 and 2.60) which describe the spatial variation (non-dimensional parallel distance $//$) of the density $(\partial n/\partial //)$ and the parallel Mach number $\left(\partial M_{//}/\partial //\right)$ in the presheath [VG99a, Pel02]. Dividing both coupled differential equations, the density as a

function of the parallel Mach number is described by the differential equation 2.62. An approximate analytical solution of $\partial n/\partial M_{//}$ is then expressed by equation 2.63. Using the convention of figure 2.21, i.e. $\beta_0 = \pi/2 - \theta$, we find for flat collectors

$$I_{i,sat_{down}^{up}} = n_{sh_{down}^{up}} ec_s A \cos\beta_0 \tag{2.72}$$

and $$R_{flat} = \exp\left[c\left(M_{//,\infty} - M_{\perp}\tan\left(\beta_0\right)\right)\right] \tag{2.73}$$

For round collectors the ion saturation current is obtained by integrating over the collecting area

$$I_{i,sat,up} = brn_{\infty}ec_s\, \mathrm{e}^{-c_0}\, \mathrm{e}^{c_{up}|M_{//,\infty}|} \int_{\beta_0-\frac{\alpha}{2}}^{\beta_0+\frac{\alpha}{2}} \cos(\beta)\, \mathrm{e}^{-c_{up}|M_{\perp}|\tan(\beta)}\, d\beta \tag{2.74}$$

$$I_{i,sat,down} = -brn_{\infty}ec_s\, \mathrm{e}^{-c_0}\, \mathrm{e}^{-c_{down}|M_{//,\infty}|} \int_{\beta_0-\frac{\alpha}{2}+\pi}^{\beta_0+\frac{\alpha}{2}+\pi} \cos(\beta)\, \mathrm{e}^{c_{down}|M_{\perp}|\tan(\beta)}\, d\beta \tag{2.75}$$

And

$$R_{round} = -\mathrm{e}^{c|M_{//,\infty}|} \frac{\int_{\beta_0-\alpha/2}^{\beta_0+\alpha/2} \cos(\beta)\, \mathrm{e}^{-c_{up}|M_{\perp}|\tan(\beta)}\, d\beta}{\int_{\beta_0-\alpha/2+\pi}^{\beta_0+\alpha/2+\pi} \cos(\beta)\, \mathrm{e}^{c_{down}|M_{\perp}|\tan(\beta)}\, d\beta} \tag{2.76}$$

with b the radial width of the probe surface. We took $\alpha = 45°$ as defined by the IGP so that we can verify the extended model with experimental probe data measured on CASTOR.
The comparison can be done independent of the parallel Mach number $\left(M_{//,\infty} = 0\right)$ since equations 2.73 and 2.76 show the

same dependency on $M_{//,\infty}$. In figure 2.22 we compare the logarithm of R for both cases. For $\beta_0 = 0$ (and $\alpha = 45°$), the probe is perpendicularly orientated by the magnetic field and we see no difference in the results for $\ln(R)$. This again proves that both probes will measure the same parallel Mach number. A difference of $\ln(R)$ is observed when the angle β_0 and the perpendicular flow increase.

In figure 2.23, equations 2.73 and 2.76 are compared in the following way. Different perpendicular Mach numbers were imposed $(0 \le M_{\perp,imp.} \le 1)$ for calculating the values for $\ln(R)$ using equation 2.76. These values for $\ln(R)$ are then fitted with equation 2.73 to obtain the perpendicular Mach number $M_{\perp,fit}$. Over the range of positive values of β_0 the difference between the imposed and the fitted values is plotted as a function $M_{\perp,fit}$ in figure 2.23. For negative angles the results are equivalent. An overestimation of $M_\perp$ is found since the fitted perpendicular Mach number is larger than the imposed one. For $\beta_0 = 62°$ and $M_\perp = 1$, an error of the order of 75% on the measurement of $M_\perp$ is observed.

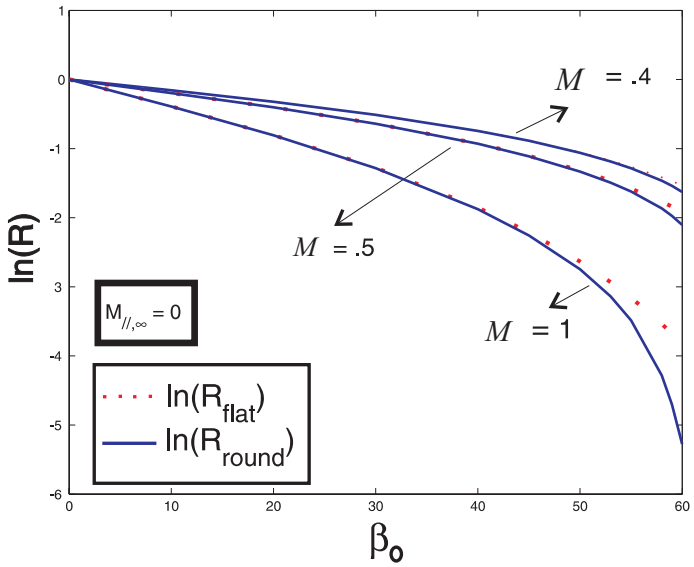

Figure 2.22: $\ln(R)$ as a function of β_0 for different conditions of $M_\perp$.

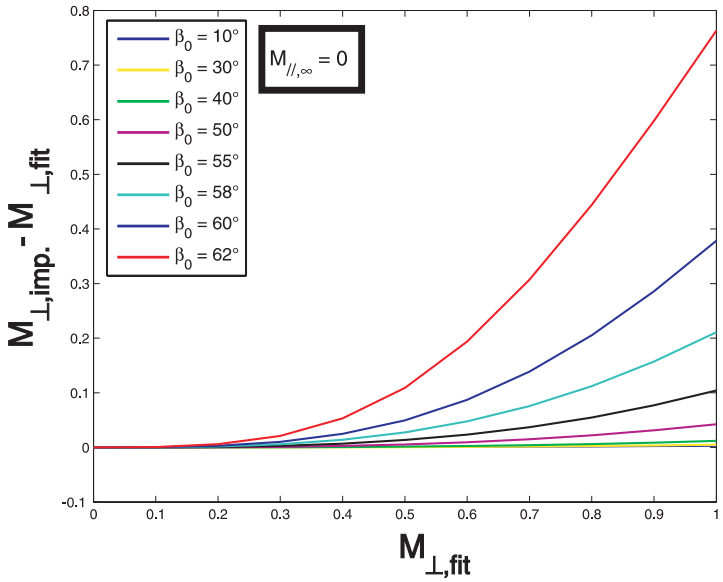

Figure 2.23: Comparison of equation 2.56 and equation 2.59 for different values of β_0.

For cases where $M_\perp \leq 0.6$ and $\beta_0 \leq 60°$, equation 2.73 can be used for round collectors while otherwise equation 2.76 is recommended.

We have applied both equations to experimental data obtained from a Gundestrup probe with round collectors $\left(\beta_0 = -45°, 0°, 45° \text{ and } \alpha = 45°\right)$ during biasing experiments on CASTOR [Spol05]. The perpendicular Mach numbers in these experiments were of the order of 0.4. Fitting the tangential relation, described by equation 2.73, to the three data points gives a $M_{\perp,flat}$ equal to 0.423. Due to its form, equation 2.76 can be used only in an iterative way for determination of the Mach numbers. The parallel Mach number has been calculated from the $\ln(R)$ for $\beta_0 = 0$. The perpendicular Mach numbers were then determined iteratively using the $M_{//}$ for each collector pair at $\beta_0 = -45°$ and $45°$. The mean value of the two perpendicular Mach numbers is $\langle M_{\perp,round} \rangle = 0.415$. This very

small difference of 2% confirms our theoretical findings as shown in figure 2.23. $M_{\perp,flat}$ and $\langle M_{\perp,round} \rangle$ are considered equal within the experimental error limits and it supports the proposal that equation 2.73 can be used, for these values of β_0 and $M_\perp$, for round collectors. However when using round collectors, we would like to stress that for larger perpendicular flows (>0.6) and for example $\beta_0 = \pm 62°$ the error can increase to more than 70% and the application of equation 2.76 is essential (figure 2.23).

2.3.5 A new advanced Gundestrup-like probe

Because equation 2.73 is more convenient to use for the interpretation of the data and we do not know in advance whether perpendicular flows higher than 0.6 will be present in the plasma during electrode biasing experiments, we have chosen flat collectors in our design [Mic02] of a new advanced Gundestrup-like probe (figure 3.1). In this way, the perpendicular flow can reach values higher than 0.6. In addition we have chosen the angles θ within the range of applicability (figure 2.19 and 2.20). The probe consists of sets of eight flat collectors poloidally distributed at two different radial positions embedded in a boron nitride insulating body. With the two collector sets the changes of flow in time can simultaneously be monitored at two radii. In addition, four cylindrical pins have been installed at the front end of the probe for comparison of the fluid velocities with the phase velocity of turbulence. The probe will be mounted on a fast scanning (up to 4 m/s) manipulator. This results in a much higher radial resolution and reduces the exposure time, which enables us to position the probe beyond the LCFS. We will be able to retrieve a complete edge profile within one discharge as will be shown in more detail in chapter 3. These features are important to study the ion density, the electron temperature, the flows and electric fields in the more inner, ergodized regions (edge) created by the Dynamic Ergodic Divertor (DED) on TEXTOR.

2.3.6 Conclusion

In this paper we validated a 1D fluid probe model using a 2D kinetic quasi-neutral Particle-In-Cell simulation code. The remarkable agreement, within the applicability of the models, supports the use of the fluid model for derivation of the Mach numbers from experimental probe data. The validated model is extended for round collectors. We formulated an expression which takes into account the effect of round collecting surfaces on the perpendicular Mach number in which the sheath edge density was integrated over the collecting area for deriving the up- and downstream currents. However, we showed that the formula for flat collectors can still be used when the perpendicular flow does not exceed a value of 0.6 and when the angle between the collecting area, and the magnetic field, is smaller than $30°$. This was confirmed with the analysis of experimental probe data obtained from a Gundestrup probe with round collectors during biasing experiments on CASTOR where the conditions for $M_{\perp}$ and β_0, as described above, are fulfilled. However, since we do not know if, in future experiments, the perpendicular flow will not exceed the value of 0.6 during electrode biasing on the larger TEXTOR tokamak and the fact that we want to use the more convenient equation 2.73 for the interpretation of the data, the choice of flat collectors for our design of a new advanced Gundestrup-like probe was required.

3

Probe diagnostic on the tokamak TEXTOR

During the full time span of this doctoral work a complete new sophisticated probe diagnostic has been developed and manufactured on TEXTOR. In this chapter a detailed description of the mechanical and electrical characteristics of this system is presented. The first experimental results of this probe system are also incorporated in order to test its sensitivity and accuracy.

3.1 Novel advanced Gundestrup-like probe for the measurements of flows and edge plasma parameters in TEXTOR

This section is set up following the manuscript, *Novel advanced Gundestrup-like probe for the measurements of flows and edge plasma parameters in TEXTOR*, by P. Peleman, S. Jachmich, Y. Xu, C. Boucher, G. Van Oost, B. Schweer, and M. Mitri to be published (accepted) in Review of Scientific Instruments, 2006. In order to promote the readability of this chapter the concise original manuscript has been extended substantially.

3.1.1 Abstract

A novel advanced Gundestrup-like probe head for local measurements of equilibrium and fluctuating plasma parameters in the plasma edge of TEXTOR is described. This probe assembly enables us to simultaneously determine the toroidal and poloidal plasma flows, the ion saturation current, density, electron temperature, floating potential, as well as their fluctuating properties. An improved analytical probe model is used to correctly relate the ratio of the ion saturation currents measured at the upstream and downstream collecting surfaces to the plasma flow. The probe is mounted on a fast reciprocating manipulator resulting in a high radial resolution of the profiles. A unique feature of the fast probe is the electrical linear motor drive which allows predefining any wave form of the radial position. The high speed of the probe drive reduces the exposure time which enables us to measure several radial profiles within a single discharge deep inside the last closed flux surface. We describe the first experimental results of flow, radial electric field, ion density, and temperature profiles measured in the plasma edge of TEXTOR. In order to verify the accuracy of these measured quantities we compare the measured radial electric field with the one calculated from the single ion momentum balance equation.

3.1.2 Introduction

A wealth of information on boundary plasma profiles, fluctuations, turbulence, and turbulence driven cross-field transport can be provided using electric probes. Among several diagnostics to measure the plasma flow velocity, a Mach probe [Oth78] is a very simple tool to obtain the ion acoustic Mach number (M_i), defined by the ratio of the plasma flow velocity to the ion acoustic velocity. A Mach probe consists typically of two oppositely facing collectors insulated from each other and aligned with the magnetic field. The ratio (R) of the measured upstream $\left(I_{sat,up}\right)$ and downstream ion saturation currents

$\left(I_{sat,down}\right)$ yields the Mach number parallel to the magnetic field [Hut87]. In order to determine also the perpendicular Mach number, additional collectors inclined with respect to the magnetic field are necessary. Such an array of collectors, poloidally distributed over the probe's circumference, is generally known as a "Gundestrup" probe [Mac92]. Such a probe was first used on the Tokamak de Varennes (TdeV). Presently there are worldwide only a few tokamaks (ISTTOK, CASTOR, Tore Supra) which are equipped with such a probe. Measuring both the poloidal and toroidal flow with a probe is therefore quite rare. In paragraph 3.1.3.1 we present a novel advanced Gundestrup-like probe head which consists of two Gundestrup arrays at different radial positions and a four-Langmuir-probe array mounted on the flat end of the head. This probe is capable of measuring the density, temperature, and floating potential in tokamak edge plasmas. In addition, the ion saturation currents collected by the Gundestrup arrays can be used to infer the speed and direction (poloidal and toroidal) of flowing plasmas.

Fast reciprocating probe assemblies have been installed on several tokamaks, stellarators, and reversed field pinch machines [Asak95, Wat97, Ped99, Serr03, Bak03, Yan05]. The fast movement is often obtained by means of a pneumatically or hydraulically driven piston which offers speed but a poor control of the acceleration, dwell time, and radial position. A versatile fast reciprocating and rotating probe system has recently been installed at the midplane of TEXTOR. The use of this fast reciprocating probe system enables us to measure several radial profiles within a single discharge deep inside the LCFS. The probe drive will be described in paragraph 3.1.3.2.

In order to test the sensitivity of the probe, measurements of the plasma edge parameters have been performed in TEXTOR in two different plasma regimes: in ohmic plasmas and in edge ergodized plasmas, imposed by the dynamic ergodic divertor (DED), where changes to the rotation profiles due to the enhanced radial conductivity are expected. The DED, recently installed at TEXTOR, is a set of 16 coils, wrapped around the vessel at the high field side and creates a

perturbation field resonant with the $q = 3$ surface [Fin01, 06]. The dynamical operation of the DED coils results in a rotation of the magnetic field pattern and hence of the plasma itself. In section 3.1.4 we present the first experimental results of the new probe diagnostic on TEXTOR carried out before and during DED operation. Furthermore, the reliability of the probe model is demonstrated by comparing radial profiles of flows and edge plasma parameters with the single ion momentum balance equation. Finally, we summarize in section 3.1.5.

3.1.3 Probe

The probe assembly consists of two main components: the probe head and the probe drive.

3.1.3.1 Probe head design

The Gundestrup-like probe head described here has a total of 20 collectors which can simultaneously obtain a large variety of edge plasma parameters. The probe consists of two sets of monographite collectors located at two different radial positions (radially separated by 1 cm). Each set consists of eight flat (based on the motivations described in section 2.3.5) square (4x4 mm) collectors poloidally distributed around the circumference of the head as shown in figure 3.1. The minimum angle between the collectors and the magnetic field is 36° which is within the minimum window ($> 30°$) of reliability of the 1D fluid probe model as investigated in section 2.3.3. The ion saturation currents of each collector pair, of which one faces the upstream while the other faces the downstream direction with respect to the magnetic field, are used to infer the speed and direction of flowing edge plasmas together with the electron temperature. In addition, a four-Langmuir-cylindrical-probe ($\phi = 3$ mm) array is mounted on the flat end of the cylindrical probe head facing the plasma ($\Delta r = 4$ mm). The saturation current and floating potential, collected by two cylindrical top pins, are used to determine the electron density n_e, the radial

electric field E_r, and the properties of turbulence as well. The top pins are made of two-dimensional graphite, a low Z material with a higher thermal conductivity compared to monographite such that the erosion of the pins due to the high temperatures which occurs at the front surface of the probe head is reduced. A boron nitride body (also low Z) electrically insulates each top and side collector from one another. The body consists of internal and external housings which are fixed at the back of the probe using a stainless steel ring. Such a probe design enables easy access for disassembly and replacement of any part of the probe head. The probe assembly is mounted on a fast reciprocating manipulator which has recently been installed on the TEXTOR tokamak.

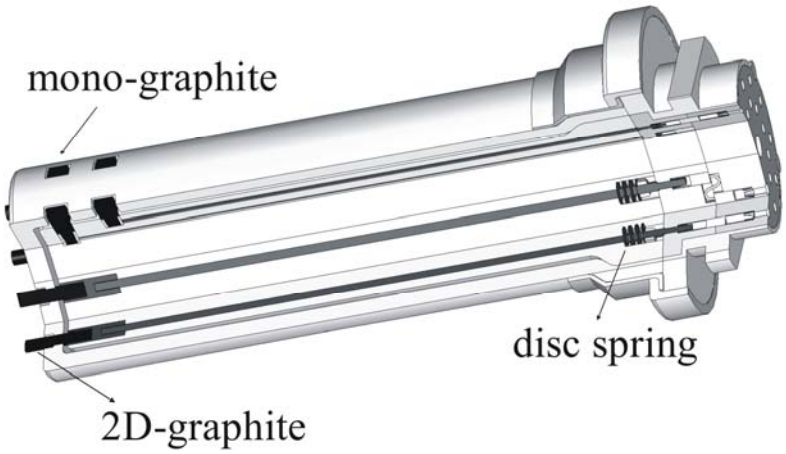

Figure 3.1: The Gundestrup-like probe head consisting of two arrays separated radially, both with eight poloidally distributed flat collectors and a four-Langmuir-probe array mounted on the flat end of the head.

3.1.3.2 Probe drive

In the past probe measurements were performed using a slow manipulator in which radial profiles were obtained by moving the probe radially on a shot-to-shot basis. In these cases, the reproducibility of the discharges is a crucial issue and even small changes in the (global) plasma parameters might be criteria susceptible to discussions. This problem can be avoided when using a fast scanning and rotatable probe system designed to provide local plasma edge parameter profiles with high temporal and spatial resolutions [Mit05]. This system is installed at the horizontal midplane of TEXTOR opposite to the location of the old slow probe manipulator as shown in figure 3.2. For measurement purposes, the probe has to be changed quickly upon request. In order to do that, the system is vented with dry nitrogen to avoid penetration of water. Then the exchange port can be opened allowing easy physical access (figure 3.3a). The system can quickly (within 3 or 4 hours) be pumped down to operation pressure (high vacuum of 10^{-6} mbar) by combining a rotary and turbo pump (pre-vacuum of 10^{-3} mbar) and subsequently a cryo pump which pumps at a rate of 1500 litres/s (figure 3.3a). Two edge welded bellows give the probe the flexibility to go into TEXTOR under high vacuum as shown in figure 3.3b.

The linear movement is a two-stage mechanism starting from an initial position close to the limiter. First the probe is slowly (0.3 ms^{-1}) moved to its standby position at 530 mm (close behind the limiter) where there is no exposure to the plasma as shown in figure 3.4. Once this position is reached, a fast (up to 2 ms^{-1}) reciprocating linear motion reaching as far as 170 mm into the plasma can be triggered.

The high precision of plasma control in TEXTOR $(\pm 2\ \text{mm})$ calls for a similar high precision of the radial positioning and movement. A unique feature of the fast probe drive is the use of two AC servo electrical motors which allows predefining any wave form for the radial position (figure 3.3b). These types of motors offer a reliable performance at maximum acceleration (90 ms^{-2}). Figure 3.4 shows the voltage and radial

position time traces of a full reciprocating cycle. The fast linear drive is numerically controlled (using a WinCC-interface) and has the flexibility of providing the user to change the three main parameters (figure 3.5), which are the (1) radial position (any penetration depth between 1 and 170 mm in 1 mm steps with a mechanical repetition accuracy of ± 0.1 mm), (2) dwell time (up to 10 s with 1 ms increments), and (3) speed (up to 2 ms^{-1} with 1 mms^{-1} increments), via two touch screens located inside the bunker and in the control room.

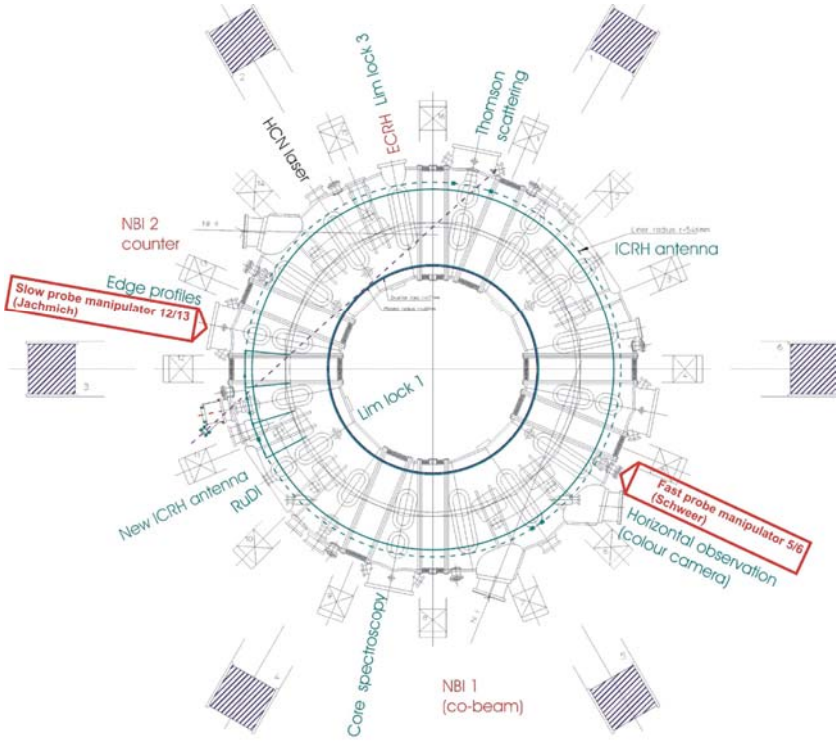

Figure 3.2: Top view of TEXTOR indicating the toroidal position of the slow and the fast probe system.

(a)

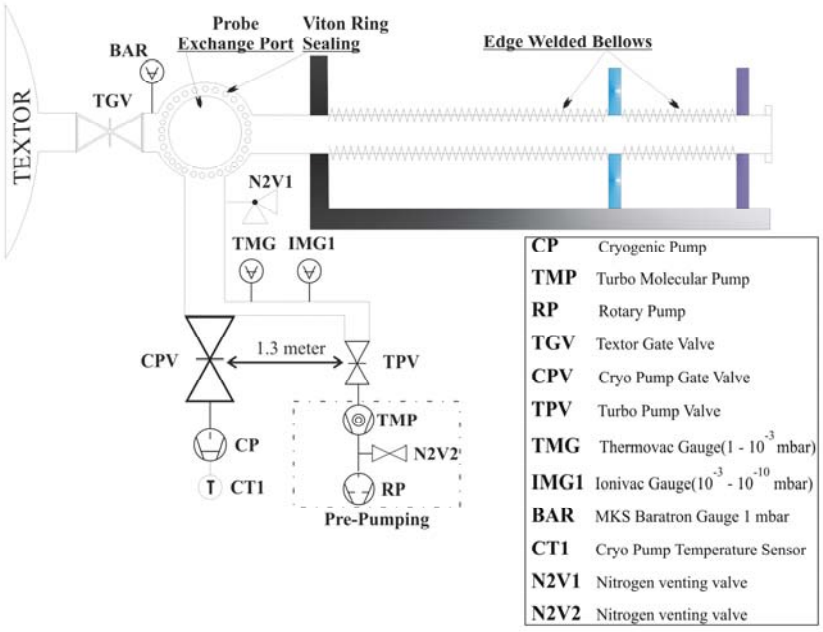

(b)

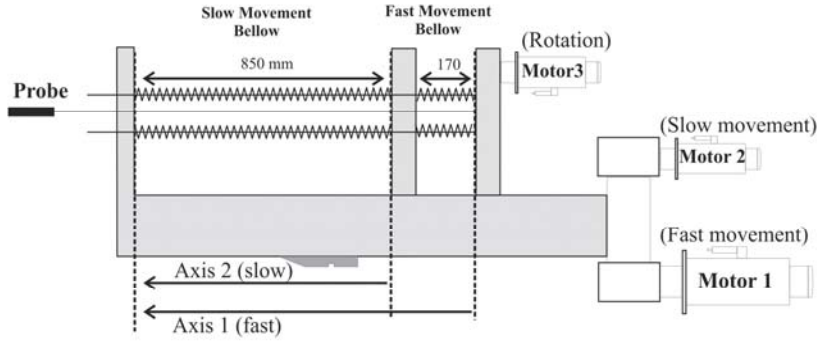

Figure 3.3: Movement and vacuum components of the fast probe. The slow and fast movement is controlled by two servo electrical motors while a third motor can induce rotation.[11]

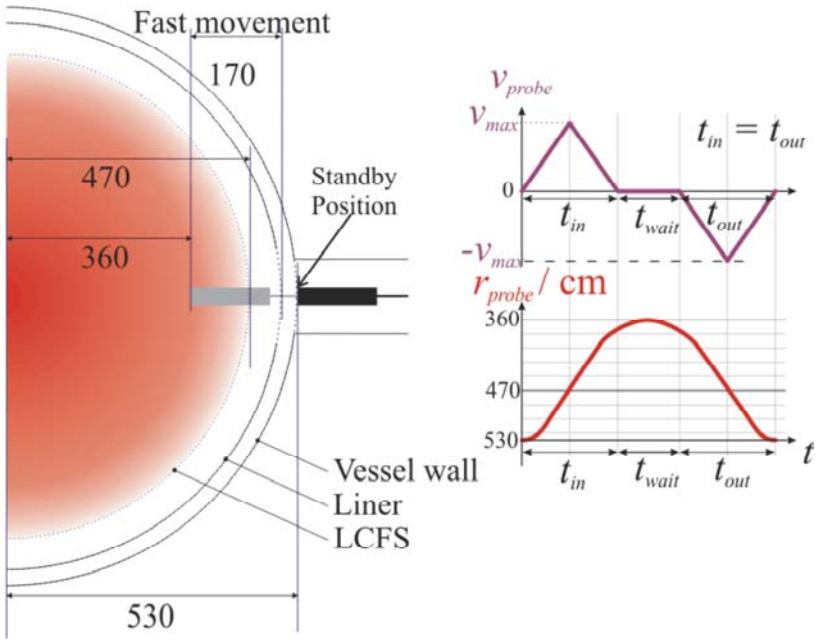

Figure 3.4: Schematic view of the fast movement originating from the standby position. A full reciprocating cycle is shown in the voltage and radial position time traces.[11]

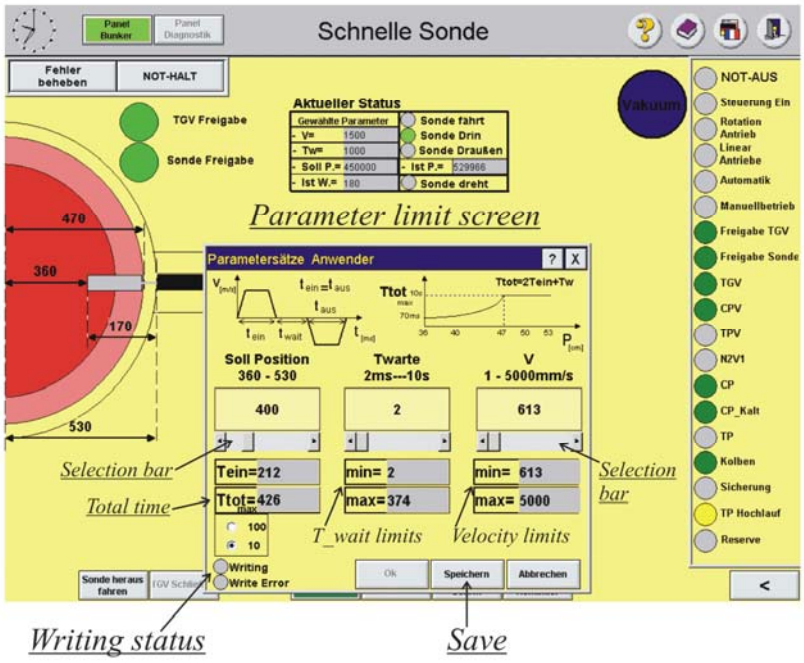

Figure 3.5: View of the WinCC main motion screen. The radial position, dwell time and speed are easily adjustable via two touch screen interfaces of which one is located inside the bunker and the other inside the control room.[11]

In addition to the linear movement, the probe system is designed to simultaneously rotate a probe at variable frequencies with a maximum of 3 Hz. However, no rotating probe measurements have been performed yet. Figure 3.6(a) represents the temporal evolution of the radial probe position. Two strokes were programmed to reciprocate the probe from 53 to 43 cm with a velocity of 0.8 ms^{-1} and a dwell time of 50 ms. These settings were found to be a good compromise in limiting

[11] Internal report, M. Mitri, 2005, [Mit05]

the exposure time of the probe head and still gathering enough data in order to be successfully analyzed. Note that a small "overshoot" occurs which is immediately (< 40 ms) countered by a reversed velocity bringing the probe back to 43 cm where it remains during the dwell time before returning to its initial position.

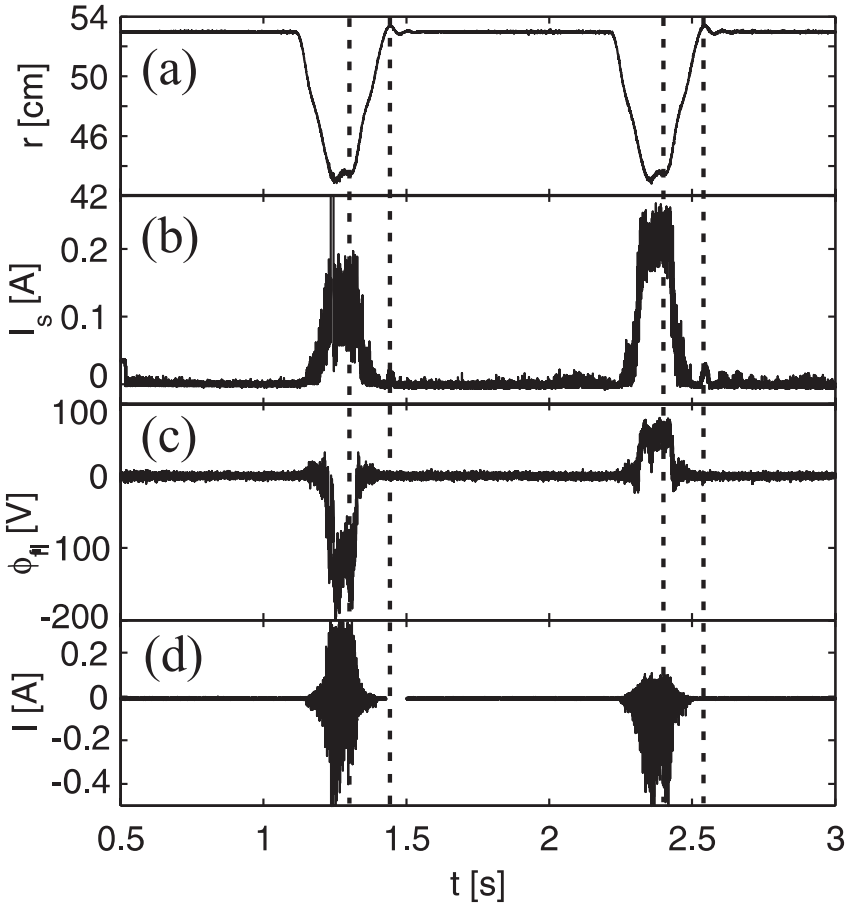

Figure 3.6: Temporal evolutions (shot No. 99777) of (a) radial position of the probe (b) I_s from one top Langmuir pin (c) ϕ_{fl} from another top pin (d) current collected from one side flat collector pair.

3.1.4 Operation and result

The discharge parameters are major radius $R_0 = 1.73\ m$, magnetic field $B_T = 1.9\ T$, plasma current $I_p = 280\ kA$, and line-averaged density $\overline{n}_{e,0} = 1.5 \times 10^{19}\, m^{-3}$. The DED has been operated with poloidal/toroidal mode number of 6/2 and is switched on at $t = 1.6$ s reaching its flat top phase at $t = 2$ s for a period of 1 s. The DED target plate is located at $r = 47.7$ cm and the plasma was shifted 2 cm inwards which gives a radial position of the LCFS of $r = 45.7$ cm. The saturation current I_s and floating potential ϕ_{fl} time traces measured by two top Langmuir pins, when reciprocating the probe before and during DED operation, are shown in figures 3.6(b) and (c) respectively. The current (I) of one Gundestrup collector pair, connected as a double probe and swept with a 200 Hz triangular voltage (V) of amplitude $\pm 200\ \mathrm{V}$, is plotted in figure 3.6(d). The data are digitized at 40 kHz to obtain a sufficient amount of data points per sweep in the *I-V* characteristic as shown in figure 3.7. The upstream and downstream ion saturation currents, the floating potential V_{fl}, and the electron temperature T_e are the four free parameters determined by fitting a non-linear function of the form

$$I = -I_{sat,up}\,\frac{1 - e^{-\frac{V-V_{fl}}{T_e}}}{R + e^{-\frac{V-V_{fl}}{T_e}}} \tag{3.1}$$

with

$$\begin{cases} R = \dfrac{I_{sat,up}}{I_{sat,down}} \\ V_{fl} = V(I=0) \end{cases} \tag{3.2}$$

The very first start values are determined from the first *I-V* characteristic with $I_{sat,up} = \max(I)$, $I_{sat,down} = \left|\min(I)\right|$, and T_e as described by equation 2.21. The start values of the subsequent fits are then the end values determined from the previous one.

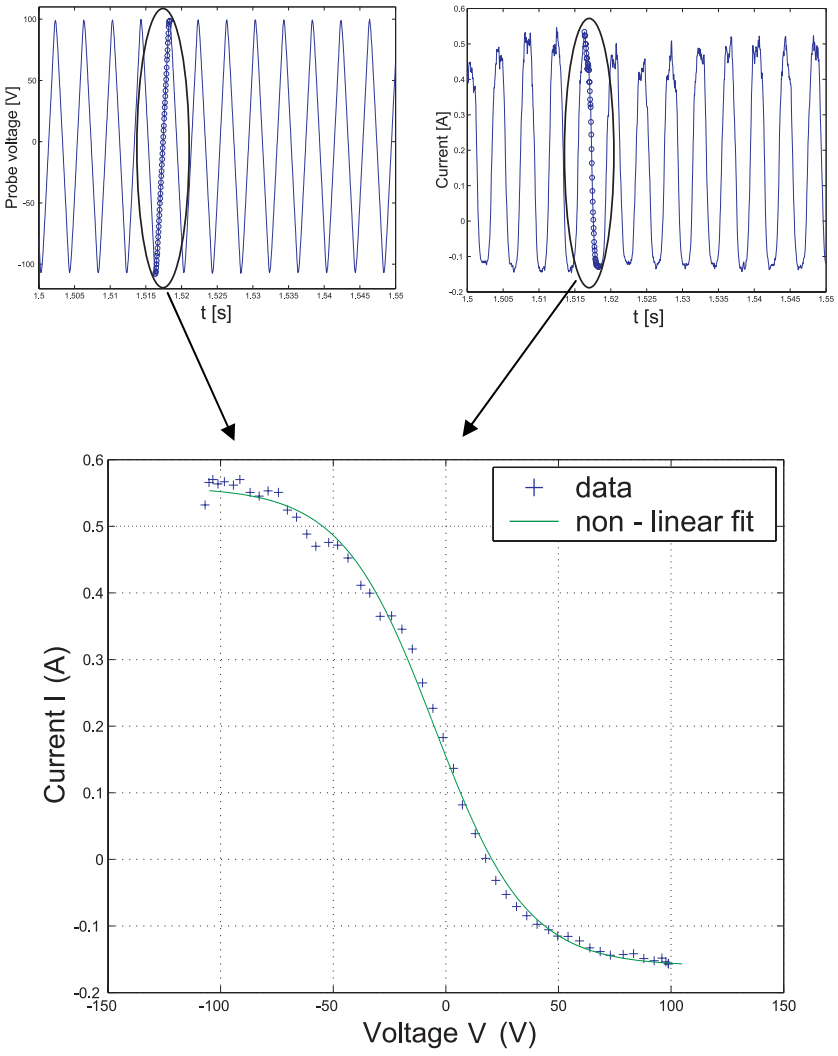

Figure 3.7: Applied probe voltage and current versus time. The sweeping frequency of the applied voltage is 200 Hz. The marked voltage and current traces (o) are used in the *I-V* characteristic (+). The green solid line represents a non-linear fit using equation 3.1.

A one-dimensional fluid probe model is used for determining both the toroidal v_ϕ and poloidal v_θ flow velocity from the probe data [VG99a, Pel05]. Here, an improved analytical expression relates the plasma flow to the measured ion saturation currents collected at the upstream and downstream collecting surfaces of the probe. The dashed lines in figure 3.6 indicate the two time periods which are used to determine the edge radial profiles plotted in figure 3.8.

The spatial resolution of the flow and T_e profiles is determined by the frequency of the applied voltage (200 Hz) and by the velocity of the probe. For a velocity of 0.8 ms^{-1}, the probe moves 4 mm during one sweep, therefore the spatial resolution of the double probe measurements varies from 4 to 8 mm, depending on the number of sweeps (one or two) used in the data analysis. A higher resolution can be achieved by increasing the sweep frequency or decreasing the probe velocity to the detriment of less data points per *I(V)* fit and longer exposure of the probe to the plasma. The radial extent (outwards) of the flow and T_e profiles is limited by the signal to noise (S/N) ratio. In the scrape-off layer (SOL) the saturation current drops strongly, producing a high (S/N) ratio. In exchange for some loss in spatial resolution, we averaged over two sweeps (one period) in order to improve the S/N. Therefore, reliable profiles were obtained up to 48.7 cm which is 3 cm into the SOL. The radial profiles of v_ϕ, v_θ, and T_e before (thin line) and during DED (thick line), are shown in figures 3.8(a)-(c), respectively.

Figure 3.8(d) shows the ion density n_i profiles which are directly calculated from

$$I_s = 0.5 A_s Z_i e n_i \left[k \left(T_i + T_e \right) / m_i \right]^{0.5} \qquad (3.3)$$

(assuming $T_i \approx T_e$) where T_i is the ion temperature, $Z_i e$ and m_i are the electric charge and mass, respectively, and A_s is the front tip collection area. The radial electric field is calculated from the negative derivative of the plasma potential defined as $\phi_{pl} = \phi_{fl} + 2.5 T_e$. Typical profiles of plasma potential and radial electric field are shown in figures 3.8(e) and (f).

3.1.5 Estimate of the error propagation

3.1.5.1 Radial electric field profiles

The difficulty to determine the radial electric field lies in the fact that only discrete values of the radial floating potential profile are available. The accuracy of the first and further derivatives is limited by the spatial resolution of the diagnostic. In the following a rough estimate of the error-bar of the radial electric field is presented. Since the voltage V (i.e. floating potential) can be measured rather precisely, a small error of 5% on the raw voltage signal is taken. The main error comes from the uncertainty in the radial position d, $\sigma_r \approx 0.5d$. The results shown in figure 3.8 are obtained with a spatial resolution of 2 mm. The slope of the profile at the position r_k has been calculated from a least square fit using three adjacent data points $\left(r_k, V_i, i = [k-1, k, k+1]\right)$. However, to calculate the error propagation a different Ansatz will be used [Jac07]:

$$r_i = a + bV_i, \tag{3.4}$$

Minimizing the χ^2 gives two equations from which a and b can be determined. The electric field in point r_k is then

$$E_{r,k} = -\frac{1}{b} = -\frac{\sum_i V_i^2 - \frac{1}{3}\left(\sum_i V_i\right)^2}{V_{k+1} - V_{k-1}} \cdot \frac{1}{d}. \tag{3.5}$$

The error of the electric field is obtained by applying Gauss's error propagation law with σ_r as the uncertainty of least square fit parameter b:

$$\sigma^2_{E_{r,k}} = -\frac{E^3_{r,k}}{V_{k+1} - V_{k-1}} \cdot \frac{\sigma_r^2}{d} \approx -0.25 \frac{\mathrm{E}^3_{r,k}}{V_{k+1} - V_{k-1}} .d \tag{3.6}$$

Thus, equation 3.6 shows that the estimated error on the radial electric field becomes: first, smaller with increasing spatial resolution and second, larger when the voltage difference at two adjacent radial positions is smaller. The relative error is typically 25-35%. For higher derivatives (as dE_r/dr in figure 4.4, chapter 4) the data have been interpolated by cubic splines, where the ordinate has been smoothed. In figure 3.8 (f) the error bars on the radial electric field are obtained using equations 3.5 and 3.6. Despite of the worst spatial resolution (d = 2 mm) the errors of the E_r - profile are still acceptable.

3.1.5.2 Electron temperature, density, plasma potential and flows

We start from a 5% uncertainty on the raw signals of $I_{i1,sat}$, $I_{i2,sat}$ (equation 2.21), the probe voltage V_{pr} and the current I_{pr}. Using the non-linear fit as described in section 3.1.4 we have determined a 95% confidence interval on the non-linear least square parameter estimates of the fitted coefficients T_e, R, $I_{i1,sat}$ and $I_{i2,sat}$. For T_e a relative error of ≈10-16% was found. Consequently, a relative error of 8-12% on the plasma potential ϕ_{pl} exists. Neglecting any error on the collecting area A_s we find a relative error on the electron density n_e of approximately 5-8%, half (due to the square root in equation 3.3) of the relative error on T_e. A similar exercise has been done in determining the relative error on v_θ and v_ϕ. The relative errors of both flows lie within a window of 20 to 25%.

The error bars shown in figure 3.8 (a)-(e) are determined from the calculations described above. It has carefully been checked that these estimations of the relative errors are representative for all the other results presented in this thesis.

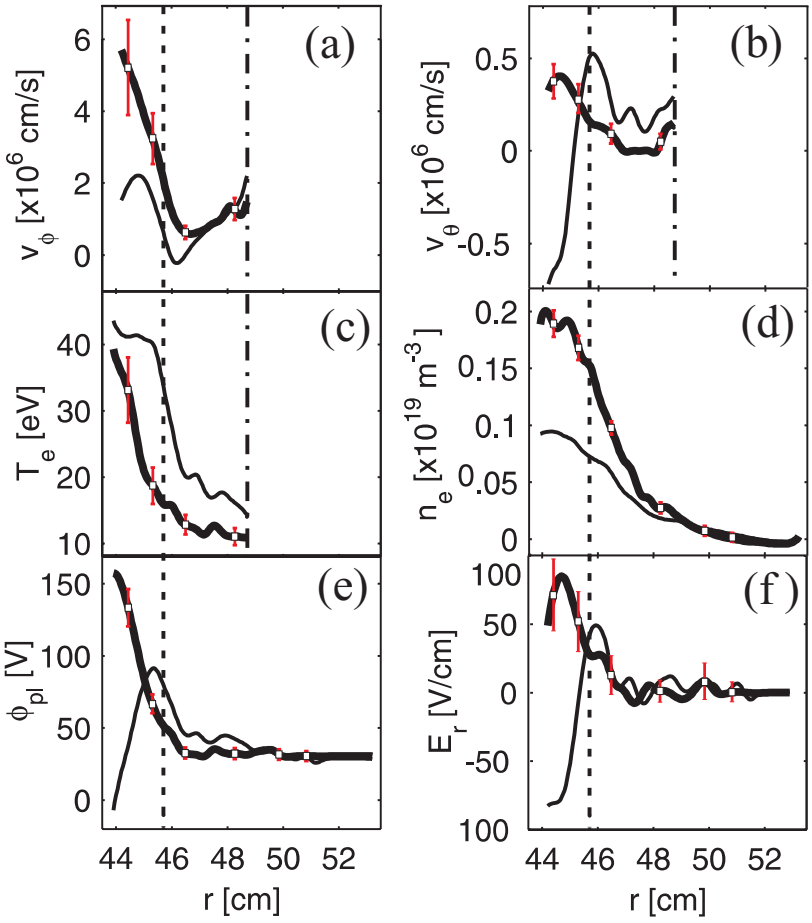

Figure 3.8: Radial profiles (shot No. 99777) of the (a) toroidal flow v_ϕ, (b) poloidal flow v_θ, (c) electron temperature T_e, (d) electron density n_e, (e) plasma potential ϕ_{pl}, and (f) radial electric field E_r before (thin line) and during (thick line) DED. The vertical dashed line marks the position of the LCFS. The dashed-dotted line indicates the end of the reliability of the Gundestrup data. The error bars (red) give an estimate of the error propagation on the different quantities.

The fundamental equation governing the electric field is the Poisson equation, $\nabla \bullet E = \rho/\varepsilon_0$ where ρ is the mass density and ε_0 the permittivity of free space. The large polarizability of a plasma and the difficulty of directly measuring charge density in fusion plasmas have led to the development of other methods for inferring the electric field. The Poisson equation is closely related to momentum because flow is the primary regulator of charge density through the charge continuity equation. Consequently, to determine E_r, it is often sufficient to specify and solve the radial force balance. It is the ion radial force balance that is of interest. Ions dominate the plasma momentum because of their large mass relative to electrons. The equilibrium radial force balance for ions is given by

$$E_r = \nabla_r p_i \big/ n_i Z_i e - v_{\theta,i} B_\phi + v_{\phi,i} B_\theta \qquad (3.7)$$

where $p_i = n_i T_i$ is the ion pressure, and B_θ and B_ϕ are the poloidal and toroidal magnetic field. With the presented probe system we are thus not only capable of measuring all the terms at the right hand side of equation 3.7, we can also directly determine the radial electric field. That is, all the quantities associated with the radial force balance are determined enabling us to verify the accuracy of our measurements by comparing the measured radial electric field $E_{r,meas}$ with $E_{r,calc}$ calculated from equation 3.7. Figure 3.9 shows the relative contribution of each term to $E_{r,calc}$ and illustrates the comparison with $E_{r,meas}$. Note that the absolute values of the diamagnetic term are plotted. In both cases the magnitude of the diamagnetic term is comparable and its contribution to $E_{r,calc}$ negligible. Since B_θ is one order of magnitude smaller than B_ϕ, the poloidal velocity term should be much larger than the toroidal one for similar v_ϕ and v_θ. Indeed, in the ohmic case the v_ϕ term remains small and contributes little (but is not negligible) to $E_{r,calc}$. Here, the electric field is mainly the result of the $\bar{E}_r \times \bar{B}$ driven poloidal flow. However, during DED, very high toroidal velocities (order of magnitude higher than v_θ) were measured which resulted in a v_ϕ term comparable to the v_θ term. Nevertheless, we found that in both cases, before and during DED, the radial profiles of

all these quantities are consistent with the first order radial single ion momentum balance equation. $E_{r,calc}$ is in good quantitative agreement with the measured radial electric field which supports the accuracy of our measurements and the underlying probe model used. Due to the unique features of this probe head and the probe diagnostic it is shown for the first time that, with a high spatial resolution, the force balance equation can be fulfilled in the plasma edge of a tokamak.

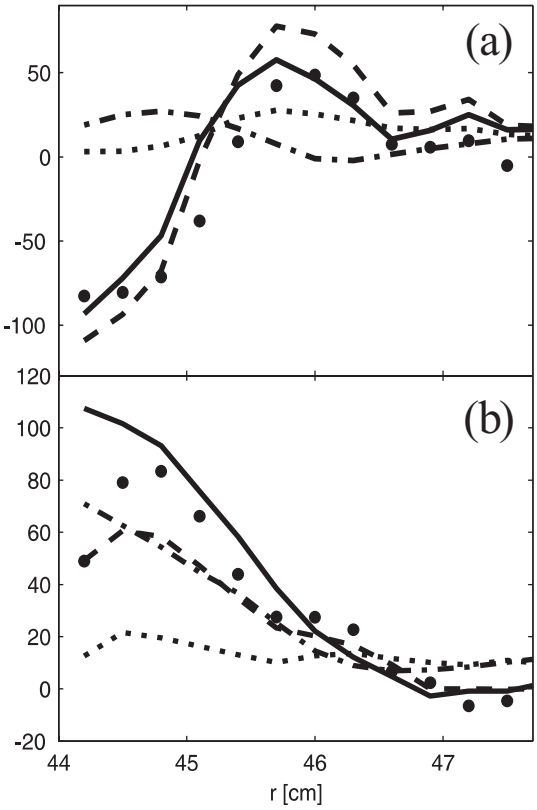

Figure 3.9: Comparison of $E_{r,calc}$ (solid line) calculated with the radial ion momentum equation and the measured (shot No. 99777) $E_{r,meas}$ (filled circles) before (a) and during (b) DED. $E_{r,calc}$ consists of $\left|\nabla_r p_i / e n_i\right|$ (dotted line), $-v_\theta B_\phi$ (dashed line), and $v_\phi B_\theta$ (dashed-dotted line).

3.1.6 Summary

The design of a new advanced Gundestrup-like probe head was described. A fast reciprocating probe system for high spatial resolution measurements is presented. First results of probe measurements, before and during DED operation, are shown and cross-checked with the radial force balance equation. In conclusion, it is shown that the measurements of flows and edge plasma parameters in TEXTOR with the presented probe diagnostic are reliable and accurate.

Now that the robustness of the new probe diagnostic has been demonstrated and taking into account the high spatial and time resolution and user-friendliness, the fast scanning probe diagnostic has become one of the most frequently used edge diagnostics on TEXTOR. Therefore, it will beyond all doubt provide useful data for DED characterization studies and possibly help to further improve the probe modelling.

3.2 Measuring system

A probe can be operated either in ion saturation current or floating potential mode.

To measure the parallel and perpendicular Mach numbers, the sixteen side collectors of the Gundestrup-like probe head are connected in pairs as floating double probes in ion saturation current. Figure 3.10 shows the electrical circuit of one pair of collectors in ion saturation mode. A TEXTOR triggered (after the start-up phase) triangular voltage signal produced by a function generator is amplified to ± 200 V with a sweeping frequency of 200 Hz. The power amplifier is protected from the plasma potential (in the case a disruption occurs) by an isolation transformer where the ground reference is decoupled. The primary winding (left side) is protected from a DC input by two electrolytic capacitors while two fast fuses protect the secondary winding against too high currents. The probe voltage and current signal are measured using a current and voltage isolation amplifier in which the current is measured by the potential drop of a small 5Ω resistor. A voltage deviator reduces the voltages to amplitudes lower than the ± 10 V limit of the ADC module. In order to minimize noise pick up induced by the length of the cables the complete measuring system is installed inside the bunker directly under (in the basement) the fast reciprocating probe system.

The radial electric field can be determined by measuring the floating potential with one of the top Langmuir pins. The scheme of such a floating potential mode is marked by the blue dashed lines in figure 3.10. Another top pin can be used to simultaneously measure the ion saturation current which is proportional to the electron density. The remaining top pins are mainly used for plasma fluctuation measurements which are not further discussed in this thesis.

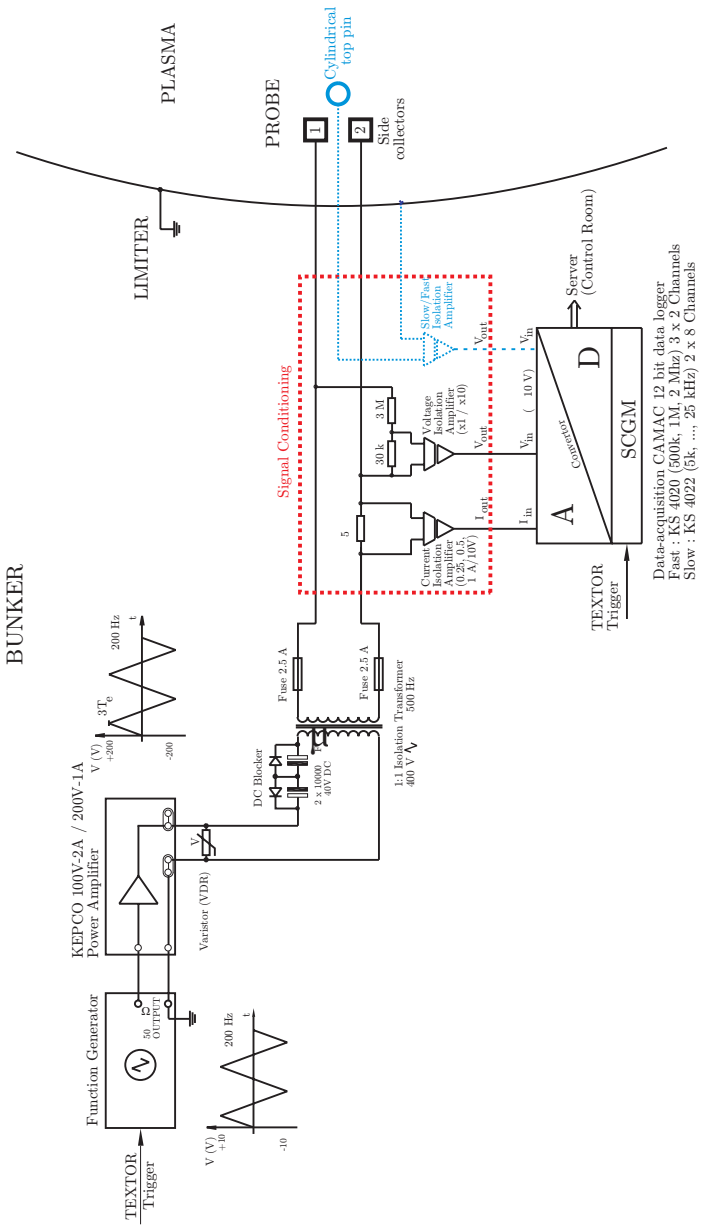

Figure 3.10: Electrical circuit of the probe system in ion saturation and floating potential mode (blue dashed line).

4

Experimental investigation of the role of flows in cross-field transport during relaxations in the plasma boundary region of the tokamak CASTOR

This chapter starts with a brief introduction to describe the importance of controlling the plasma edge. The various plasma confinement operation schemes are then summarized in order to situate the enhanced plasma confinement regime on CASTOR during edge biasing experiments. Consequently, the experimental results of highly resolved measurements of periodic radial electric field and associated relaxations observed in the biasing phase of the discharge are discussed. In particular the experimental evidence of a dynamical coupling between the parallel flow and the enhanced radial transport observed during the biasing phase is brought out.

4.1 Importance of controlling the plasma edge

The performance of the core plasma is very sensitively influenced by the behaviour of the edge plasma. It is beyond dispute that controlling the boundary of the core plasma is an important issue. In particular the role of the boundary plasma is essential for particle and energy exhaust. Indeed, the produced α-particles and the energy they carry, have to be conveyed through the SOL. The particles who interact with the wall will free wall material and these impurities should be kept away from the core plasma and the particle and energy fluxes directed towards the vessel should stay below the technical limits of the materials used for the first wall, divertors or limiters.

4.1.1 Confinement regimes in a tokamak

Conditioning of the wall by carbonisation, boronisation and siliconisation are passive plasma boundary controlling methods which effectively reduce the amount of impurities and recycling [Jack91]. These passive techniques are mostly used to condition the machine prior to successful operation.

A first very promising active confinement technique is the so-called Radiative Improved (RI) mode. This method has been developed on TEXTOR and is achieved by controlled seeding of the plasma boundary by carefully chosen impurities as Si and Ne. The underlying idea is to create a cold mantle which radiates around the core plasma inducing a better particle and energy confinement.

The standard plasma operation in a tokamak with auxiliary heating is the low confinement mode or L-mode. The improvement of high confinement regime, known as the H-mode, was first observed in large divertor tokamaks like ASDEX, DIII-D and JET when the neutral beam power exceeds a certain threshold [Wag82, Bur89, Camp90]. The energy confinement of such a spontaneous H-mode was to be enhanced up to a factor 2 compared to the L-mode. Later it was found that a similar plasma behaviour can be produced in ohmically heated limiter

plasmas by applying sufficient voltage to a probe or electrode (edge biasing or polarization) located several centimetres inside the plasma [Tayl89, Weyn92, Aski92]. In both conditions the onset of the H-mode is characterised by a sharp reduction in recycling and a sudden appearance of a strong radial electric field in the outer centimetre or so of the plasma. It has been shown that the change in the electric field is the cause, rather than the effect, of the improvement [Jac98, VOost03, Groeb90]. This very localized radial electric field creates a strong shear in the $E_r \times B_\phi$ poloidal flow which is strongly reducing the cross-flow transport in a region identifiable as a transport barrier as will be discussed in section 4.2.4.1. Such barriers are now widely utilized in fusion plasmas. Before the discovery of the first robust and reproducible transport barrier by Wagner et al. [Wag82], plasma confinement and fusion energy production were seriously limited by small-scale turbulent fluctuations. These had long seemed irreducible, because they are driven by the steep gradients of temperature and density needed to confine and insulate hot fusion plasmas away from material surfaces. With shear suppression, the heat loss caused by these fluctuations was controlled for the first time.

H-mode plasmas have an Edge Transport Barrier (ETB) with a large edge pressure gradient. Several possible explanations have been proposed for the spontaneous H-mode transition (see, e.g. [Sha89, Weyn92;93, Roz92, VS03]). However, difficulties in evaluating the hot (due to neutral beam power) ion orbit loss and in measuring the profiles of the electric fields, flows and other edge parameters have made it impossible to make a definite comparison between theory and experiment. By contrast, triggering of an H-mode by applying a voltage can be done in a controlled way, and the lower edge temperature allows the electric field and related quantities to be measured by means of probes. These biasing schemes are not seen as a control mechanism for future reactors (like ITER) but are nevertheless very important to better understand the mechanisms between (enhanced) turbulent driven cross-field transport and related quantities as will be shown in this chapter.

Presently there are two major candidates for confinement regimes of future tokamaks.

Firstly there is the Advanced Tokamak Scenario [ITER01]. This auspicious scenario was first discovered in the 1990s [Koid94, Strait95] and the properties of an enhanced confinement in the core plasma and the potential for fully non-inductive current drive are important for the steady-state operation of future reactors. Here, an Internal Transport Barrier (ITB) is formed starting from either a L- or H-mode plasma by subtly modifying the plasma current. The ITB confinement regime has steeper temperature and density (thus pressure) gradients compared to the standard H-mode. The barrier is sometimes only visible on the ion-channel (ion ITB) while in other cases only the electrons are affected (electron ITB). It is believed that the dominant heating of the electrons and ions plays an important role in the distinction of the type of barriers, although the phenomenon is not yet fully understood.

Secondly there is the ELMy H-mode operation which is planned to be the Standard Tokamak Scenario for ITER [ITER01]. When the pressure gradient during H-mode exceeds a certain limit, instabilities develop and so-called Edge Localised Modes (ELMs) occur [Zohm96]. These ELMs reduce the edge pressure gradient periodically during which energy and particles are expelled towards the wall. On the one hand these phenomena are beneficial for expelling impurities and α - particles but on the other hand harmful due to the large heat loads and particle impact onto the divertor target plates. Although ELMs have extensively been studied on JET for many years, many questions still remain.

Figure 4.1 summarizes the possible confinement regimes in a tokamak.

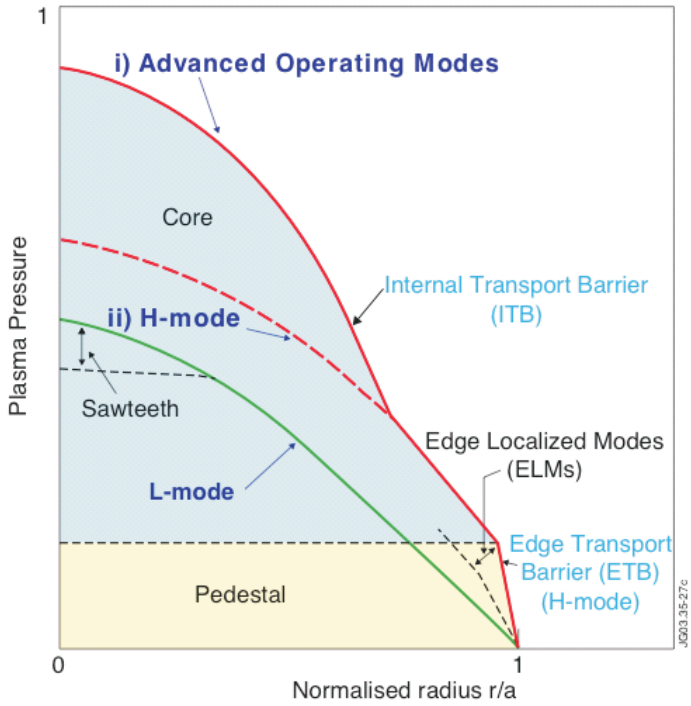

Figure 4.1: Schematic view of the different confinement regimes in a tokamak.[12]

4.1.2 Context of this chapter

Recently improved confinement events, dubbed as ICEs, were reported on the tokamak ISTTOK (Instituto Superior Tecnico TOKamak, Lissabon) during emissive electrode biasing [Silva04]. Above a certain threshold of the bias current ICEs were observed characterized by a further improvement in confinement during short periods. A new approach to study the relation between gradients and transport in ohmic (no ELMs) plasmas, using a statistical description of turbulent transport in terms of probability density functions (PDFs), has been

[12] Source: JET Figure Database, JG03.05-27c, 2003

proposed [Hid03a,b, Gon02]. They concluded that the bursty and strongly non-Gaussian behaviour of turbulent transport is strongly coupled with fluctuations in parallel flows. It is thus clear that fluctuating instabilities in edge plasmas appear in many different tokamaks and plasma conditions.

CASTOR is probably one of the best equipped tokamaks for diagnosing the edge plasma in detail. In particular the extensive variety of many different probe systems, which are easily accessible, allows thorough investigation of the plasma boundary [Stöc06]. During edge biasing experiments, above a certain threshold of the radial electric field, we observed periodic oscillations on all edge quantities. Strong bursts of particles towards the limiter are seen during these plasma instabilities. Although these instabilities are certainly not ELMs (completely different plasma conditions) they seem to behave interestingly similar and their fundamental physics might possibly be related [Gon03].

Simulations of plasma flows, including the effect of diamagnetic, $E \times B$, and $B \times \nabla B$ drifts, have previously been investigated [Roz92, Chan94, Rog99]. In general, the perpendicular (or poloidal) flow is mainly driven by the $j_r \times B_\phi$-force and was found to be in quantitative and qualitative agreement with the measured profiles [VS03]. The calculated SOL parallel (or toroidal) flow profiles, however, can qualitatively reproduce the measured radial profile of parallel flows but the amplitude of measured parallel flow [Ere00] is significantly larger than those predicted from simulation. These findings may suggest that there is a missing ingredient in previous simulations to explain the generation of parallel flows in the plasma boundary.

Our research is particularly focussed on the generation of edge plasma flows during radial electric field fluctuations as they are believed to play a crucial role in understanding cross-field transport in magnetically confined plasmas. We have experimentally investigated the possible link between parallel flow and radial transport during plasma instabilities during an enhanced plasma confinement triggered via edge biasing experiments on CASTOR.

4.2 Highly resolved measurements of periodic radial electric field and associated relaxations in edge biasing experiments

As basis for this section an enlarged version of the manuscript '*Highly resolved measurements of periodic radial electric field and associated relaxations in edge biasing experiments*' by P. Peleman, Y. Xu, M. Spolaoré, J. Brotankova, P. Devynck, J. Stöckel, G. Van Oost, and C. Boucher, is used. This paper is accepted for publication in 2006 in the Journal of Nuclear Materials.

4.2.1 Abstract

High time-space resolved measurements of the radial electric field E_r and plasma rotations have been performed during edge biasing experiments in the CASTOR tokamak. During polarization, edge sheared $E_r \times B_\phi$ poloidal flow is routinely generated, triggering a transition to a global improved confinement and a formation of an edge transport barrier. Furthermore, on top of the biasing-imposed DC E_r, we observed, for the first time, concurrent fast periodic oscillations (dubbed as relaxations) on E_r, plasma rotations, edge recycling and the ETB as well. Although the global confinement improvements are not much affected by the relaxation event, the local edge plasma parameters and the ETB are substantially modulated during the oscillating phases. Moreover, throughout the relaxation period a possible link between the modulated radial transport and the toroidal plasma flow is found. The results support the paradigm of the non-linear dynamical coupling and energy transfer between the turbulence eddies and plasma flows.

4.2.2 Introduction

The importance of the edge radial electric field (E_r) and its shear for plasma transport has already been recognized for a long time. Many theoretical models successfully studied the link between E_r and the formation of edge or internal transport barriers triggering an improved confinement [Sha89, Ten02, VS03]. The transition from low (L-mode) to high confinement (H-mode) can occur spontaneously or can be induced by an externally imposed electric field through edge biasing [Strin93, Weyn92, 93]. A biased electrode can drive a radial current in the plasma edge resulting in a $j_r \times B_\phi$ force and thus a sheared $E_r \times B_\phi$ poloidal flow, which may suppress turbulence and related transport [VOost03]. Therefore, the radial electric field perturbs the plasma edge and acts as a trigger mechanism to modify the plasma confinement. However, hitherto a thorough understanding of the flow shear and its role in inducing confinement improvements is still a challenge for fusion researchers. Consequently, detailed studies on this subject are still needed.

In this chapter, we report the experimental results performed during edge biasing experiments in the Czech Academy of Science Torus (CASTOR) tokamak. In addition to the improvement of global confinement, fast relaxation events on E_r and related quantities during the biasing phase are also observed for the first time. The paper is organized as follows. In section 4.2.3, we describe the experimental set-up of the biasing experiments. The results and discussions are presented in section 4.2.4. Section 4.2.5 gives a summary and conclusions.

4.2.3 Experimental set-up

Biasing experiments were conducted on the CASTOR tokamak which has a major radius $R_0 = 40$ cm and a minor plasma radius $a = 6.6$ cm. An electrode was inserted from the top of the torus well inside the last closed flux surface (LCFS) $(r/a = 0.6)$. To create an edge radial electric field E_r and its

shear, a biasing voltage abruptly ramped from 0 to +260V was applied during the flat-top phase of a discharge, which typically has the following parameters: central chord-averaged plasma density $\bar{n}_{e,0} = 1.0 \times 10^{19} \mathrm{m}^{-3}$, plasma current $I_p = 12\ kA$ and $B_T = 1.3$ T in ohmically heated hydrogen plasmas. A conventional rake probe, consisting of 16 radially separated Langmuir probe pins (radial separation between two adjacent pins = 2.54 mm), located 40° toroidally from the electrode and inserted from the top of the torus, was used to simultaneously measure the floating potential ϕ_f and ion saturation current I_s at various radial positions. A Gundestrup probe, located 180° toroidally from the electrode and placed on top of the torus, was inserted from the top of the vessel to measure the toroidal and poloidal flow velocities. The Gundestrup probe consists of eight collector plates surrounding a cylindrical boron nitride body [Gunn01]. The data were digitized at a sampling rate of 1 MHz for both the rake and Gundestrup probe. The H_α diagnostic, located 180° toroidally from the conventional rake probe, monitors the radiation due to recycling with a sampling frequency of 40 kHz. The experimental set-up from a top view of CASTOR is shown in figure 4.2.

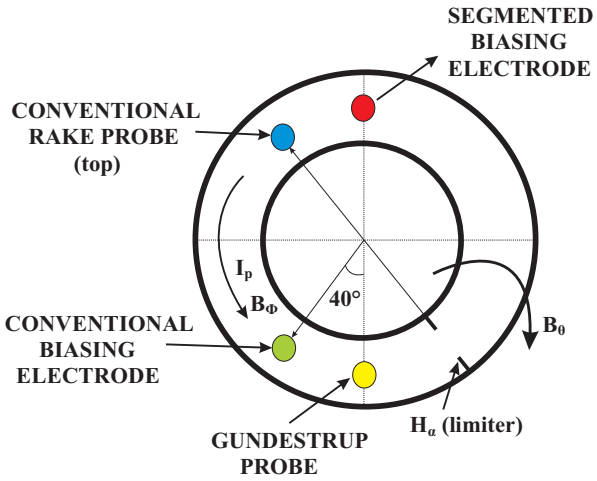

Figure 4.2: The experimental set-up, a view from the top.

4.2.4 Experimental results and discussion

4.2.4.1 Global confinement improvement

The effects of the positive edge electrode biasing on the main plasma parameters are shown in figure 4.3 for a time interval of interest (full discharge duration ≈ 30 ms). The figure shows time traces of the electrode voltage (V_E) and current (I_E), central line-averaged density $\bar{n}_e$, H_α emission and the ratio of $\bar{n}_e/H_\alpha$ along with the radial electric field E_r measured at $r = 60$ mm by the rake probe (radial derivative of ϕ_f on two adjacent pins). Before biasing, the electrode was grounded so no current flows between the electrode and the vessel. At about 10 ms, a positive biasing voltage $V_E \approx 260$ V is abruptly applied and maintained constant thereafter for ~ 5 ms, during which a current $I_E = -20$ A is drawn by the electrode, as seen in figure 4.3(a). In figure 4.3(b), it can be seen that during biasing, $\bar{n}_e$ is built-up gradually and reaches 1.7×10^{19} m^{-3} at $t = 14$ ms before falling off to its original pre-bias value of 1×10^{19} m^{-3}. In the initial stage of the biasing, from 10 to 12.5 ms, we can see a clear reduction in recycling indicated by a drop in H_α emission, and thus, a net increase of the ratio $\bar{n}_e/H_\alpha$ (which is roughly proportional to the particle confinement time τ_p) by a factor of 2.5 with respect to the pre-bias case. All of these results indicate an improvement of the global particle confinement induced by the electrode biasing, as observed earlier [VOost03]. After 12.5 ms, the H_α increases simultaneously with the C_{III} signal (not shown here), suggesting an overheating on the electrode head which contaminates the plasma in these last milliseconds of the bias. In figures 4.3 (c)-(e), the signals display periodic oscillations, which will be discussed in section 4.2.4.2.

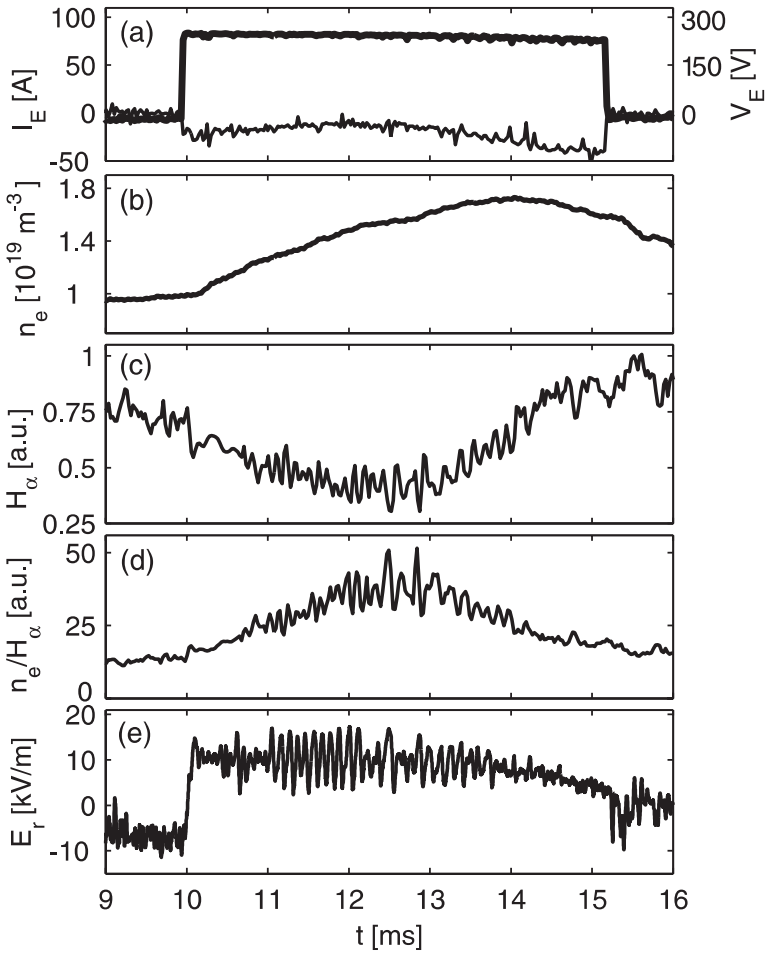

Figure 4.3 Time evolution of plasma parameters during a typical edge electrode biasing experiment on CASTOR (shot No. 24076). (a) the electrode voltage V_E (thick line) and current I_E (thin line), (b) the central line-averaged electron density $\overline{n}_e$, (c) H_α radiation, and (d) the ratio of $\overline{n}_e/H_\alpha$. Shown in (e) is the time trace of the radial electric field measured at $r = 60$ mm.

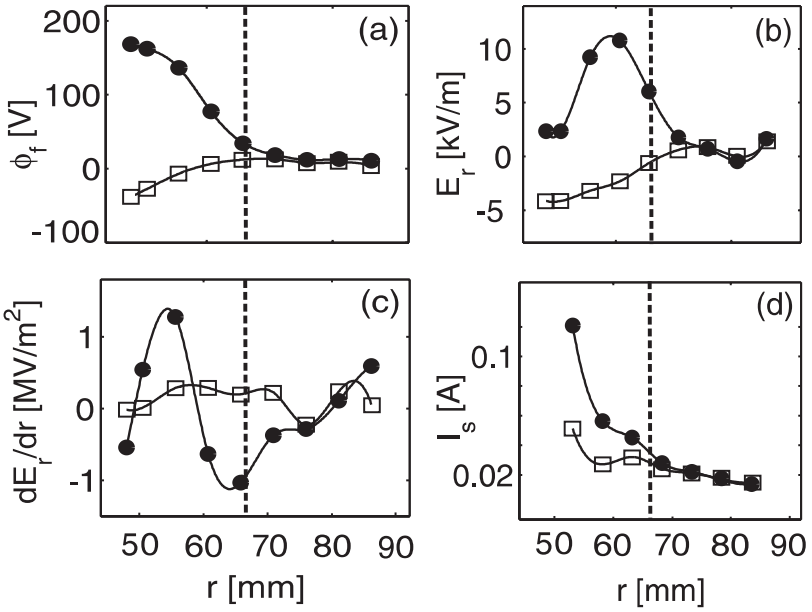

Figure 4.4 Radial profiles of (a) the floating potential ϕ_f, (b) the radial electric field E_r, (c) the E_r shear, and (d) the ion saturation current I_s averaged over 4 ms before (open symbols) and during (filled symbols) the biasing, where ϕ_f and I_s are measured by a rake probe (shot No. 24076). The vertical dashed line marks the position of the LCFS.

Figure 4.4 further illustrates the influence of biasing on the radial dependence of edge plasma equilibrium parameters. In the figures, the radial profiles of the floating potential ϕ_f, E_r and its shear dE_r/dr, and ion saturation current I_s are obtained by averaging over a time window of 4 ms before (open symbols) and during (filled symbols) the biasing phase. Here, E_r is calculated directly from the radial derivative of ϕ_f neglecting the contribution from the T_e gradient, and therefore somewhat underestimated. These approximations are justified

due to the very slight changes in edge T_e and ∇T_e before and during the biasing phase observed in similar biasing experiments. In the same context, it is assumed that the I_s profiles mainly reflect the changes in plasma density as $I_s \propto nT_e^{1/2}$. The radial position of the LCFS is around $r_{LCFS} = 66$ mm (indicated by dashed line in figures 4.4 and 4.7). During the biasing phase, the radial dependence of ϕ_f is strongly modified (see figure 4.4(a)), leading to a narrow positive and single-peaked E_r structure with a maximum of 11 kV/m at $r \approx 61$ mm, just inside the LCFS (see figure 4.4(b)). As a consequence, a strong stable positive $\left(\sim 1.3\ \mathrm{MV/m^2}\right)$ and negative $\left(\sim -1\ \mathrm{MV/m^2}\right)$ E_r shear is generated inside and across the LCFS, respectively, as shown in figure 4.4(c). The maximum shear decorrelation rate of the $E_r \times B_\phi$ poloidal flow, $\tau_s^{-1} \propto dv_{E\times B}/dr$, is thus about $1 - 1.3 \times 10^6$ s^{-1}. On the other hand, we have calculated the decorrelation rate of local turbulence scattering, τ_{c0}^{-1}, from the e-folding time, i.e. the width of the peak, of the normalized autocorrelation function (ACF, figure 4.5) of I_s fluctuation data detected before biasing, which gives $\tau_{c0}^{-1} = 2.2 \times 10^5$ s^{-1}. Thus, the flow shear rate significantly exceeds the turbulence decorrelation rate and hence reduces turbulence and turbulent transport [Stö99, Bur92, Roz92, VOost03, Tayl89, Ten97]. The mechanism of reduced turbulent transport in the presence of stable flow shear is rather simple and is schematically shown in figure 4.6. When a fluid eddy is placed in a stable laminar background flow of which the speed varies transverse to the flow direction, the eddy is stretched and distorted as different fluid parcels in the eddy are advected (carried along) at different speed. When the eddy (or cell) is isolated, it can be stretched to many times its original scale length. When the eddy is part of a turbulent flow, however, it loses coherence (or correlation) and the strong shear in the poloidal flow tears the turbulent cells apart. In the absence of the background shear flow, the time scale for the loss of coherence defines the turbulent scattering decorrelation time τ_{c0}. In the presence of a background shear flow of which the rate $\left(\tau_s^{-1}\right)$ of differential advection exceeds the turbulent scattering decorrelation rate $\left(\tau_{c0}^{-1}\right)$, eddies stretch to a flow-wise eddy decorrelation length in

a fraction of the time they would normally take to become decorrelated were there no shear. Consequently, the decorrelation time is significantly shortened. Therefore, the rate of turbulent transport across the background shear flow is also reduced. This follows because the turbulent intensity and shear-wise eddy decorrelation length are reduced, thus reducing the speed and step size of a random-walk transport process.

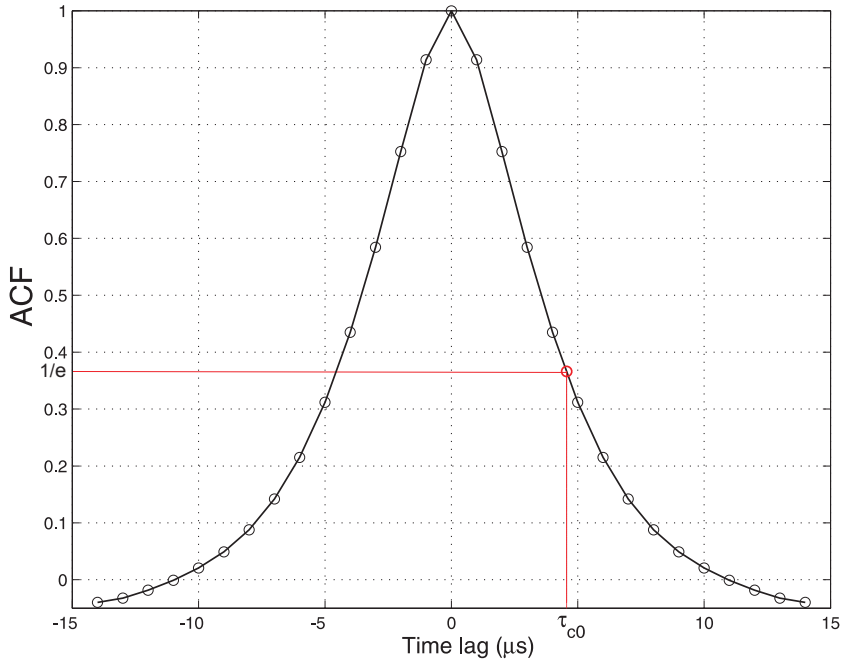

Figure 4.5 (a) Autocorrelation function (ACF) of the ion saturation current fluctuations before biasing measured at $r = 60$ mm. The e-folding time of the ACF equals the decorrelation time of the local turbulent scattering $\tau_{c0} = 4.6\ \mu s$.

The reduction in both I_s and ϕ_f fluctuations during biasing has been observed in the present experiments. The reduced turbulent transport leads to the formation of an edge pedestal and thus steepening of the edge density profile during biasing, as shown in figure 4.4(d). From all the above facts, we conclude that a clear and reproducible transition to a improved confinement is induced by the edge electrode biasing along with the creation of a particle edge transport barrier just inside the LCFS. This barrier is characterized by a (i) substantial increase of the edge density gradient; (ii) reduction in recycling indicated by a drop in H_α signal; (iii) substantial increase of the global particle confinement time; (iv) suppression of the density and potential fluctuation level.

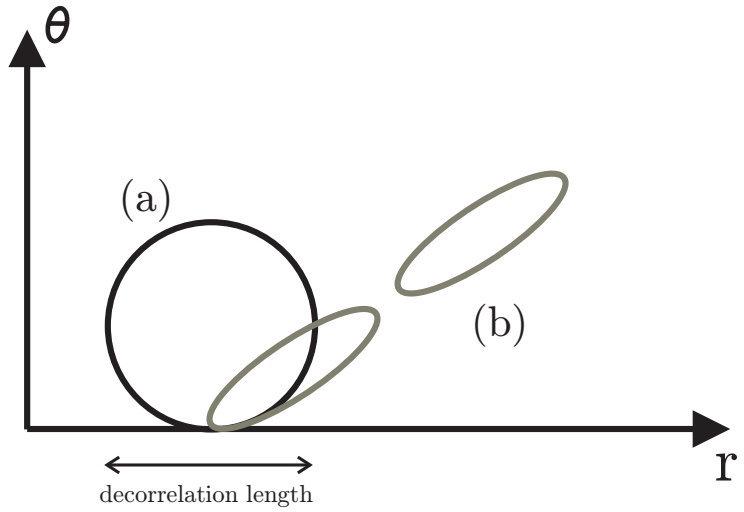

Figure 4.6 A reference eddy [(a), no shear flow] sheared by poloidal shearing (b) with radial velocity $u_r(\theta) = \alpha\theta$. If the eddy is isolated it stretches into the shape indicated by the grey colour. In turbulence, the eddy loses correlation in a decorrelation length, represented as a break-up into two eddies. The decorrelation reduces the θ scale relative to that of the reference eddy.

4.2.4.2 Periodic relaxation on E_r and related quantities

In these experiments, an important finding is the periodic relaxation behaviour of E_r and related quantities during the biasing period. The high sampling rate performed on the electrostatic measurements at the edge allowed the investigation of fast features with a good time resolution. In particular during the biasing phase the onset of a quite regular oscillating behaviour has been observed on electrostatic quantities measured at the edge. As shown in figure 4.3(e), the E_r signal in the biasing phase (between 11-14 ms) clearly exhibits periodic oscillations ($f \sim 10$ kHz, amplitude 7 kVm^{-1}) on top of a DC E_r value (~ 11 kVm^{-1}). The concurrent oscillations in H_α and τ_p can also be seen in figure 4.3(c) and (d), respectively. These oscillations do not affect the global confinement properties, since the averaged values of H_α and τ_p evolve continuously with time. Nevertheless, a modulation on the ETB can still be seen from the edge density profile on top of its average level.

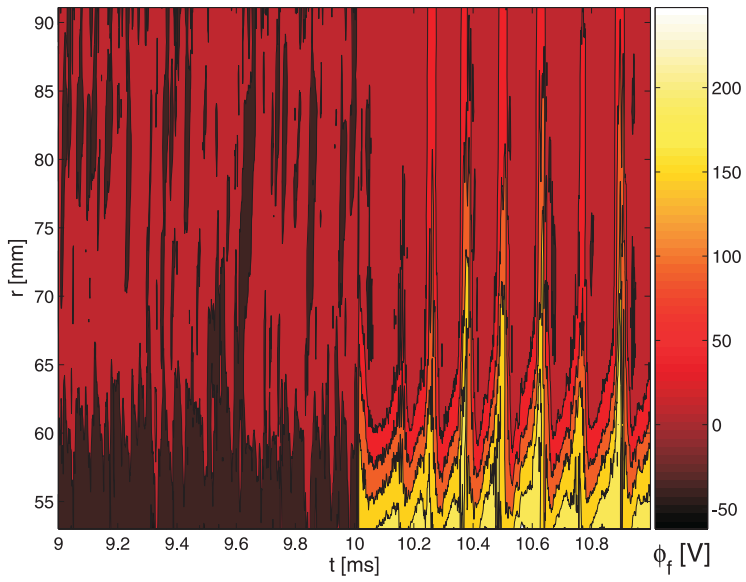

Figure 4.7 Contour plot of ϕ_f over the full radial extend of the rake probe (53- 91 mm) in a time window [9.00,11.00] ms; biasing starts at 10 ms (shot No. 24000).

The 2-D picture shown in figure 4.7 blatantly shows the sudden appearance of these oscillations. We dub this phenomenon as a relaxation event (RE). This contour plot represents the time behaviour of all the 16 pins of the rake probe showing the radial extension of the oscillating features (REs), i.e. almost 40 mm in the plasma edge region. Figures 4.8(a) and (b) focus on one of the ϕ_f and E_r structures respectively in a time window of 0.1 ms. The peak turns out to be asymmetric, with the arising phase slower than the crash. In reference to one RE figure 4.8(b) shows the floating potential profiles at three different time steps: a strong ϕ_f gradient characterizes the region inside the LCFS, with a radial electric field up to 19 kV/m that precedes the peak $(t_a = 10.59 \text{ ms})$, then E_r falls to a value four times lower during the peak $(t_b = 10.632 \text{ ms})$ and finally recovers its initial value $(t_c = 10.66 \text{ ms})$.

(a)

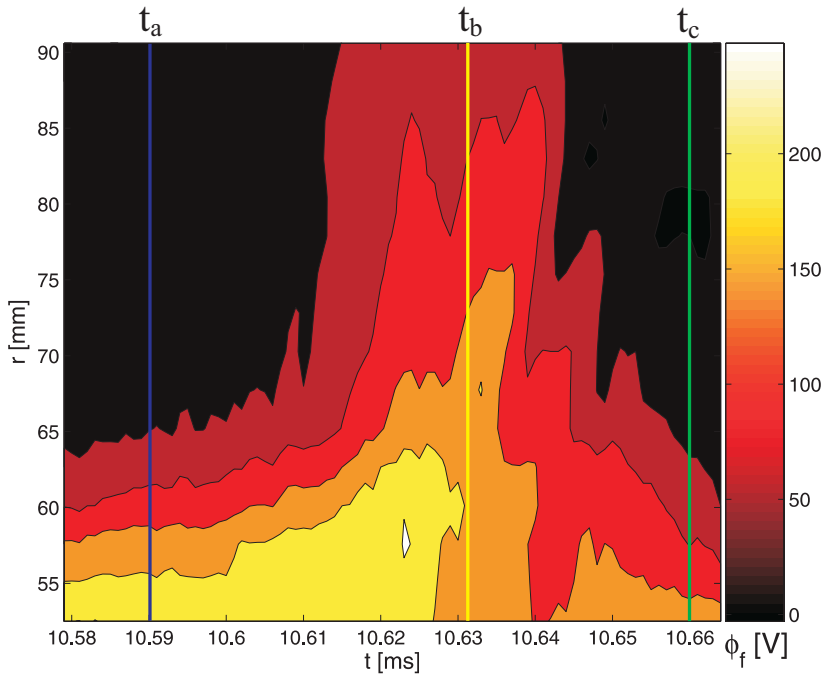

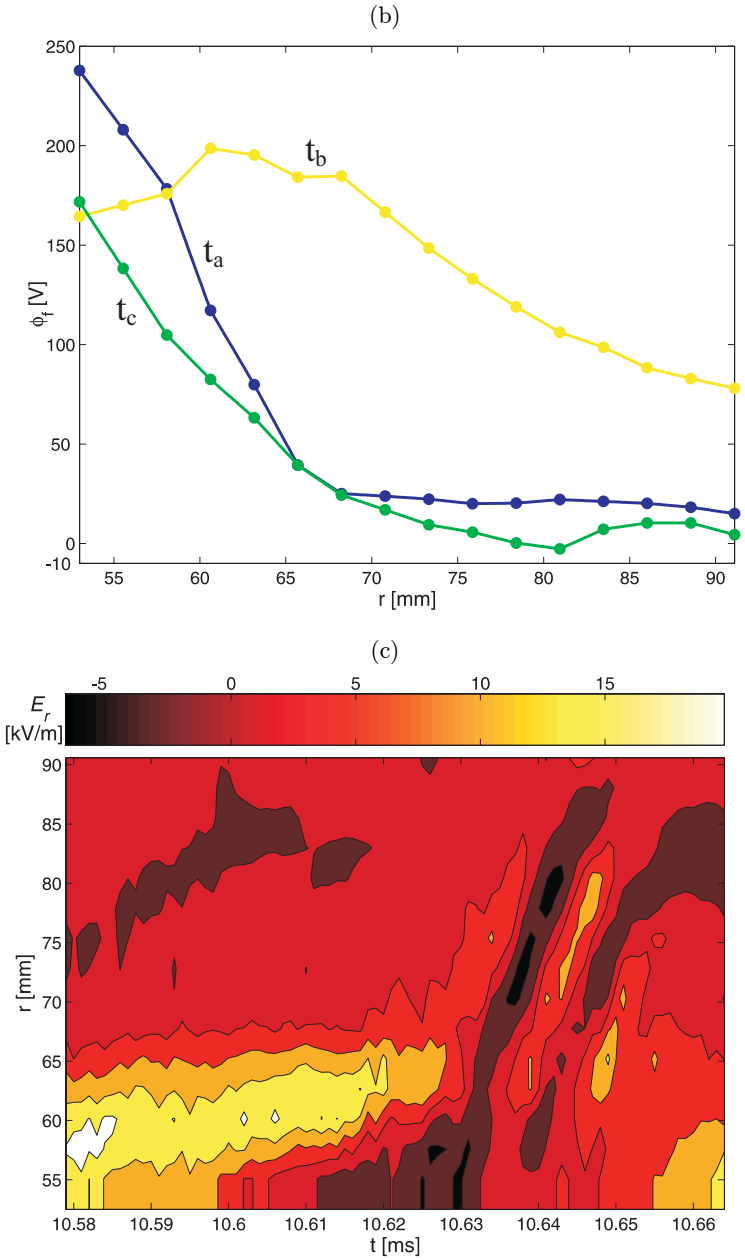

Figure 4.8 Detail of time behaviour of ϕ_f (a) and E_r (c) profiles during one relaxation event and (b) $\phi_f(r)$ measured at three different time instants: before (t_a), during (t_b) and after (t_c) the crash (shot No. 24000).

Plotted in figure 4.9 is the radial dependence of density $(\propto I_s)$ at three different times. The reference one (open squares - pre-bias) is the same as that shown in figure 4.4(d), i.e. the average value detected prior to the biasing phase. The other two are measured at time t_1 and t_2, when the oscillating E_r is maximum and minimum, respectively, as indicated in figure 4.10. Figure 4.9 clearly shows that (i) during biasing the average density gradient, i.e., average of profiles of t_1 and t_2, is much steeper than that of the pre-bias profile; (ii) with oscillation of E_r, the density profiles change from a very steep one at t_1 to a less steep one at t_2, indicating a modulation of the ETB during the improved confinement stage. Meanwhile, it is found that the edge poloidal and toroidal plasma rotations also oscillate simultaneously with E_r at the same time period. The details of the RE are shown in figure 4.10 for a time window of 0.35 ms. Plotted in figure 4.10 are time traces of E_r, H_α, poloidal (v_θ) and toroidal (v_ϕ) plasma flow velocities measured at $r = 60$ mm and I_s measured at two different radial positions $(I_{s1}$ at $r_1 = 53$ mm, I_{s2} at $r_2 = 68$ mm$)$ across the ETB region. The absolute value of the density gradient around the transport barrier $\left(\propto |\nabla I_s| = \left|(I_{s2} - I_{s1})/(r_2 - r_1)\right|\right)$ is shown in figure 4.10(e).

In figure 4.10(c), v_θ and v_ϕ are deduced from Gundestrup probe measurements using an improved one-dimensional fluid probe model (see chapter 2) in which a constant $T_e = 35$ eV is assumed [Pel05, Pel06a]. From the figures, we can see that E_r, v_θ and $|\nabla I_s|$ are changing in phase while v_ϕ and H_α vary out of the phase with E_r. The lowest order single ion radial force balance equation $E_r = \nabla_r p_i / n_i Z_i e - v_{\theta,i} B_\phi + v_{\phi,i} B_\theta$ has been checked using the measured quantities, where p_i denotes the ion pressure and $Z_i e$ the electric charge. It has been found that the equation is well fulfilled throughout the oscillation phase. Moreover, the in-phase-oscillations between E_r and v_θ and the out-of-phase-oscillations between E_r and ∇I_s $(\propto \nabla p_i)$ indicate that the diamagnetic term ∇p_i alone cannot account for the development of the E_r oscillations, but are rather dominated by the poloidal flow oscillations.

The overall feature of the E_r relaxation can be further illustrated by a one-period process. First, E_r increases gradually to its threshold value (18 kV/m) at t_1. Meanwhile, v_θ and $|\nabla I_s|$ increase, whereas H_α drops indicating an increase of poloidal sheared flows, decrease of the local particle flux and the strengthening of a local transport barrier (see profile at t_1 in figure 4.9). From t_1 to t_2, with the relaxation of E_r from its maximum to bottom, the concomitant drop in $|\nabla I_s|$ and increase in H_α reveal a fading of the local barrier, as shown also in figure 4.9 by the profile at t_2. It is interesting to see that, throughout the above process, the behaviour of the toroidal flow, v_ϕ, is completely different from that of E_r and v_θ, but follows the variation of the radial transport. For example, from t_1 to t_2, with the fading of the local transport barrier, the flattening of the edge density profile implies an enhancement of outflux. Spolaore [Spol05] used a conditional averaging technique to estimate the radial propagation velocity of these expelled particles (blobs of density) towards the wall during the relaxation event. This resulted in a value of about 0.4 km/s. The enhanced radial outflux may transfer energy to the toroidal flow via dynamical coupling and thus increases v_ϕ substantially. This coupling can occur through the turbulence-driven Reynolds stress. Similar phenomena for the non-linear dynamical interaction between the turbulent transport and the toroidal flow have been reported on JET [Hid03a,b] in non-biasing experiments, where, in particular, the large scale components $(\sim 12.5$ kHz$)$ show dominant effects. In our case, the periodic link between the turbulent transport and the parallel flow takes place at an almost fixed frequency of $f \approx 10$ kHz, which is probably triggered by E_r and interestingly close to the dominant frequencies in JET.

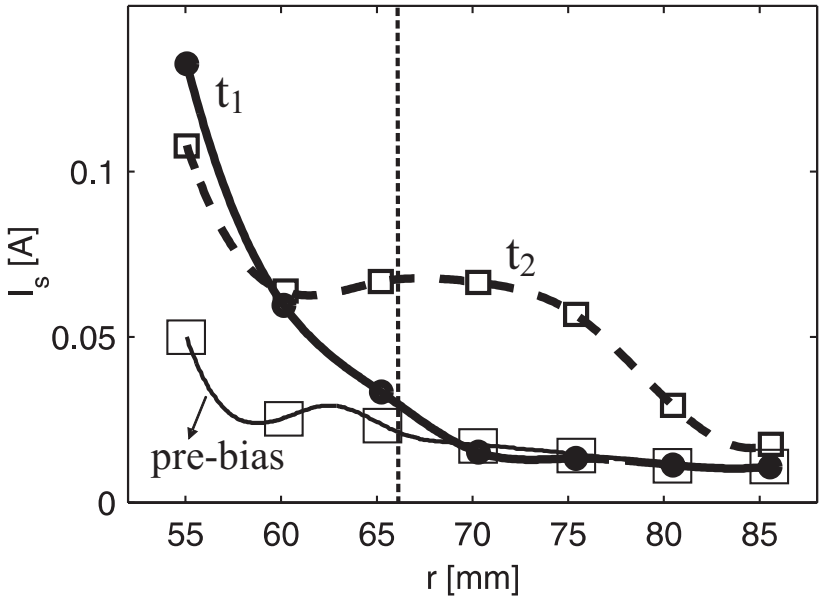

Figure 4.9 Radial profiles of ion saturation current measured by a rake probe at three different times. The curve of "pre-bias" is the averaged value detected before the biasing phase (the same as in figure 4.4(d)). The other two are the I_s -profiles measured at times t_1 and t_2 indicated in figure 4.10. The vertical dashed line marks the position of the LCFS (shot No. 24000).

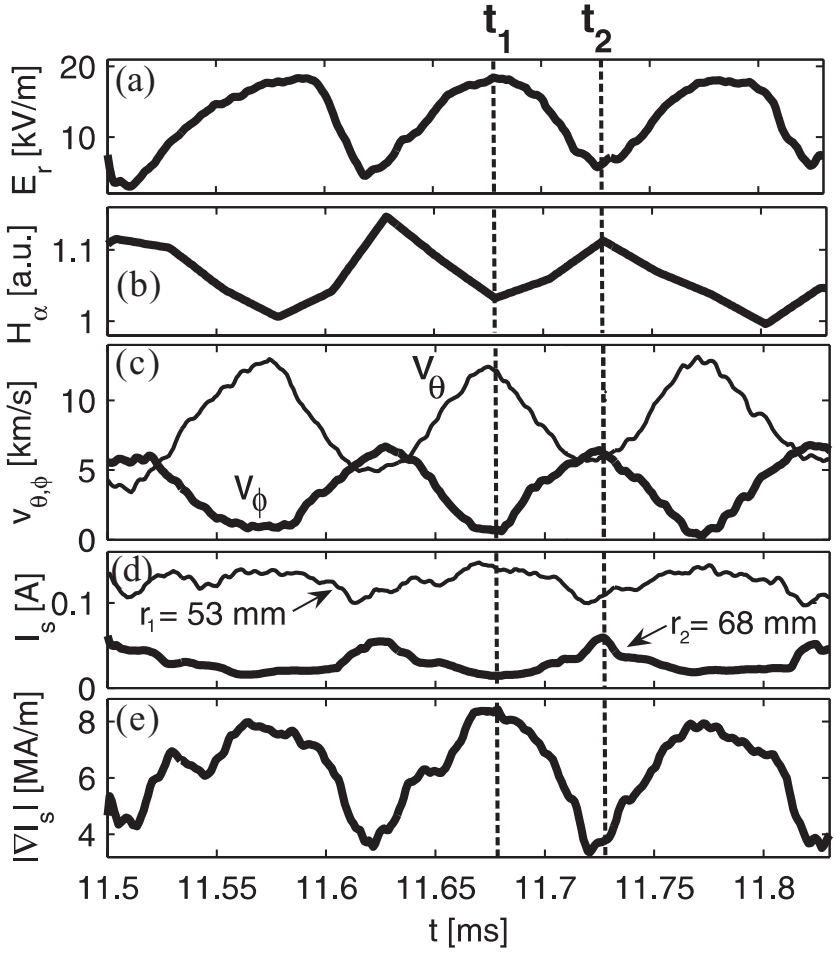

Figure 4.10 Time evolution of (a) E_r, (b) H_α, (c) poloidal v_θ (thin line) and toroidal v_ϕ (thick line) velocities measured at $r = 60\ mm$, (d) I_{s1} (thin line) and I_{s2} (thick line) measured by a rake probe at $r_1 = 53\ mm$ and $r_2 = 68\ mm$, respectively, and (e) $|\nabla I_s| = |(I_{s2} - I_{s1})/(r_2 - r_1)|$ showing oscillations of the signals. (shot No. 24000). The two dashed vertical lines mark the times when a relaxation of E_r starts (t_1) and ends (t_2).

4.2.5 Conclusion

In conclusion, the results of highly resolved spatio-temporal measurements of the edge radial electric field E_r and plasma rotations during the edge biasing experiments in the CASTOR tokamak have been presented. With biasing, a clear and reproducible transition to an improved confinement is routinely observed along with the formation of an edge transport barrier. Furthermore, for the first time we observed the concurrent fast periodic relaxations on E_r, plasma rotations, edge recycling and the edge transport barrier during the globally improved confinement phase on top of the biasing-imposed DC E_r. The oscillation event does not much affect the global confinement properties, but modulates the local edge plasma parameters and the transport barrier as well. During the oscillating phase, E_r and associated quantities well obey the radial force balance E_r-equation, suggesting a radial equilibrium of the local parameters unaffected in the process. In addition, a possible link between the relaxation of the radial transport and the parallel flow was evidenced during the relaxation process of E_r, which supports the paradigm of the non-linear dynamical coupling and energy transfer between the turbulence eddies and zonal (or mean) flows.

The fact that these features occur in the plasma boundary of two completely different tokamaks under entirely different plasma conditions might suggest that the physics are of universal nature. The results suggest that parallel turbulent force is an important ingredient to explain flow momentum redistribution in the boundary of fusion plasmas (i.e. flow physics requires a three-dimensional (3D) description). These findings are consistent with numerical simulations pointing out the role of turbulent forces on both perpendicular and parallel flow components during the development of zonal flows [Hall04]. Because of the 3D nature of the shear flow physics in fusion plasmas and the experimental evidences shown, several components of the production term, including radial-parallel $\left(\left\langle \tilde{v}_{//}\tilde{v}_r \right\rangle\right)$ and radial-perpendicular $\left(\left\langle \tilde{v}_{\perp}\tilde{v}_r \right\rangle\right)$ components of Reynolds stress, should be considered [Verg05]. It remains a

challenge for experimentalists to measure simultaneously the evolution of the whole production term during the development of the observed relaxations.

Acknowledgement

This work was supported by a fund for scientific research-Flanders, Belgium (FWO, Project No. G.0098.05), and partly by a fund of the international association for the promotion of co-operation with scientists from the new independent states of the former Soviet Union (INTAS, Project No. 2001-2056).

5

Overall conclusions

For more than a decade it has become increasingly clear that edge or boundary plasmas play an important role in magnetic fusion experiments. In particular, the cross-field transport of energy and particles, originating in the edge plasma due to different mechanisms, limits the confinement time of the hot and dense core plasma and strongly imposes constraints on the ultimate material choice for the first wall and other plasma facing objects in next generation tokamaks. Therefore, fusion research dedicated to a better understanding of edge plasmas and controlling it is of essential importance. Tokamaks like CASTOR and TEXTOR have engaged to specialize in edge studies and plasma-surface interactions by employing extensive equipment of edge diagnostics. The work presented in thesis is focussed on both tokamak machines.
The electrical probe method is one of the most straightforward techniques in plasma diagnostics to study the plasma boundary. However, probes suffer from the first law of diagnostics; the ease of interpretation is inversely proportional to the ease of implementation [Matt94].

In this thesis the historical developments of a one-dimensional fluid probe theory, for the determination of parallel and perpendicular Mach numbers (directly related to the plasma flow), has been reviewed in detail. The resulting transport equations constitute a set of coupled differential equations. For practicability this model uses an analytical expression to

approximate the exact numerical solutions of the differential equations. A numerically based full-parameter study has been performed to carefully examine the reliability of this analytical model resulting in the formulation of an improved analytical expression. This ameliorated expression now takes into account all related and dependent quantities and more clearly defines the region of the model's applicability. Subsequently, the improved model has been validated by comparing it to a kinetic, two-dimensional and quasi-neutral Particle-In-Cell simulation code. The remarkable agreement, within the applicability of both models, supports the use of the improved analytical fluid probe model for derivation of the Mach numbers from experimental probe data.
Worldwide two different types of Gundestrup probes are employed: probes with flat collectors, for example in TEXTOR, and with round collectors, as in CASTOR. The afore-mentioned probe model has been extended to be able to correctly determine the Mach numbers from data retrieved from a probe with round collectors. The effect of a round collecting surface on the perpendicular flow has been investigated and it was found that the parallel flow appeared to be insensitive to the shape of the collector. For round collectors, an expression which takes into account the curvature consequences on the determination of the perpendicular Mach number is then proposed.

Furthermore, the development of an advanced Gundestrup probe head is presented. This complex probe assembly has made it possible to simultaneously determine a large variety of edge plasma parameters, i.e. the toroidal and poloidal plasma flows, the ion saturation current, density, electron temperature, floating potential (thus electric field), as well as their fluctuating properties. Its design rests mainly on the probe modelling discussed above. This probe head has been installed on a versatile fast scanning and rotating probe system which very recently (Nov. 2005) became in operation on the TEXTOR tokamak. Measurements of the local plasma edge parameter radial profiles with high temporal and spatial resolution were possible due to the high-tech features of the

reciprocating linear movement of the probe drive system. Finally, it has been shown that the measurements of flows and other edge plasma parameters in TEXTOR with the presented probe diagnostic are reliable and accurate.
Now that the robustness of the new probe diagnostic has been demonstrated and taking into account the high spatial and time resolution and user-friendliness, the fast scanning probe diagnostic has become one of the most frequently used edge diagnostics on TEXTOR. Therefore, in the future, it will beyond all doubt provide useful data for further DED characterization studies.

Recently, experimental evidence of a dynamical coupling between turbulent transport and toroidal flows has been reported on JET [Hid03a]. This empirical link could provide new insights in the physics of edge plasmas in order to explain the discrepancy between the measured and theoretical radial transport. We report a similar observation on CASTOR during edge biasing experiments. In the biasing phase a clear and reproducible transition to an improved confinement is induced by the edge electrode polarization along with a creation of a particle edge transport barrier just inside the LCFS.
An important finding has been the periodic relaxation behaviour of the radial electric field and related quantities during the biasing period. These periodic oscillating features of these relaxation events have been studied in detail. In particular, a clear and reproducible relationship between the turbulent driven radial transport and the toroidal flow has been found. Hence, this edge plasma behaviour does not only concur with the results on a much bigger tokamak as JET, the completely different plasma conditions in which these experiments took place could indicate that the mechanism to couple transport and toroidal flows might be a universal feature of edge tokamak plasmas. The results suggest that parallel turbulent force is an important ingredient to explain flow momentum redistribution in the boundary of fusion plasmas.

Bibliography

[Asak95] N. Asakura, S. Tsuji-lio, Y. Ikeda, Y. Neyatani, and M. Seki, *'Fast reciprocating probe system for local scrape-off layer measurements in front of the lower hybrid launcher on JT-60U'*, Rev. Sci. Instrum., 66:5428, 1995.

[Aski92] L. G. Askinazi, V. E. Golant, S. V. Lebedev, V.A. Rozhanskii, and M. Tendler, *'Radial current in a tokamak caused by a biased electrode',* Nucl. Fusion, 32:271, 1992.

[Bael91] M. Baelmans, *'PhD thesis'*, Institüt fur Plasmaphysik, Jülich, 1991.

[Bak03] J.G. Bak, S.G. Lee, and the KSTAR Project Team, *'KSTAR edge probe diagnostics'*, Rev. Sci. Instrum., 74:1578, 2003.

[Bohm49a] D. Bohm, *'Minimum ion kinetic energy for a stable sheath'*, National Nuclear Energy Series, 5:77, Mc Graw-Hill book Company Inc., 1ste edition, 1949.

[Bohm49b] D. Bohm, *'The characteristics of electrical discharges in magnetic fields'*, edited by A. Guthrie and R.K. Wakerling, 1949.

[Brag65] S. I. Braginski, *'Transport processes in a plasma'*, Reviews of plasma physics, Vol. I, Plenum Publishing Corporation, 1965.

[Bur89] K. H. Burrell, *et al.*, '*Confinement physics of H-mode discharges in DIII-D*', Plasma Phys. Control. Fusion, 31:1649, 1989.

[Bur92] K. H. Burrell, T. Carlstrom, E. Doyle, D. Finkenthal, P. Gohil, R. J. Groebner, D. L. Hillis, J. Kim, H. Matsumoto, R. A. Moyer, T. H. Osborne, C. L. Rettig, W. A. Peebles, T. L. Rhodes, H. StJohn, R. D. Stambaugh, M. R. Wade, and J. G. Watkins, '*Physics of the L-mode to H-mode transition in tokamaks*', Plasma Phys. Control. Fusion, 34:1859, 1992.

[Camp90] D. S. Campbell and the JET TEAM, '*Confinement and stability in JET: recent results*', Plasma Phys. Control. Fusion, 32:949, 1990.

[Chan94] A. V. Chankin and P. C. Stangeby, '*The effect of diagmagnetic drift on the boundary conditions in tokamak scrape-off layers and the distribution of plasma fluxes near the target*', Plasma Phys. Control. Fusion, 36:1485, 1994.

[Chen74] F. Chen, '*Introduction to Plasma Physics*', Book, New York: Plenum Press, 1974.

[Chod82] R. Chodura, '*Plasma-wall transition in an oblique magnetic field*', Phys. Fluids, 25:1628, 1982.

[Chod88] R. Chodura, '*Basic problems in edge plasma sheath criterion*', Phys. Plasmas, 28:303, 1988.

[Chod95] R. Chodura, '*The Bohm-Chodura plasma sheath criterion*', Phys. Plasmas, 2(3), 1995.

[Chu91] K. S. Chung and I.H. Hutchinson, '*Effects of a generalized presheath source in flowing magnetized plasmas*', Phys. Fluids, B3:11, 1991.

[Den80] R. Denavit and W. Kruer, *'How to get started in particle simulation'*, Comments Plasma Phys. Cont. Fusion, 6(1):35, 1980.

[Ere00] S.K. Erents, A. V. Chankin, G. F. Matthews, and P. C. Stangeby, *'Parallel flow in the JET scape-off layer'*, Plasma Phys. Control. Fusion, 42:905, 2000.

[Fin01] K.H. Finken, S.S. Abdullaev, T. Eich, D.W. Faulconer, M. Kobayashi, R. Koch, G. Mank, and A. Rogister, *'Plasma rotation induced by the Dynamical Ergodic Divertor'*, Nucl. Fusion, 41:503, 2001.

[Fin06] K.H. Finken, *'The Dynamic Ergodic Divertor'*, Fusion Sci. Technol., 49:240, 2006.

[Glass60] S. Glasstone and R.H. Lovberg, *'Controlled thermonuclear reactions, an introduction to theory and experiment'*, Colonial Press Inc. USA, 1960.

[Gon02] B. Goncalves, C. Hidalgo, M. A. Pedrosa, K. Erents, G. Matthews, B. van Milligen, E. Sanchez, and C. Silva, *'Experimental investigation of dynamical coupling between density gradients, radial electric fields and turbulent transport in JET plasma boundary region'*, Nucl. Fusion, 42:1205, 2002.

[Gon03] B. Goncalves, C. Hidalgo, M. A. Pedrosa, C. Silva, R. Balbin, K. Erents, M. Hron, A. Loarte, and G. Matthews, *'Edge localized modes and fluctuations in the JET SOL region'*, Plasma Phys. Control. Fusion, 45:1627, 2003.

[Groeb90] R. J. Groebner, K. H. Burrell, and R. P. Seraydarian, *'Role of electric field and poloidal rotation in the L-H transition'*, Phys. Rev. Lett., 64:3015, 1990.

[Gunn98] J. P. Gunn, *'Two-dimensional quasineutral PIC simulation of a Gundestrup probe'*, Czech. J. Phys., 48(S2):293, 1998.

[Gunn01] J. P. Gunn, *'Direct measurements of $E \times B$ flow and its impact on edge turbulence in the CASTOR tokamak using an optimized Gundestrup probe'*, Czech. J. Phys., 51(10):1001, 2001.

[Hall04] K. Hallatschek, *'Turbulent saturation of tokamak-core zonal flows'*, Phys. Rev. Lett., 93:065001, 2004.

[Hamm96] D. Hammer, F. Dyson, N. Fortson, B. Novick, and W. Panofsky, *'Inertial Confinement Fusion (ICF) Review'*, Nucl. Sci. Techn., A721603, 1996.

[Hid03a] C. Hidalgo, B. Goncalves, M. A. Pedrosa, K. Erents, M. Hron, and G. F. Matthews, *'Experimental investigation of dynamical coupling between turbulent transport and parallel flows in the JET plasma-boundary region'*, Phys. Rev. Lett., 91(6):065001, 2003.

[Hid03b] C. Hidalgo, B. Goncalves, M. A. Pedrosa, C. Silva, R. Balbin, M. Hron, A. Loarte, K. Erents, G. F. Matthews, and R. Pitts, *'Experimental evidence of fluctuations and flows near marginal stability and dynamical interplay between gradients and transport in the JET plasma boundary region'*, J. Nucl. Mat., 313:863, 2003.

[Hut87] I.H. Hutchinson, *'A fluid theory of ion collection by probes in strong magnetic fields with plasma flow'*, Phys. Fluids, 30:3777, 1987.

[Hut88a] I.H. Hutchinson, *'Ion collection by probes in strong magnetic fields with plasma flow'*, Phys. Rev. A, 37:4358, 1988.

[Hut88b] I.H. Hutchinson, *'Reply to the comments of Stangeby'*, Phys. Fluids, 31(9):2728, 1988.

[Hut00] I.H. Hutchinson, *'Plasma particle flux'*, In principles of plasma diagnostics, Cambridge University Press, ISBN 0-521-32622-2, 50-86, 2000.

[ITER01] ITER, Summary of the ITER Final Design Report – presented by the ITER Director, July 2001.

[Ito88] S. I. Itoh and K. Itoh, *'Model of L- to H-mode transition in tokamak'*, Phys. Rev. Lett., 60:2276, 1988.

[Jac98] S. Jachmich, G. Van Oost, R. R. Weynants, and J. A. Boedo, *'Experimental investigations on the role of $E \times B$ flow shear in improved confinement'*, Plasma Phys. Control. Fusion, 40:1105, 1998.

[Jac07] S. Jachmich, *'Effects of radial electric field on transport and confinement in tokamak plasmas'*, PhD-thesis, to be published, 2007.

[Jack91] G. L. Jackson, J. Winter, T.S. Taylor, K. H. Burrell, J. C. DeBoo, C. M. Greenfeld, R.J. Groebner, T. Hodapp, K. Holtrop, E. A. Lazarus, L. L. Lao, S. I. Lippmann, T. H. Osborne, and DIII-D Team, *'Regime of very high confinement in the boronized DIII-D tokamak'*, Phys. Rev. Lett., 67:3098, 1991.

[John50] E.O. Johnson and L. Malter, *'A floating probe method for measurements in gas discharges'*, Phys. Rev. Lett., 80:58, 1950.

[Joy97] G. Joyce, *'Electrostatic particle-in-cell simulation technique for quasineutral plasma'*, J. Comp. Phys., 138:540, 1997.

[Klee98] M. Kleemann, *'Potentials and limits of renewable sources of energy'*, Fus. Techn., 33:401, 1998.

[Koch06a] R. Koch, *'The ion cyclotron, lower hybrid and Alfvèn wave heating methods'*, Seventh Carolus Magnus Euro-Summer School on Plasma and Fusion Energy Physics, Trans. Fusion Sci. Techn., 49:187, 2006.

[Koch06b] R. Koch, *'Plasma heating by neutral beam injection'*, Seventh Carolus Magnus Euro-Summer School on Plasma and Fusion Energy Physics, Trans. Fusion Sci. Techn., 49:167, 2006.

[Koid94] Y. Koide, M. Kikuchi, M. Mori, S. Tsuji, S. Ishida, N. Asakura, Y. Kamada, T. Nishitani, Y. Kawano, T. Hatae, T. Fujita, T. Fukuda, A. Sakasai, T. Kondoh, R. Yoshino, and Y. Neyatani, *'Internal transport barrier on q=3 and poloidal plasma spin-up in JT60-U high-β_p discharges',* Phys. Rev. Lett., 72:3662, 1994.

[Lang23] I. Langmuir, *'The effect of space charge and initial velocities on the potential distribution and thermionic current between parallel plane electrodes'*, Phys. Rev., 21:419, 1923.

[Lang24] I. Langmuir and H. Mott-Smith, Gen. Electr. Rev., *'Langmuir probe technique'*, 27:449, 1924.

[Lang29] I. Langmuir, *'The interaction of electron and positive ion space charges in cathode sheath'*, Phys. Rev., 33:954, 1929.

[Law57] J. Lawson, *'Some criteria for a power producing thermonuclear reactor'*, Proc. Phys. Soc. B, 70:6, 1957.

[Liew85] P. C. Liewer, *'Measurements of microturbulence in tokamaks and comparisons with theories of turbulence and anomalous transport'*, Nucl. Fusion, 25:543, 1985.

[Lin97] J.D. Lindl, '*Inertial Confinement Fusion: The Quest for Ignition and Energy Gain Using Indirect Drive*', Book AIP Press, ISBN 156396662X, 1997.

[Mac92] C.S. MacLatchy, C. Boucher, D.A. Poirer and J. Gunn, *'Gundestrup: A Langmuir/Mach probe array for measuring flows in the scrape-off layer of TdeV'*, Rev. Sci. Instrum., 63:3923, 1992.

[Matt94] G. F. Matthews, *'Tokamak plasma diagnoses by electrical probes'*, Plasma Phys. Control. Fusion, 36:1595, 1994.

[Mic02] F. Michon, *'Sonde'*, Rapport de Stage, INRS Energie et Matériaux, Canada, 2002.

[Mit05] M. Mitri, *'Control of a fast reciprocating probe for the TEXTOR fusion experiment'*, Master Thesis, Internal Report, Research Centre Jülich, Institute of Plasma Physics, University of Duisburg-Essen, Duisburg, May 2005.

[Mott26] H.M. Mott-Smith and I. Langmuir, *'The theory of collectors in gaseous discharges'*, Phys. Rev., 28:727, 1926.

[Ong06] J. Ongena and G. Van Oost, *'Energy for future centuries. Prospects for fusion power as a future energy source'*, Seventh Carolus Magnus Euro-Summer School on Plasma and Fusion Energy Physics, Trans. Fusion Sci. Techn., 49:3, 2006.

[Oth78] H. Ohtsuka, H. Kimura, S. Shimomura, H. Maeda, S. Yamamoto, M. Nagami, N. Ueda, A. Kitsunezaki, and T. Nagashima, *'Probe measurements in the scrape-off layer of a tokamak'*, Plasma Phys. Contr. Fus. 20:749, 1978.

[Ped99] M.A. Pedrosa, A. Lopez-Sanchez, C. Hidalgo, A. Montoro, A. Gabriel, J. Encabo, J. de la Gama, L.M. Martinez, E. Sanchez, R. Perez, and C. Sierra, *'Fast movable remotely controlled Langmuir probe system'*, Rev. Sci. Instrum., 70:415, 1999.

[Pel02] P. Peleman, S. Jachmich, M. Van Schoor, C. Boucher, F. Michon, and G. Van Oost, *'Study of the accuracy of Mach probes to Measure the parallel and perpendicular flow in the plasma edge'*, 29th European Physical Society (EPS) conference on Plasma Phys. and Contr. Fusion, Montreux, Switzerland, ECA 26B, 2.126, 2002.

[Pel05] P. Peleman, S. Jachmich, M. Van Schoor, G. Van Oost, *'Investigation of the reliability of a 1-D fluid probe model for Mach probe measurements'*, Czech. J. Phys., 55(3):381, 2005.

[Pel06a] P. Peleman, S. Jachmich, M. Van Schoor, G. Van Oost, W. Knaepen, and C. Boucher, *'Comparative Study of Flat and Round Collectors Using a Validated 1D Fluid Probe Model'*, Contrib. Plasma Phys., 46(5-6):432, 2006.

[Pel06b] P. Peleman, S. Jachmich, Y. Xu, C. Boucher, G. Van Oost, B. Schweer, and M. Mitri, *'Novel advanced Gundestrup-like probe for the measurements of flows and edge plasma parameters in TEXTOR'*, to be published (accepted), Rev. Sci. Instrum., 2006.

[Pel06c] P. Peleman, C. Boucher, J. Brotankova, P. Devynck, J. Stöckel, M. Spolaore, and G. Van Oost, *'Highly resolved measurements of periodic radial relaxation in edge biasing experiments'*, to be published (accepted), J. Nucl. Mat., 2006.

[Riem91] K. U. Riemann, *'The Bohm criterion and sheath formation'*, J. Phys. D: Appl. Phys., 24:493, 1991.

[Riem94] K. U. Riemann, *'Theory of the collisional presheath in an oblique magnetic field'*, Phys. Plasmas, 1:552, 1994.

[Reit06] D. Reiter and S. Wiesen, *'Helium removal and recycling'*, Trans. Fus. Techn., 49:248, 2006.

[Ritz89] Ch. P. Ritz, R. V. Bravenec, P. M. Schoch, R. D. Bengtson, J. A. Boedo, J. C. Forster, K. W. Gentle, Y. He, R. L. Hickok, Y. J. Kim, H. Lin, P. E. Phillips, T. L. Rhodes, W. L. Rowan, P. M. Valanju, and A. J. Wooton, *'Fluctuation-induced energy flux in the tokamak edge'*, Phys. Rev. Lett., 17:1844, 1989.

[Rog99] T. D. Rognlien, G. D. Porter, and D. D. Ryutov, *'Influence of ExB and del B drift terms in 2-D edge/SOL transport simulations'*, J. Nucl. Mat., 266:654, 1999.

[Roz92] V. A. Rozhansky and M. Tendler, *'The effect of radial electric field on the L-H transitions in tokamaks'*, Phys. Fluids B, 4:1877, 1992.

[Roz01] V. A. Rozhansky, S. P. Voskoboynikov, E. G. Kaveeva, D. P. Coster, and R. Scheider, *'Simulation of tokamak edge plasma inducing self-consistent electric fields',* Nucl. Fusion, 41:38, 2001.

[Serr03] G. Serrianni, W. Baker, and S. Dal Bello, *'High-spatial resolution edge electrostatic probe system for RFX'*, Rev. Sci. Instrum., 74:1558, 2003.

[Sha89] K. C. Shaing and E. C. Crume, *'Bifurcation of poloidal rotation and surpression of turbulent fluctuations: A model for the L-H transition in tokamaks'*, Phys. Rev. Lett. 63(21):2369, 1989.

[Silva04] C. Silva, I. Nedzelskiy, H. Figueiredo, R. M. O. Galvao, J. A. C. Cabral, and C. A. F. Varandas, *'Improved confinement events triggered by emissive electrode biasing on the tokamak ISTTOK'*, Nucl. Fusion, 44:799, 2004.

[Spol05] M. Spolaore, P. Peleman, J. Brotankova, P. Devynck, H. Figueiredo, G. Kirnev, E. Martines, J. Stöckel, G. Van Oost, J. Adamek, E. Dufkova, I. Duran, M. Hron, and V. Weinzettl, *'Relaxation phenomena induced by edge biasing experiments in the CASTOR tokamak'*, Czech. J. Phys., 55(12):1597, 2005.

[Sta90] P.C. Stangeby and G.M. McCracken, *'Plasma boundary phenomena in tokamaks'*, Nucl. Fusion, 30:1225, 1990.

[Sta95a] P.C. Stangeby, *'The Bohm-Chodura plasma sheath criterion'*, Phys. Plasmas, 2:702, 1995.

[Sta95b] P.C. Stangeby and A.V. Chankin, *'The ion velocity (Bohm-Chodura) boundary condition at the entrance to the magnetic presheath in the presence of diamagnetic and ExB drifts in the scrape-off layer'*, Phys. Plasmas, 2:707, 1995.

[Stö99] J. Stöckel, K. Dyabilin, I. Duran, J. Horacek, M. Hron, K. Jakubka, L. Kryska, S. Nanobashvili, I. Nanobashvili, M. Tendler, G. Van Oost, F. Zacek, *'Structure of edge turbulence at plasma polarization on the TEXTOR tokamak'*, 26th European Physical Society (EPS) conference on Plasma Phys. and Contr. Fusion, Maastricht, Netherlands, P4.058, 1999.

[Stö06] J. Stöckel, J. Adamek, P. Balan, O. Bilyk, J. Brotankova, R. Dejarnac, P. Devynck, I. Duran, J. P. Gunn, M. Hron, J. Horacek, C. Ionita, M. Kocan, E. Martines, R. Panek, P. Peleman, R. Schrittwieser, G. Van Oost, F. Zacek, *'Advanced probes for edge plasma diagnostics on the CASTOR tokamak'*, to be published in J. Phys., 2006.

[Strait95] E. Strait, L. Lao, M. Mauel, B. Rice, T. Taylor, K. Burell, M. Chu, E. Lazarus, T. Osborne, S. Thompson, and A. Turnbull, *'Enhanced confinement and stability in DIII-D discharges with reversed magnetic shear'*, Phys. Rev. Lett., 75:4421, 1995.

[Strin93] T. E. Stringer, *'Explanation of the L-H mode transition induced by applied voltage'*, Nucl. Fusion, 33(9):1249 , 1993.

[Tayl89] R. J. Taylor, M. L. Brown, B. D. Fried, H. Grote, J. R. Liberati, G. J. Morales, P. Pribyl, D. Darrow, and M. Ono, 'H-mode behaviour induced by cross-field currents in a tokamak', Phys. Rev. Lett., 63:2365, 1989.

[Tayl97] T. Taylor, *'Physics of tokamaks'*, Plasma Phys. Control. Fusion, 39:B47, 1997.

[Ten97] M. Tendler, Plasma Phys. Control. Fusion, *'Different scenarios of transitions into improved confinement modes'*, 39:B371, 1997.

[Ten02] M. Tendler, G. Van Oost, and J. Stockel, *'Models for transitions into regimes with enhanced confinement'*, Comments on Modern Physics, C203-204, 2002.

[Toki02] K. Tokimatsu, J. Fujino, Y. Asaoka, Y. Ogawa, K. Okano, T. Yoshida, R. Hiwatari, S. Konishi, S. Nishio, K. Yamaji, and Y. Kaya, *'Studies of Nuclear Fusion Energy Potential Based on a Long-Term World Energy and Environmental Model'*, NEDO (New Energy and Industrial Technology Development Organization), IAEA, 2002.

[Verg05] M. Vergote, M. Van Schoor, Y. Xu, S. Jachmich, R. Weynants, M. Hron, J. Stöckel, *'The possible role of Reynolds stress in the creation of a transport barrier in tokamak edge plasmas'*, Czech. J. Phys., 55(3):389, 2005.

[VG99a] H. Van Goubergen, R.R. Weynants, S. Jachmich, M. Van Schoor, G. Van Oost, and E. Desoppere, *'A 1D fluid model for the measurement of perpendicular flow in strongly magnetized plasmas'*, Plasma Phys. Control. Fusion, 41:L17-L22, 1999.

[VG99b] H. Van Goubergen, *'Experimental and theoretical investigation of flows in the edge plasma of the TEXTOR-94 tokamak using Mach probes'*, PhD-thesis, Ghent University, 1999.

[VS98a] M. Van Schoor, *'The influence of biasing on the flows in the core and the scrape-off layer of a tokamak'*, PhD – thesis, Laboratory Report No. 115, 1998.

[VS98b] M. Van Schoor and R. R. Weynants, *'Radial current and flows in the scrape-off layer of a tokamak'*, Plasma Phys. Control. Fusion, 40:403, 1998.

[VS03] M. Van Schoor, S. Jachmich, and R. R. Weynants, *'An experimental and theoretical study on the formation of electric field induced flow shear in the tokamak edge'*, J. Nucl. Mat., 313-316:1326, 2003.

[VOost01] G. Van Oost, J. Stockel, M. Hron, P. Devynck, K. Dyabilin, J. P. Gunn, J. Horacek, E. Martines, and M. Tendler, *'Potential structures and flow measurements with separatrix biasing in the CASTOR tokamak'*, J. Plasma Fus. Res. Series, 4:23, 2001.

[VOost03] G. Van Oost, J. Adamek, V. Antoni, P. Balan, P. Devynck, I. Duran, L. Eliseev, J. P. Gunn, M. Hron, C. Ionita, S. Jachmich, G. S. Kirnev, E. Martines, A. Melnikov, R. Schrittwieser, C. Silva, J. Stockel, M. Tendler, C. Varandas, M. Van Schoor, V. Vershkov, and R. R. Weynants, *'Turbulent transport reduction by ExB velocity shear during edge biasing: recent experimental results'*, Plasma Phys. Control. Fus., 45:621, 2003.

[Wag82] F. Wagner, G. Becker, K. Behringer, D. Campbell, A. Eberhagen, W. Engelhardt, G. Fussman, O. Gehre, J. Gernhardt, G. V. Gierke, G. Haas, M. Huang, F. Karger, *et al.*, *'Regime of improved confinement and high beta in neutral-beam-heated divertor discharges of the ASDEX tokamak',* Phys. Rev. Lett., 49:1408, 1982.

[Waid96] G. Waidmann, *'Operational limits in tokamak machines'*, Trans. Fus. Techn., 29:55, 1996.

[Wat97] J.G. Watkins, J. Hunter, B. Tafoya, M. Ulrickson, R.D. Watson, R.A. Moyer, J.W. Cuthbertson, G. Gunner, R. Lehmer, P. Luong, D.N. Hill, M. Mascaro, J.I. Robinson, R. Snider, and R. Stambaugh, *'Fast reciprocating Langmuir probe for the DIII-D divertor'*, Rev. Sci. Instrum., 68:373, 1997.

[Wes06] E. Westerhof, *'Electron cyclotron waves'*, Seventh Carolus Magnus Euro-Summer School on Plasma and Fusion Energy Physics, Trans. Fusion Sci. Techn., 49:195, 2006.

[Weyn92] R. R. Weynants, G. Van Oost, G. Bertschinger, J. Boedo, P. Brys, T. Delvigne, K. H. Dippel, F. Durodie, H. Euringer, K. H. Finken, D. S. Gray, J. D. Hey, D. L. Hillis, J. T. Hogan, L. Konen, R. Leners, A. M. Messiaen, A. Pospieszczyck, U. Samm, R. P. Schorn, B. Schweer, G. Telesca, R. Van Nieuwenhove, P. E. Vandenplas, *'Confinement and profiles changes induced by the presence of positive or negative radial electric fields in the edge of the TEXTOR tokamak'*, Nucl. Fusion, 32:837, 1992.

[Weyn93] R. R. Weynants and G. Van Oost, *'Edge biasing in tokamaks'*, Plasma Phys. Control. Fusion, 35:B177, 1993.

[Weyn94] R.R. Weynants, *'Fusion Machines'*, Trans. Fus. Techn., 25:19, 1994.

[Wolf96] G.H. Wolf, *'Status of tokamak experiments'*, Trans. Fus. Techn., 29:392, 1996.

[Woot90] A. J. Wootton, B. A. Carreras, H. Matsumoto, K. McGuire, W. A. Peebles, Ch. P. Ritz, P. W. Terry, and S. J. Zweben, *'Fluctuations and anomalous transport in tokamaks'*, Phys. Fluids B, 2:2879, 1990.

[Yan05] L. Yan, W. Hong, J. Qian, C. Luo, and L. Pan, *'Fast reciprocating probe system on the HL-2A tokamak'*, Rev. Sci. Instrum., 76:093506, 2005.

[Zohm96] H. Zohm, *'Edge localized modes'*, Plasma Phys. Control. Fusion, 38:105, 1996.